# Nuclear fission induced by heavy ions*

J. O. Newton

*Department of Nuclear Physics, Australian National University, Australia*
Fiz. Elem. Chastits At. Yadra **21**, 821–913 (July–August 1990)

This review covers recent experimental and theoretical developments in the field of heavy-ion induced fission. The basic ideas of the macroscopic theory of fission barriers and of the equilibrium statistical model and its application to nuclear fission are discussed. Experimental data and analysis of fission-fragment angular distributions, fragment angular momenta, fission and fusion excitation functions, the fission-like decay of systems with fissilities less than the Businaro–Gallone limit, and the prefission emission of particles and $\gamma$ rays are reviewed. Prefission neutron data suggest that the relaxation time for the collective fission degree of freedom is much longer ($> 10^{-20}$ s) than previously thought, implying overdamped motion of the nuclear fluid and the failure of the equilibrium statistical model. The basic ideas of dissipative nuclear dynamics and its application to fission are described.

## 1. INTRODUCTION

The year 1989 is the 50th anniversary of the discovery of nuclear fission (Ha 39, Me 39), perhaps one of the more momentous events in the history of mankind. The subsequent rapid development to produce nuclear bombs and nuclear power gave great impetus and financial support for the study of nuclear-structure physics. Curiously enough, the study of fission has until recently been outside the mainstream of nuclear research. This is probably because the accelerators of the 50's and 60's mostly provided beams of light ions, well suited for studying individual quantum states of low angular momentum or reactions involving the transfer of one or two nucleons. Fission, being an example of large-scale collective motion, appeared far removed from the ideas of the shell model and perhaps dull when viewed by analogy with a rather featureless oscillating liquid drop.

This situation has changed in recent years, owing to the new generation of accelerators capable of producing beams of heavy ions with energies high enough to overcome the Coulomb barriers of all stable nuclei. These have made possible the study of new examples of large-scale collective motions, involving major rearrangements of nuclear matter, such as deep-inelastic collisions and heavy-ion fusion. Further, the discovery of fissioning isomers (Po 62) and the development of the macroscopic–microscopic method to calculate the nuclear potential-energy surface (My 66, St 66) showed the strong connection between shell structure and fission barriers, at least for low temperatures.

Perhaps the most exciting development in the past few years is the discovery that dissipative effects (nuclear "viscosity") play an important role in fission induced by heavy ions. While the necessity to include strong dissipation in deep-inelastic collisions was clear and well recognized, it had been assumed for many years that the viscosity involved in fission was very weak and played a minor role. No doubt there are many common features between the deep-inelastic reactions and fission, but there are also marked differences. For example, deep-inelastic collisions are mainly peripheral, involving only necked-in shapes, and have a relatively small average mass-transfer between target and projectile and a very large energy-dissipation ($\sim 100$ MeV), whereas fission begins at a nearly spherical shape which eventually divides into two nearly equal parts and the dissipative loss to the collective motion is only $\sim 10$ MeV. Thus, we might expect that a study of fission will produce its own unique insights into the problem of large-scale nuclear dynamics. A complete picture may only emerge from a study of all of the reactions involving large mass-transfer and dissipation, e.g., fission, fusion, and deep-inelastic and fast fission (fission without compound nucleus formation).

This review will be mainly concerned with developments in heavy-ion induced fission during the last few years and will have an emphasis on the very recent results on dissipative effects. Since heavy-ion bombardment usually results in compound systems with high excitation energies and angular momenta, shell effects might be expected to be small, and the subject of low-energy fission, where they are important, will not be addressed. Other recent reviews of fission have been given by Va 73, Gr 76, De 82, Og 85.

## 2. BASIC THEORY AND MEASUREMENT

In this section we outline the ideas behind the present interpretation of fission induced by heavy ions, and possible measurements which can be made. For simplicity it is assumed that the fission results entirely from a compound system. More detailed considerations will be given, where appropriate, in later sections.

When a compound nucleus is formed, it can decay in many ways but principally by light-particle emission (neutrons, protons, or $\alpha$ particles) or by fission. Unless the nucleus is very neutron deficient, when the binding energies are unusually high for neutrons and low for charged particles, neutron emission dominates over that for protons and $\alpha$ particles. The competition between neutron decay and fission is illustrated in Fig. 2.1. Typical excitation energies in the compound nucleus range from 50 MeV to over 100 MeV, so that there is the possibility of four or more neutrons being emitted before a particle-stable evaporation residue (ER) is reached. Fission can compete with neutron emission at each stage, from the compound nucleus (first-chance fission) or after the emission of $x - 1$ neutrons ($x$th-chance fission).

As will be seen later, the unambiguous interpretation of fission measurements is far from easy. Consequently, many different and independent studies of a given system should be made if there is to be any hope of real physical insight. In addition, systematic in-depth studies of a wide range of nuclei would be very valuable. A wide variety of measurements is possible and should be carried out as functions of bom-

 0090-4759/90/040349-35$04.00  

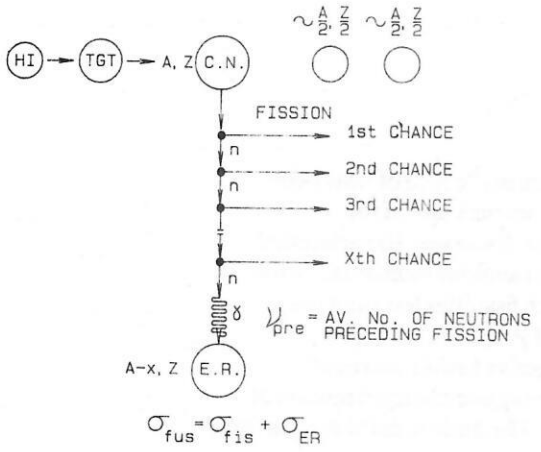


FIG. 2.1. Illustration of a heavy-ion induced reaction leading to fission and neutron decay.

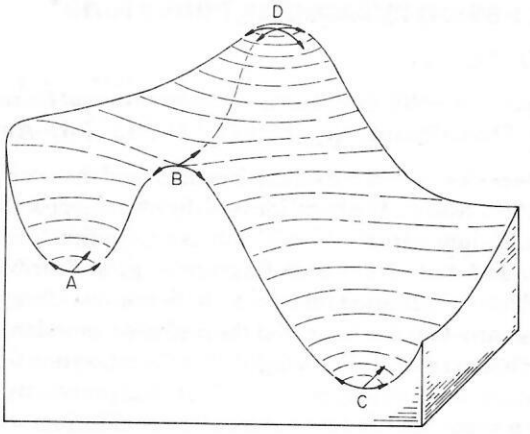


FIG. 2.2. Sketch of a two-dimensional potential-energy surface illustrating different types of equilibrium points. The hollow $A$ is a metastable minimum separated from the "absolute" minimum $C$ by a saddle point $B$ with one degree of instability. The mountain top $D$ has two degrees of instability (from Co 74).

barding energy (angular momentum). Some of the more important are: (i) fission cross sections $\sigma_{\text{fis}}$; (ii) $\sigma_{\text{ER}}$; (iii) average number of particles preceding fission, $\nu_{\text{pre}}$, $\pi_{\text{pre}}$, and $\alpha_{\text{pre}}$; (iv) angular distributions and correlations of fission fragments; (v) mass and charge distributions of fission fragments; (vi) kinetic-energy distributions of fission fragments; (vii) gamma-ray multiplicities from decay of fragments; (viii) statistical giant-dipole $\gamma$ rays correlated with fission.

### 2.1. The fission barrier

Although all naturally occurring nuclei with $A > 92$ are unstable to decay by fission, such decay is only observed in the heaviest of them and even then only with very long half-life, e.g., $\sim 10^{16}$ yr for $^{238}$U. To undergo fission the nucleus must first stretch out from its initially roughly spherical shape, then assume a necked-in shape, and finally at scission separate into two roughly equal fragments. A potential barrier exists between these initial and final states. Because of the large masses of the two fragments the process is almost classical and the probability of tunneling through the barrier is almost negligibly small; hence the long half-lives for spontaneous fission. To properly map the nuclear potential surface is a complex process and requires a many-parameter description. A relatively simple approximation, which may be appropriate at temperatures high enough to wash out shell effects, is the liquid-drop model (LDM); the nucleus is viewed as a classical charged liquid drop with a sharp surface. The surface energy of the drop ($\propto A^{2/3}$) favors the spherical shape, whereas the (repulsive) Coulomb energy ($\propto Z^2/A^{1/3}$) tends to disrupt the drop. The fissility parameter is defined as

$$x = E_C^0/2E_S^0 = [50.883\,(1 - 1{,}7826\,I^2)]^{-1}\,Z^2/A, \quad (2.1)$$

where $E_C^0$ and $E_S^0$ are the Coulomb and surface energies of a spherical drop, and $I = (N - Z)/A$. When $x = 1$, the drop is completely unstable against small quadrupole deformations and the fission barrier vanishes.

The top of the barrier is an equilibrium point (albeit unstable) on the nuclear potential surface. On a two-parameter representation of the surface, the barrier is at the top of a pass through a mountain range and hence is called the saddle point. This is illustrated in Fig. 2.2, which shows four types of equilibrium points. Of course, there are different fission barriers corresponding to different mass asymmetries. For $x > 0.396$ the lowest of these corresponds to mass symmetry and hence, as observed, symmetric fission is favored. However, this is not the case for $x \leqslant 0.396$ (the Businaro–Gallone point). The height of the barrier $E_f$ is the difference between the energy of the saddle point and that of the stable equilibrium shape (spherical in this model); it is a function of $x$ only. The shape corresponding to the saddle point is a sphere for $x = 1$ and for decreasing $x$ passes successively through shapes corresponding roughly to ellipsoids of revolution, necked-in symmetric dumbbell-type shapes, and ending in two touching spheres for $x = 0$ (see Fig. 2.3).

The simple liquid-drop model is not applicable to heavy-ion induced fission because of the high angular momenta involved. The effect of angular momentum is to reduce the fission barrier, as might be expected from the effect of the centrifugal force. It also moves the Businaro–Gallone point to lower values of $x$ (Mo 75). The barrier is the difference in energy between the rotating equilibrium and saddle-point shapes. Assuming that these shapes are independent of

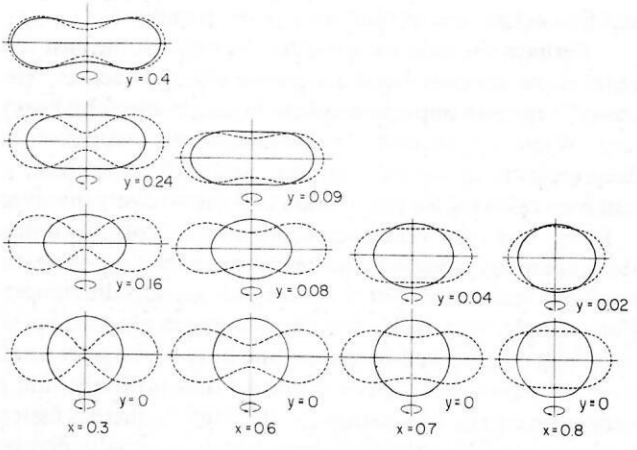


FIG. 2.3. Equilibrium (full) and saddle-point shapes (dashed lines), for various values of the parameters $x$ and $y$, calculated from the RLDM (from Bl 82).

angular momentum, this difference is

$$E_f(J) = E_f(0) + \frac{\hbar^2}{2\mathcal{J}_{\text{sad}}} J(J+1) - \frac{\hbar^2}{2\mathcal{J}_{\text{eq}}} J(J+1), \quad (2.2)$$

where $\mathcal{J}_{\text{sad}}$ and $\mathcal{J}_{\text{eq}}$ are the moments of inertia for the saddle point and equilibrium shapes. Since $\mathcal{J}_{\text{sad}} > \mathcal{J}_{\text{eq}}$, $E_f(J)$ falls with increasing $J$. In a classical paper Cohen, Plasil, and Swiatecki (Co 74) introduced the rotating liquid-drop model (RLDM) which does take account of angular momentum. Since rotation tends to disrupt the nucleus in a similar though not identical, way to Coulomb repulsion, it is natural to introduce another "fissility" parameter

$$y = E_R^0/E_S^0 = \frac{1{,}9249}{(1-1{,}7826I^2)} \frac{J^2}{A^{7/3}}, \quad (2.3)$$

where $E_R^0$ is the rotational energy of a spherical nucleus with angular momentum $J\hbar$. The potential-energy surface and the height of the fission barrier $E_f(J)$ are functions of $x$ and $y$ only. Shapes corresponding to equilibrium and saddle point for various values of $x$ and $y$ are shown in Fig. 2.3. For low angular momenta the equilibrium shapes are approximately oblate spheroids (Hiskes shapes). However, if $x < 0.73$ (Si 86), and above a critical value $y_{\text{I}}$, the Hiskes shapes become higher in energy than triaxial, approximately ellipsoidal shapes rotating about the shortest axis. As $y_{\text{I}}$ is exceeded these shapes rapidly achieve an approximately axially-symmetric prolate configuration rotating about an axis perpendicular to the "symmetry" axis and with large deformation. These are known as Beringer–Knox shapes. The saddle-point configurations are also usually slightly triaxial and prolate and are known as Pik–Pichak shapes. At $y_{\text{II}}$ when the fission barrier becomes zero, the equilibrium and saddle shapes coincide. For $x > 0.73$ the triaxial Beringer–Knox configurations never become lower in energy than the oblate Hiskes shapes. As seen in Fig. 2.3, the effect of increasing rotation on the saddle-point shapes is somewhat similar to that of increasing $x$ in that the neck radius increases and (except for lower values of $x$) the maximum elongation decreases.

Clearly, approximating the nucleus by a liquid drop with a sharp surface is rather extreme. Mustafa *et al.* (Mu 82) have introduced a modified rotating liquid-drop model (RFRM) which includes the Yukawa-plus-exponential folding function introduced by Krappe *et al.* (Kr 79) to account for the finite range of the nuclear force and the finite surface thickness. This has since been improved by Sierk (Si 86), who used more elaborate computing techniques, better modeling of the nuclear shapes, and improved parameters than for the RLDM. In addition he has made accurate global approximations to the calculated results for $E_f(J)$ and saddle-point moments of inertia for any measurable nucleus with $20 \leqslant Z \leqslant 100$. These can be incorporated in other computer codes, such as statistical-model codes, where these quantities are required. This global approximation is of great value, since individual calculations take considerable time even on a supercomputer. Fission barrier heights as functions of $J$ calculated by Sierk are shown in Fig. 2.4, while the critical angular momenta $J_{\text{I}}$ and $J_{\text{II}}$ corresponding to $y_{\text{I}}$ and $y_{\text{II}}$ are shown in Fig. 2.5, for both the RLDM and the RFRM, as functions of $A$. A general result of including finite-range effects is to reduce the fission barriers for $A \leqslant 200$ over those for the RLDM (see Fig. 2.5). This is in agreement

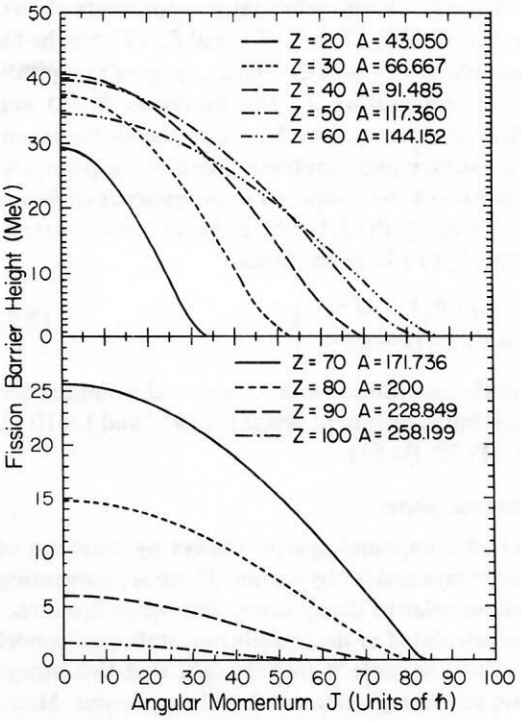


FIG. 2.4. Fission barrier heights as a function of $J$ for various $\beta$-stable nuclei, calculated with the RFRM (from Si 86).

with a number of experimental data (Be 77, An 79, Pl 80, Oe 80, Bl 82, Si 82, Hi 82, Bl 82a, Pl 82, Hi 83, Be 83, Pl 83, Pl 84, Le 86). There are also slight modifications to the saddle-point shapes and related moments of inertia and an increase in the Businaro-Gallone point to about $x = 0.48$ for $J = 0$.

The RLDM and RFRM calculations are essentially made for nuclei at zero temperature, since the parameters in the models such as surface energy are based on fits to ground-state masses. By analogy with classical systems one would expect that the effect of increasing temperature would be to increase the mean radius of the system and to decrease the free surface energy, thus reducing the fission barrier.

In the liquid-drop parametrization of Nix (Ni 69) the fission barrier, which is the free energy of deformation at the saddle point, is given by (Ha 73, Sa 76, Pi 82)

$$F_f(y_T, T) = [B_S(y_T) - 1]F_S(T) + [B_C(y_T) - 1]E_C(T), \quad (2.4)$$

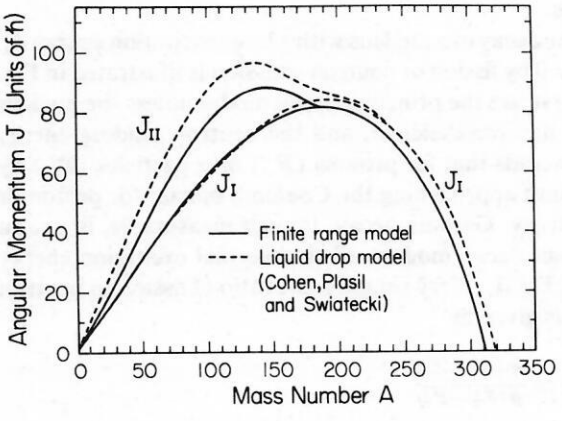


FIG. 2.5. Critical angular momenta $J_{\text{I}}$ and $J_{\text{II}}$ as a function of $A$ for $\beta$-stable nuclei, calculated with the RLDM and RFRM (from Si 86).

where $y_T = 1 - x(T)$ is the deformation coordinate of Nix, and $x(T) = E_C(T)/2F_S(T)$, $F_S(T)$, and $E_C(T)$ are the fissility, free surface energy, and Coulomb energy of the spherical nucleus at temperature $T$. The functions $B_S(y)$ and $B_C(y)$, which are tabulated by Nix, give the shape dependence of the surface and Coulomb energies, respectively. Some calculations of the temperature dependence of fission barriers (Ha 73, Sa 76, Pi 82, Ba 85) indicate that the quantities $F_s(T)$ and $E_c(T)$ have the forms

$$\left.\begin{aligned} F_S(T) &= E_S(0)[1-\beta T^2], \\ E_C(T) &= E_C(0)[1-\alpha T^2]. \end{aligned}\right\} \qquad (2.5)$$

The values of the quantities $\alpha$ and $\beta$ are probably not certain at the moment but appear to be about $1\times10^{-3}$ and $1\times10^{-2}$, respectively (Pi 82, Ba 85).

### 2.2. The statistical model

An excited compound system decays by emission of particles, and $\gamma$ rays and/or by fission. These are competing processes whose relative decay rates, and hence cross sections, can be calculated in the equilibrium statistical-model framework. Until recently it was thought that this model was adequate to treat phenomena involving fission. However, experimental data (Ch 70, Fr 75, Ga 81, Ho 83, Za 86, Hi 86, Ga 86, Ga 87, Hi 88, Hi 89a, Ne 88, Ro 89) suggest that dynamical effects should be included.

The principal assumptions of the model are that all significant degrees of freedom of the nucleus are in thermal equilibrium and that the fission decay rate is equal to the transition rate at the saddle point (transition state) as postulated by Bohr and Wheeler (Bo 39). The latter assumption is equivalent to saying that if the saddle point is passed, by however little, the nucleus always proceeds on to fission. The standard expressions used in statistical-model calculations are based on the Hausser–Feshback formulas (Ha 52). There are theoretical difficulties in applying these to heavy-ion reactions (Ma 79), although they appear to "work well" in practice for the widths $\Gamma_p$ for particle decay. Improvements have been proposed by Karmayan (Ka 78) and by Swiatecki (Sw 83), who suggests that particle decay should be treated instead by the transition-state method as for fission. So far these have been included in statistical-model calculations. The details of the statistical model have been well covered by many authors; see, for example Fe 60, Th 68, Vo 68, Va 73, Gr 76, Ma 79, Ha 52, De 82, Sto 85. Here a very simplifed approach is used only to make clear a number of features.

The decay of a nucleus with a large excitation energy $E_x$ and $J = 0$ by fission or neutron emission is illustrated in Fig. 2.6. These are the principal decay modes unless the nucleus is very neutron-deficient, and the neutron binding energy ($B_\nu$) exceeds that for protons ($B_\pi$) or $\alpha$ particles ($B_\alpha$) by an amount approaching the Coulomb barrier for proton or alpha decay. Gamma decay, though measurable, is not an important decay mode until the thermal excitation energy approaches $B_\nu$. Very roughly, the ratio of fission to neutron widths is given by

$$\frac{\Gamma_f}{\Gamma_\nu} \simeq \frac{\rho(E_x - E_f)}{\rho(E_x - B_\nu)}$$

$$\simeq \exp\{2[\sqrt{a_f(E_x-E_f)} - \sqrt{a_\nu(E_x-B_\nu)}]\}. \qquad (2.6)$$

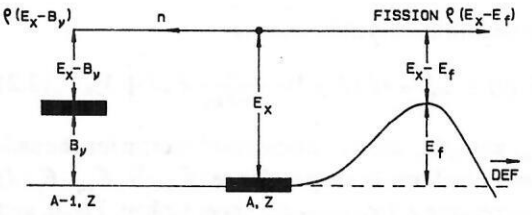


FIG. 2.6. Decay of an excited nucleus by fission or neutron emission. Maximum excitation energies in the nucleus following neutron decay and at the saddle point are shown. The curve on the right is a schematic illustration of the fission barrier as a function of deformation.

Here we have assumed the level density to be given by the simple expression $\rho(E) \propto \exp(2\sqrt{aE})$. The level-density parameters correspond to those at the saddle point ($a_f$) and in the nucleus to which neutron decay occurs ($a_\nu$). The value for $a_\nu$ is usually chosen to be in the range $(A/7.5)$–$(A/10)$, while $a_f/a_\nu$ is usually taken to be unity or to slightly exceed unity. For high excitation energy, $E_x \gg E_f, B_\nu$; hence Eq. (2.6) can be approximated as

$$\frac{\Gamma_f}{\Gamma_\nu} \simeq \exp\left\{2\sqrt{a_\nu E_x}\left[\left(\sqrt{\frac{a_f}{a_\nu}} - 1\right) - \frac{1}{2E_x}\left(E_f\sqrt{\frac{a_f}{a_\nu}} - B_\nu\right)\right]\right\}. \qquad (2.7)$$

From this one can see that the most important parameters are $a_f/a_\nu$ and $E_f$, since $B_\nu$ usually can be obtained either from measured masses (at lower $E_x$) or from semi-empirical liquid-drop masses at higher $E_x$, where shell and pairing effects are expected to be unimportant.

If we take $a_f/a_\nu = 1$, Eq. (2.7) becomes

$$\frac{\Gamma_f}{\Gamma_\nu} \simeq \exp\left[\sqrt{\frac{a_\nu}{E_x}}(B_\nu - E_f)\right]. \qquad (2.8)$$

From this it follows that:

(i) $\Gamma_f/\Gamma_\nu \leqslant 1$ when $B_\nu < E_f$ and $\Gamma_f/\Gamma_\nu \geqslant 1$ when $B_\nu > E_f$;

(ii) $\Gamma_f/\Gamma_\nu$ *decreases* with decreasing $E_x$ if $E_f > B_\nu$, with the consequence (see Fig. 2.1) that $\nu_{\text{pre}}$ is small;

(iii) $\Gamma_f/\Gamma_\nu$ *increases* with decreasing $E_x$ if $E_f < B_\nu$, giving larger values for $\nu_{\text{pre}}$ provided that $\Gamma_f/\Gamma_\nu$ does not become very large compared with unity;

(iv) when $\Gamma_f/\Gamma_\nu \gg 1$, $\nu_{\text{pre}}$ again becomes small, since nearly all of the population leads to first-chance fission and little is left for higher-chance fission.

Heavy ions bring in increasing angular momentum, with consequent lower values of $E_f(J)$, as the bombarding energy increases. Hence from (i)–(iv) above it follows that the statistical model predicts that $\nu_{\text{pre}}$ will be small at low and high bombarding energies with a maximum in between (see Fig. 2.7). As will be seen later, this prediction is incorrect.

Realistic calculations require the use of a massive computer code to carry out computations over all $J$, energies of outgoing neutrons, protons, alphas, gamma rays, fission fragments, etc. Nevertheless the qualitative results in (i)–(iv) are generally borne out by the detailed calculations. Codes which are commonly used at the present time are ALERT1 (Bl 81, Bl 82, Bl 82b), CASCADE (Pu 77), GROGIF (De 77), and PACE2 (Ga 80). The latter, in contrast to the others, which are "grid calculations," is a Monte-

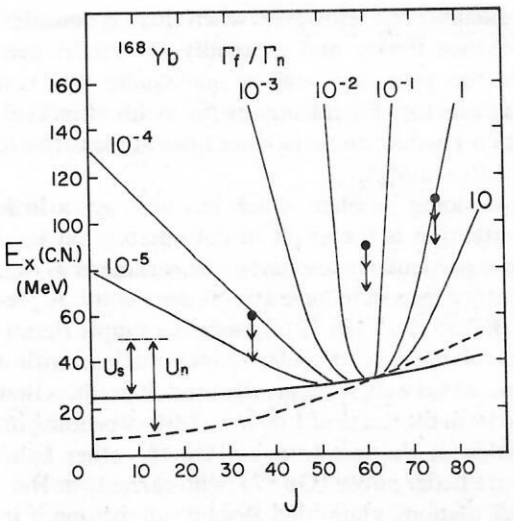


FIG. 2.7. Contours of $\Gamma_f/\Gamma_n$ as a function of excitation energy and $J$ for $^{168}$Yb. The energies of the rotating saddle-point shape (thick line) and rotating equilibrium shape plus $B_n$ (dashed line) are shown. Thermal excitation energies at the saddle point ($U_s$) and in the nucleus following neutron decay ($U_n$) are indicated for a low value of $E_x$ (and $J$). The filled circles indicate typical values of $E_x$ and $J$ for nuclei formed in the $^{18}O + ^{150}Sm$ reaction, and the vertical arrows show the energy carried away in neutron emission. The nuclei formed with $J = 35$, 60, and 75 correspond, respectively, to the cases (ii), (iii), and (iv) discussed in the text (from Hi 86).

Carlo code. It has the advantage that it is possible to follow particular decay sequences in detail, but the results usually involve non-negligible statistical errors, particularly for the weaker decay modes. An earlier, simpler and quicker running code, ALICE (Bl 76, Pl 78), is now only used for qualitative orientation purposes.

### 2.3. Inputs to statistical-model codes

Quite apart from the validity of the basic assumptions of the equilibrium statistical model, a variety of assumptions and approximations are involved in statistical-model codes. Earlier versions of the codes incorporated the RLDM to give values for $E_f(J)$ and the yrast line (an yrast state is the state of lowest energy for a given $J$). These values of $E_f(J)$ could be multiplied by an arbitrary factor $k_f$ or adjusted by a constant amount $\Delta_f$, both independent of $J$ (Bl 82), to get better fits to experiment. The RLDM values have now mostly been replaced by those from the global approximation to the more realistic RFRM (Si 86); it is still convenient to retain a multiplying factor $k_f$ to check for possible inaccuracies in the RFRM values for $E_f(J)$.

#### *2.3.1. Level densities*

The branching ratios in the statistical model depend strongly on level densities [Eq. (2.6)]. Unfortunately, our knowledge of these is still very poor, except at excitation energies which are very low or just above the neutron threshold, where individual levels can be indentified and counted. Above about 8 MeV and for high angular momenta the information is indirect and not very definitive. A number of reviews and discussions of level densities both from a theoretical and experimental point of view are available (Er 60, Bo 69, Ga 72, Hu 72, Da 80, Ig 85). The task of calculating, for every nucleus of interest, level densities as functions of excitation energy and angular momentum is a formidable one, even with present computers. Because of this it has been customary in statistical codes to mainly use very simple models whose parameters are adjusted to give "agreement with experiment." That normally used for higher or all excitation energies is the so-called Fermi-gas model. Strictly speaking it is not the Fermi-gas model but rather the equidistant model, since it refers to a system with equally spaced single-particle levels; in a Fermi gas the single-particle level density increases as the square root of particle kinetic energy. Nevertheless it represents a good approximation to the Fermi-gas model in the region of interest for heavy-ion induced fission ($E_x$ up to $\sim 100$ MeV) because the corresponding nuclear temperatures of a few MeV are small compared with the Fermi energy of $\sim 37$ MeV.

The level-density formula from the equidistant model for a given angular momentum and both parities is (Bo 69)

$$\rho(U, J) = \frac{(2J+1)\, a^{1/2}}{12} \left(\frac{\hbar^2}{2\mathcal{I}}\right)^{3/2} \frac{\exp\left[2\,(aU)^{1/2}\right]}{U^2}, \qquad (2.9)$$

where $U = E_x - E_{\rm rot}$ is the thermal excitation energy, and $E_{\rm rot} = (\hbar^2/2\mathcal{I})J(J+1)$ may be interpreted as the excitation energy tied up in collective rotation. In most statistical-model codes $E_{\rm rot}$, which defines the yrast line, is derived either from the RLDM or from the RFRM. The quantity $\mathcal{I}$ is related to the mean-square single-particle angular-momentum projection $\langle m^2\rangle$ by $\mathcal{I} = \hbar^2 g\langle m^2\rangle$ and is the rigid-body moment of inertia for the nucleus. The level-density parameter $a$ is related to the single-particle level density $g$ by $a = \pi^2 g/6$. Applying to a real nucleus, $g$ should be taken as the sum of the neutron and proton single-particle level densities at the Fermi surface. Two temperatures are commonly defined. The nuclear temperature $T$ for a given $J$ is given by

$$\frac{1}{T} = \frac{d\,(\ln\omega)}{dU} = \left(\frac{a}{U}\right)^{1/2} - \frac{5}{4U}, \qquad (2.10)$$

where $\omega$ is the density of states (each level has $2J+1$ degenerate magnetic substates). The thermodynamic temperature $t$ is defined by

$$t = \frac{dS}{dU} = \left(\frac{U}{a}\right)^{1/2}, \qquad (2.11)$$

where $S$ is the entropy. These two temperatures become essentially equal when $aU \gg 1$; this occurs at modest excitation energies for medium and heavy nuclei, where $a$ may typically have a value of $\sim 20$ MeV$^{-1}$. Sometimes for low $U$ a constant-temperature form,

$$\rho(U) = C \exp\left(\frac{2U}{T}\right). \qquad (2.12)$$

better describes the level density. Some authors (Gi 65, Ig 75, Pu 77, Re 81) use composite formulas, for example, matching an expression similar to Eq. (2.12) at low $U$ to that of the equidistant model at higher $U$.

The temperature $T$ roughly defines the region around the Fermi surface where the single-particle levels are either partially filled or partially empty, i.e., it defines the number $n$ of single-particle levels which contribute to the level density. Hence $n \cong gT$, which is a small number. For example, with $a = A/8$ MeV$^{-1}$, $A = 160$, and $U = 20$ MeV, we have $n \approx 13$, whereas $\rho \approx 10^{12}$ MeV$^{-1}$. The nuclear single-particle levels are not equidistant but are stongly bunched, giving rise to the well known shell structure. As a consequence we may expect variations of $g$ and $a$ as the Fermi surface of different

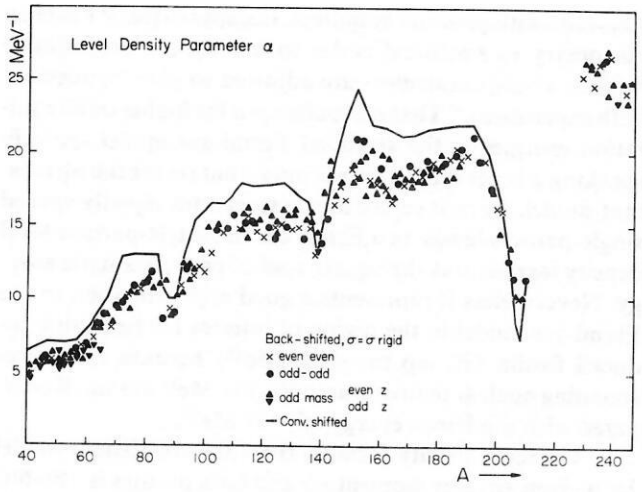


FIG. 2.8. Level-density parameter $a$ as a function of mass number, deduced from the back-shifted model (symbols). The line represents the average result from the conventional shifted model (from Di 73).

nuclei moves through regions of low single-particle level densities near closed shells to high densities in midshell nuclei. This effect is larger, the smaller the value of $n$, i.e., the smaller the value of $T$. At the neutron threshold ($U \approx 8$ MeV) the effect is very pronounced, as seen in Fig. 2.8. At higher excitation energies the variation of $g$ and $a$ with nucleon number is expected to wash out. It has been shown in the case of *periodic* single-particle level schemes, which approximate shell structure, that the equidistant-model formula (2.9) becomes valid at *high excitation energies* provided that $U$ is replaced by an effective value $U - \Delta E$ (Ka 66, Ka 69, Ba 70). The energy shift $\Delta E$ depends on the location of the Fermi level with respect to the periodic structure; it has positive values near closed shells and negative midshell. Since shell structure is nonperiodic, this procedure is not strictly correct and hence $\Delta E$ is not indpendent of $U$ or of $J$.

The pairing interaction reduces the level density at low excitation energy because of blocking of levels near the Fermi surface. However, pairing is weakened and finally destroyed by temperature and angular momentum. After the pairing has broken down the equidistant model is again applicable but an energy shift has to be applied; typical shifts which have been applied are $2\Delta$ for doubly even nuclei, $\Delta$ for odd-mass nuclei, and 0 for odd–odd nuclei, with $\Delta \approx 12/A^{1/2}$ MeV. An alternative formulation in terms of a temperature-dependent parameter $a(T)$ has been recently given (Ci 85, Ba 87).

At high excitation energies and angular momenta, where shell and pairing effects are expected to wash out, it seems appropriate to use liquid-drop masses and binding energies rather than those for the ground states. If this is done, it is no longer necessary to apply the shift $\Delta E$ arising from shell structure. This procedure is usually adopted for statistical analysis of heavy-ion induced fission. The most frequently used liquid-drop masses are those of Myers and Swiatecki (My 67), though the Myers droplet parametrization with the Wigner term (My 77) has also been used for this purpose and claimed to be an improvement (Le 86). Insofar as fission takes place at high values of $U$, the procedure of using liquid-drop masses and the equidistant model may be a reasonable one. However, when there is considerable multi-chance fission and especially for nuclei near closed shells, this procedure may be inadequate. Nor is it likely to be satisfactory for calculating the yields of individual evaporation-residue products, since these are sensitive to low values of $U(\sim 8$ MeV).

A long-standing problem which has been given little theoretical attention is the effect of deformation on level density. This is particularly relevant to the parameter $a_f/a_\nu$, which is usually assumed to have a value near unity. A prescription of Bishop *et al.* (Bi 72), based on a simple Fermi-gas model involving a rectangular-shaped nucleus with a trapezoidal potential well, is frequently used. It predicts that $a_f/a_\nu$ should be in the range of 1.00 to $\sim 1.04$, depending on the deformation at the saddle point. On the other hand Gottschalk and Ledergerber (Go 77), who carried out Hartree–Fock calculations, claim that Bishop's derivation is in error and that $a_f/a_\nu$ should have a value of $\sim 0.98$. Carjan *et al.* (Ca 79), who carried out microscropic calculations based on a realistic set of single-particle levels, conclude that $a_f/a_\nu$ should have a value of $\sim 1.065$ for $^{194}$Hg at high excitation energy. Recently Bertsch (Be 80) has considered the question of level density as a function of shape but has not addressed the specific problem of $a_f a_\nu$. Toke and Swiatecki (To 81) have considered surface-area and curvature corrections to the level density of a diffuse Fermi gas, leading to values of $a_f/a_\nu > 1.1$ for fissility $x \lesssim 0.7$.

Another uncertainty in level densities is the effect of collective levels, rotations and vibrations; it may have a special reference to the value of $a_f/a_\nu$. It is well known that at low excitation energies level densities are considerably enhanced, especially in deformed nuclei, by the presence of these levels, which of course appear at the expense of higher-lying excitations. Rotational enhancement factors of the order of $10^2$ can occur. Questions which arise are: (i) How high in excitation energy do collective levels need to be taken into account? (ii) Is it necessary to take account of the missing levels at high excitation energy? (iii) What happens in the transition region? The first question was addressed by Bjornholm *et al.* (Bj 73), who estimated that the transition temperature would be $\sim 41 A^{-1/3}|\delta|$ MeV, where $\delta$ is a deformation parameter. This estimate was confirmed by more detailed calculations on the basis of the SU3 model by Hansen and Jensen (Ha 83). For $A \sim 150$–$200$ and RLDM equilibrium states $\delta \sim -0.04$, whereas for deformed nuclei in their ground states and nuclei at the saddle point $\delta \sim 0.25$ and 1.0, respectively. The transition temperatues for these cases are therefore about 0.3, 1.8, and 7 MeV, respectively, implying corresponding excitation energies around 2, 60, and 1000 MeV. The value of $\sim 60$ MeV for deformed nuclei is comparable with that calculated by Moretto (Mo 72) for washing out of the shell effects which cause the deformation.

Vigdor and Karwowski (Vi 82) have discussed the effects which the presence of the collective enhancement and its decay with increasing temperature may have in statistical-model calculations. In particular they argue that the average deformation for a highly excited nucleus is not at the minimum of the RLDM potential. It is rather at some large prolate deformation in between those of the spherical and saddle-point shapes. At this deformation the level density as a function of deformation is a maximum, the increase due to rotational enhancement more than offsetting the decrease

arising from increased shape potential-energy. If this were not the case, the absence of collective enhancement at the RLDM equilibrium point and full enhancement at the saddle point would have a profound effect on $\Gamma_f/\Gamma_\nu$. Schmidt *et al.* (Sc 84) have considered the effects of this temperature-induced deformation on the washing out of spherical shell effects in nuclear level densities.

Experimental evidence on the value of the level-density parameter at high excitation energy and angular momentum is scarce. In principle values may be deduced from the shapes of particle evaporation spectra, but sequential decay makes interpretation difficult. A method which has recently been used to deduce values for $a$ is the study of statistical giant-dipole-resonance (GDR) $\gamma$ rays emitted by states of high excitation energy and spin (Ne 81). This method has the advantage over particle measurements that most of the $\gamma$ rays arise from the decay of the highest-energy states. A number of authors (Ki 87, Mu 88, Sn 86, St 88, To 86) have successfully fitted data with values of $A/a$ between $\sim 7$ and 12 MeV for initial excitation energies $< 100$ MeV. However, with the *assumption* that the GDR strength and energy agree with the ground-state values, $A/a$ appears to have a value of about $8 \pm 1$ MeV. Recent studies of the particle decay of systems with masses of $\sim 160$ (Ne 86) and $\sim 180$ (Hi 86a, Hi 87) suggest that $A/a$ varies from $\sim 8$–$9.5$ MeV at lower excitation energies ($T \leqslant 3$ MeV) to 10–13 MeV at energies of $\sim 400$ MeV, as shown in Fig. 2.9. A measurement with the Heidelberg crystal ball indicates a value of $8.8 \pm 1.3$ MeV for spin $\sim 52\hbar$ and low $T$ in $^{155}$Er (He 88). Theoretical calculations (Bo 87, Ha 86) are in qualitative agreement with this decrease of $a$ with excitation energy.

From this brief outline it is clear that there are still many uncertainties in level-density calculations. Fortunately only *relative* level densities are involved in the statistical model. Further, as one can see from Eq. (2.6), these ratios do not usually involve very large differences in excitation energies. If they did, the branching ratios such as $\Gamma_f/\Gamma_\nu$ would be either extremely small or extremely large, because of the very strong energy dependence of the level density, and hence of little experimental interest. Probably because of this, the sensitivity to the exact form of the level-density expression is not great, except in special cases, and it is often possible to fit fission excitation-functions rather well over extended ranges of bombarding energy. However, it should be always borne in mind that there are a variety of parameters coming into statistical-model calculations and that free adjustment of them may simply compensate for deficiencies in others, such as those involved in level-density formulas. It should also be appreciated that the transition-state model loses it validity when $T \geqslant E_f$ (Kr 40, St 73). Our knowledge of many of these other parameters has increased considerably in recent years and is continuing to do so. We may therefore hope that many of these uncertainties will be resolved or at least greatly reduced.

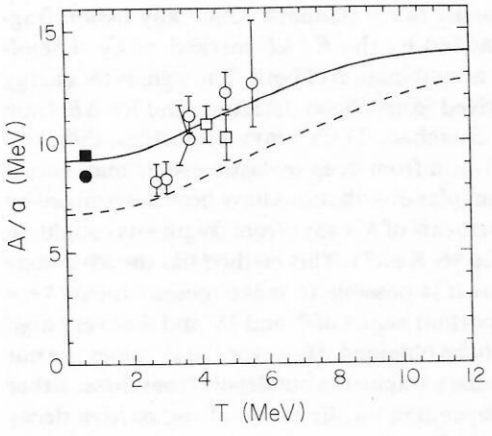


FIG. 2.9. Inverse level-density parameter as a function of $T$. Open squares and circles are, respectively, the results of Nebbia *et al.* (Ne 86) for $A \approx 160$, and of Hilscher *et al.* (Hi 86a, Hi 87) for $A \approx 180$. The filled circles and squares are mean values at low excitation energies, deduced by Dilg *et al.* (Di 73). The full and dashed lines are the results of theoretical calculations (Ha 86) (from Hi 87a).

### *2.3.2. Fusion cross sections and angular-momentum distributions*

Calculated fission cross sections are sensitive to $J$, particularly for light compound systems where $E_f(0) \gg B_\nu$. Hence they are sensitive both to the magnitude of $\sigma_{\text{fus}}$ and to the distribution assumed for the partial cross sections $\sigma_{\text{fus}}(L)$. Note that in statistical codes it is usual to take $J$ equal to the orbital angular-momentum quantum number $L$. This is a good approximation for high angular momenta.

Many recent measurements have shown that sub-barrier fusion cross sections show strong deviations from those predicted by simple one-dimensional Coulomb-barrier calculations. These deviations depend on the deformation or softness of projectile and target nuclei and on particle transfer between them; i.e., they are structure-dependent. Essentially there is a multidimensional barrier problem. For recent reviews of this subject, see Be 85, Be 86, Mo 85, Re 86, Re 86a, St 85a, St 86, Va 86. Although the deviations are probably understood qualitatively, a quantitative theoretical description is not yet available; even it it were, it would be very complex. It follows that it is necessary to *meaure* the fusion cross sections which are used as inputs to statistical-model calculations; it is not reliable to use a semi-empirical global fit, such as provided by the Bass model (Ba 77) even for light projectiles. For heavier projectiles and hence more symmetric systems dynamical effects have to be taken into account (Bj 82, Do 86, Si 86a, Sw 82, Bl 86). The fusion cross section is usually taken to be the sum of the fission and evaporation-residue cross sections.

Incomplete fusion (ICF) reactions occur when bombarding energies $E$ exceed a threshold velocity usually taken to be about 10 MeV/nucleon; they increase in probability as $E$ increases. Note, however, that Tserruya *et al.* (Ts 88) found that there is no threshold velocity for ICF reactions in three $^{12}$C-induced reactions (see Fig. 2.10). These reactions can involve pre-equilibrium (PE) emission of particles preferentially in the beam direction with much greater energies than expected from equilibrium emission. In another type of incomplete fusion reaction, sometimes known as massive transfer, only part of the lighter reactant is captured. A number of theoretical approaches, none entirely satisfactory, have been developed for these reactions. Hence ICF may result in some uncertainty in statistial-model analysis of fission data particularly when $E$ exceeds $\sim 10$ MeV/nucleon. Reviews and recent papers on this topic are given in Bl 85, Ch 86, Ge 82, Hi 87, Ra 87a, Sc 84a, Si 83, Ts 88, Vi 82a.

The angular-momentum distribution for fusion is also affected by the same factors which cause deviations in sub-

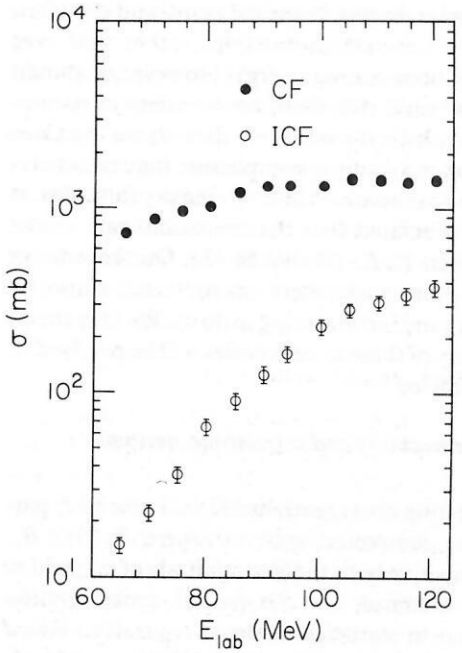


FIG. 2.10. Excitation functions for complete fusion (CF) and incomplete fusion (ICF), shown by closed and open circles, respectively, for the $^{12}C + ^{160}Gd$ reaction (from Ts 88).

barrier fusion cross sections. For example, it is obvious classical that the collision of a spherical projectile with a prolate target nucleus will result in a more smeared out angular-momentum distribution than the sharp cut-off distribution obtained with a spherical target. Further, the reaction will occur to lower energies with the deformed target because the Coulomb barrier is lower at the tips of the prolate shape than it is for the spherical target nucleus. However, the precise relationship between the form of $\sigma_{\rm fus}(L)$ and $\sigma_{\rm fus}$ is not yet clear. Early analyses used the sharp cut-off distribution, which is grossly inadequate for systems with low fissility. A later one (Hi 82) used the parabolic-barrier approximation together with a method due to Vaz and Alexander (Va 74) which took into account deformation. However, more recently it has become common to use the arbitrary Fermi-distribution expression (Ch 86a, Gi 85, Ha 85, Le 86, Ne 88, Pl 83, Va 83, Vi 82b)

$$\sigma_{\rm fus}(L) = \pi\lambda^2 (2L+1)\, T_L = \frac{\pi\lambda^2 (2L+1)}{1+\exp[(L-L_0)/\delta L]}\,, \qquad (2.13)$$

where $\delta L$ determines the diffuseness and $L_0$ is defined by the fusion cross section. There is no theoretical justification for this expression and, for example, the use of an expression with a Gaussian rather than an exponential-type falloff makes a significant difference for light systems such as $^{168}Yb$ (Ch 86a) (see Fig. 3.11). Further, there is no justification for taking $\delta L$ as independent of bombarding energy as is usually done. Simple fusion models such as the zero-point motion (ZPM) model (Es 81), which takes into account collective excitations of target and projectile, and also some recent measurements (Va 86a, Mu 86) indicate that it is a function of $E$ (Bo 88).

#### *2.3.3. Transmission coefficients*

From the method of detailed balance it can be shown that the width for emission of particle $p$ is given by (Ha 52)

$$\Gamma_p = \frac{1}{2\pi\rho(E_x)} \int_{\varepsilon_p=0}^{E_x-B_p} \rho(E_x - B_p - \varepsilon_p,\ J) \times \sum_{S=|j-s|}^{j+s} \sum_{L=|J-S|}^{J+S} T_L(\varepsilon_p)\, d\varepsilon_p, \qquad (2.14)$$

where $E_x$, $J$, and $B_p$ are the excitation energy, spin, and particle binding energy of the emitting nucleus, $\epsilon_p$ is the kinetic energy of the emitted particle, and $T_L$ is its transmission coefficient. The $T_L(\epsilon_p)$ refer to incoming particles with energy $\epsilon_p$ incident on a nucleus of excitation energy $E_x - B_p - \epsilon_p$. They cannot be measured experimentally, so that in statistical codes they are usually approximated by optical-model transmission coefficients $T_L^{\rm OM}(\epsilon_p)$ based on global fits to elastic scattering data. However, the $T_L^{\rm OM}(\epsilon_p)$ refer to particles scattered from nuclei in their ground states and also to the total reaction cross section and not the fusion cross section as they should. The latter may not involve serious error for the light particles ($A \leqslant 4$) which are the most important; see Mc 80 and Vi 82a for discussions of this topic. However, it is possible that the former may, since hot rotating nuclei are likely to be more diffuse and have different deformation to the ground state; see, for example, Refs. Ch 87, Th 88, where evidence is presented for strong deformation in hot rotating nuclei near $^{200}Pb$, and Ref. Br 88. This would have its greatest effect on charged particles rather than on neutrons, owing to reductions of the Coulomb barriers (Bl 80, Bl 81, Aj 86). There is experimental evidence for substantial barrier reductions (Al 82, La 87, Ra 87, Mo 87, Ne 86, Ri 82, Va 84) but the effect is not fully understood in detail. It is clear that the subject of the particle transmission coefficients needs more attention and understanding.

For fission, which is a much more classical process than light-particle emission because of the large reduced mass, it is usual to take the transmission coefficient as unity above the barrier and zero below it; this is probably an adequate approximation for heavy-ion induced fission.

## 3. EXPERIMENTAL DATA AND ANALYSIS

### 3.1. Experimental Methods

The experimental methods for measuring fission and evaporation-residue excitation functions and angular distributions are usually fairly standard. Generally fission fragments are identified by the $E/\Delta E$ method or by time-of-flight/$E$, or by a combination of both. The signals for energy are usually derived from silicon detectors, and for $\Delta E$ from gas ionization chambers. With heavy projectiles, difficulty in separating fission from deep-inelastic events may occur. In a few cases angular distributions have been determined by off-line measurements of $K$ x rays from fragments caught on catcher foils (Lu 86, Ke 87). This method has the advantage over others that it is possible to make measurements very close to the important angles of 0° and 18° and that very high $Z$ resolution can be obtained. However the $Z$ values are not those of the primary fragments but depart from these, either down or up, depending on the mode of radioactive decay (EC, $\beta^+$, or $\beta^-$). Evaporation residues can be identified by time of flight or with the aid of on-line mass separators.

The method used for measuring prefission neutrons may be less familiar. It takes advantage of the fact that the intensity of neutrons emitted from the fission fragments

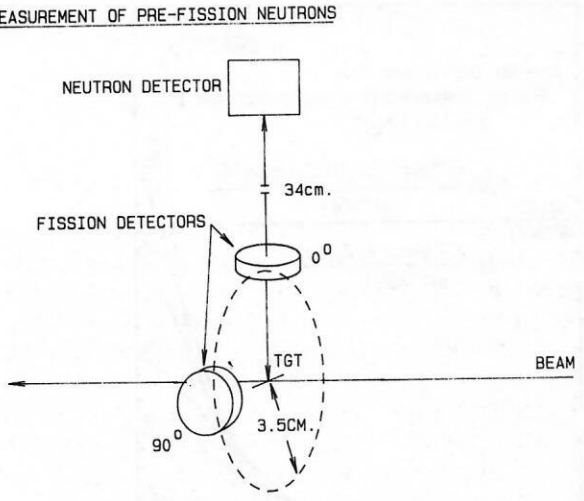


FIG. 3.1. Schematic illustration of prefission neutron measurements.

moving with comparable velocities is strongly correlated with the fragment direction, whereas those from the relatively slowly moving compound system are only weakly correlated with the beam direction. A schematic illustration of the method is given in Fig. 3.1. Coincidences are taken between neutrons and fission fragements, and the neutron time of flight is determined. Kinematic focusing ensures that the postfission neutron intensity in coincidence with the 0° fission detector is much greater than that with the 90° detector. The neutron velocity spectra may be analyzed into components $\nu_{pre}$ and $\nu_{post}$ by an iterative computer program; an example is shown in Fig. 3.2. In this analysis it is assumed that the neutrons are emitted either from the slowly moving compound system or from the *fully accelerated* fragments. This is not strictly correct, as some neutrons are emitted when the fragments are accelerating (Hi 84). Hence allowance must be made for this effect in comparing results

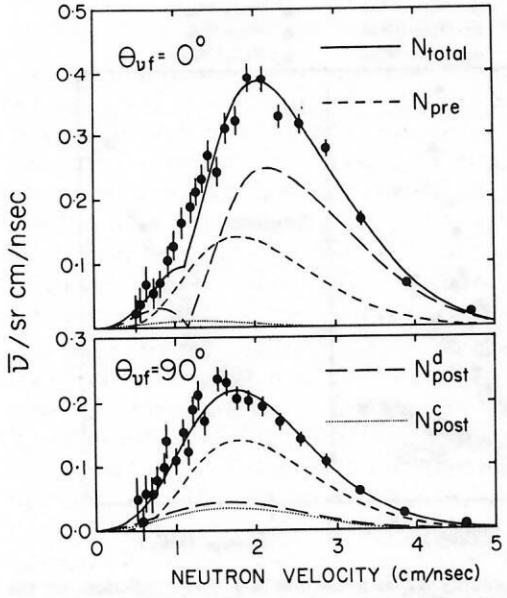


FIG. 3.2. Neutron velocity spectra at 0° and 90° to the direction of the fission-fragment detector for 115-MeV $^{19}$F on $^{159}$Tb. The deduced spectra for total, prefission, postfission detected fragment ($N^d_{post}$) and complementary fragment ($N^c_{post}$) are indicated (from Ne 88).

with those from the statistical model. The correction is minor except for very heavy systems such as $^{251}$Es (He 84), where the energy gain from saddle to scission is very large. Some authors (Ga 81, Ga 87, Ho 83), who have carried out measurements at high energies-per-nucleon above the Coulomb barriers, have used more complex arrangements and have not confined the detectors to the plane perpendicular to the beam direction. At these higher energies it is essential to carry out measurements at various angles to the beam direction so that the presence of PE-neutron emission may be identified and appropriately taken into account.

### 3.2. Fission-fragment angular distributions

The angular distributions are usually discussed in terms of transition-state theory. If rotating compound nuclei are formed in a reaction between particles of zero spin, their total angular-momentum vectors (**J**) lie in the plane perpendicular to the beam direction, i.e., $M = 0$ (Fig. 3.3a). A simple classical liquid-drop picture suggests that the nuclei fission in a plane perpendicular to **J**. Therefore if their lifetime is long compared with their rotational periods, the probability of their fissioning at angle $\theta$ to the beam direction is independent of $\theta$. Likewise it is independent of the aximuthal angle $\phi$, so that the probability of observing a fragment in $d\theta d\phi$ is $d\theta d\phi/2\pi^2$. Hence the angular distribution $W(\theta)$ is given by

$$W(\theta)\, d\Omega = W(\theta) \sin\theta d\theta d\phi = d\theta d\phi/2\pi^2, \qquad (3.1)$$

i.e., $W(\theta) \propto 1/\sin\theta$. Angular distributions approaching this form are seen for very large $J$, but are much less strongly peaked near $\theta = 0$ for smaller $J$.

There is no reason why the angular momentum along the fission axis should be zero; though collective rotation cannot take place around the nuclear symmetry axis (fission axis), angular momentum $K\hbar$ can be carried by intrinsic excitations. In this case the angular momentum $R\hbar$ which initiates the fission of the nuclear drop is no longer perpendicular to the beam axis, but tilted through an angle $\alpha \sim K/J$ (Fig. 3.3b). One consequence is that $W(\theta)$ is less sharply peaked than $1/\sin\theta$. Another is that the fission barrier is a function of $K$ as well as $J$. This effect, which should also be included in statistical-model calculations, does not seem to be of much importance (Pr 84). If the moments of inertia parallel and perpendicular to the fission axis are $\mathcal{J}_{\parallel}$ and $\mathcal{J}_{\perp}$, respective-

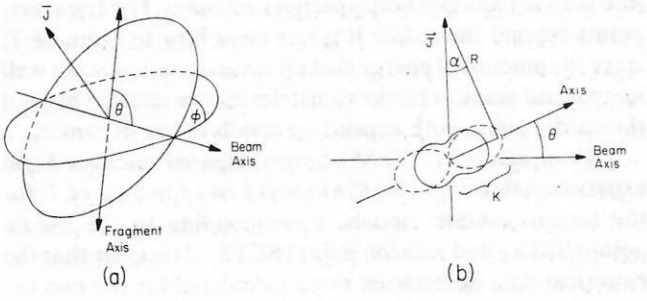


FIG. 3.3. (a) Illustration of nucleus fissioning perpendicular to **J** at angles $\theta$, $\phi$ to the beam axis. (b) Illustration of tilting of rotational and fragment axes due to an angular-momentum component $K\hbar$ along the nuclear symmetry axis. The forms represent the saddle (solid line) and scission (dashed line) point shapes.

ly, the rotational energy may be written

$$E_{\rm rot}(J,K) = \frac{\hbar^2}{2\mathscr{I}_\perp}(J^2-K^2) + \frac{\hbar^2}{2\mathscr{I}_\parallel}K^2$$
$$= \frac{\hbar^2}{2\mathscr{I}_\perp}J^2 + \frac{\hbar^2}{2\mathscr{I}_{\rm eff}}K^2, \qquad (3.2)$$

where

$$\mathscr{I}_{\rm eff}^{-1} = \mathscr{I}_\parallel^{-1} + \mathscr{I}_\perp^{-1} \qquad (3.3)$$

and is zero for a sphere. If the $K$ degree of freedom is equilibrated, then at temperature $T$ there is a distribution of $K$ values approximately proportional to $\exp[\hbar^2K^2/2\mathscr{I}_{\rm eff}T]$, i.e., a Gaussian distribution in $K$ centered on $K=0$ with variance

$$K_0^2 = T\mathscr{I}_{\rm eff}/\hbar^2. \qquad (3.4)$$

In order to calculate an angular distribution it is usual to assume that, at some transition point on the path to fission, the $K$ distribution is equilibrated and then frozen for the remainder of the path. The transition point has usually been chosen as the saddle point because this is a quasi-equilibrium point of the nuclear potential and because it used to be assumed that the transition time from saddle to scission ($\tau_{ss}$) was very short. Recent developments (see Sec. 3.5) suggest that $\tau_{ss} \sim 10^{-20}$ s, much longer than previously thought, while the relaxation time of the tilting mode is also thought to be $\sim 10^{-20}$ s (Bu 86, Do 86b, Lu 86). It is therefore possible that an effective transition point might lie between saddle and scission (Al 87, Fr 86) or, as an extreme possibility, at the scission point. It is also possible that in some cases $K$ does not become equilibrated at all.

If it is assumed that the separation axis coincides with the symmetry axis at scission, the form of the expression for the angular distribution is independent of where the transition point is located. For a particular value of $J$, the angular distribution depends only on the parameters $p = \hbar^2J^2/4\mathscr{I}_{\rm eff}T = (J/2K_0)^2$; the larger is $p$, the more nearly the angular distribution approximates $1/\sin\theta$. A complete angular distribution is obtained by an appropriately weighted average for all the $J$ contributing to fission; calculated examples are shown in Fig. 3.4. Of course, the values for $\mathscr{I}_{\rm eff}$ and $T$ do depend on the location of the transition point and on $J$. It is possible to estimate $\mathscr{I}_{\rm eff}$ at the saddle point from the RLDM or RFRM, or at scission if assumptions are made about the shape (see, e.g., Fig. 3.3b). Clearly $\mathscr{I}_{\rm eff}$ decreases as the effective transition point moves towards the scission point. The temperature $T$ at the saddle point can be estimated from the thermal excitation energy there, having taken into account any presaddle particle emission. For transition points beyond the saddle it is less clear how to estimate $T$, since the amount of energy tied up in deformation is not well known and because further particles can be emitted beyond the saddle point; both depend on details of the dynamics.

Friefelder *et al.* (Fr 86) have compared calculated and experimental results (Ba 85a) for $K_0^2$ as a function of $T$ for the transition-state models, corresponding to the saddle point (SPTS) and scission point (SCTS). It is clear that the empirical data lie between those calculated for the two extreme models (Fig. 3.5). The SPTS model calculations show a large scatter because $\mathscr{I}_{\rm eff}$ depends strongly on $Z^2/A$ and $J$ at the saddle point (Fig. 2.3), whereas it does not at the scission point. While the scatter of the data conforms better

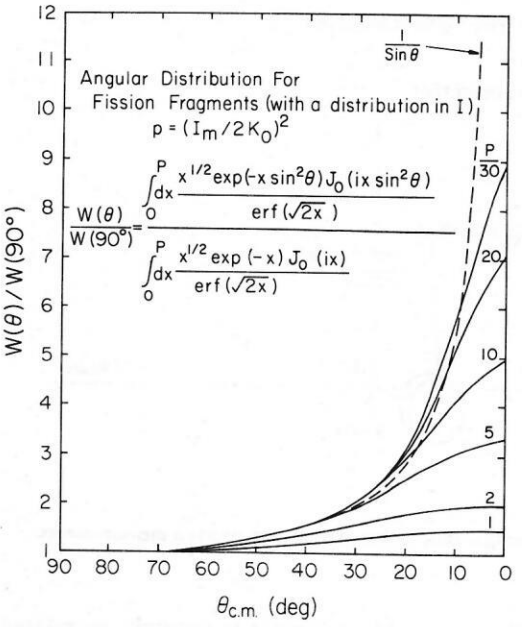


FIG. 3.4. Calculated angular distributions for fission fragments obtained by summing over the sharp cut-off angular-momentum distribution of $I$ from 0 to $I_m$ (from Va 83a).

to the SCTS calculations, they lie well above them. This suggests that, if $K$ equilibration has been achieved, the effective transition-state configurations must be less deformed than those at scission.

Generally speaking it appears that for reactions which do not involve large angular momenta and where the compound nuclei have temperatures much lower than the fission barrier, the SPTS model seems to give a reasonable description of fission angular distributions (Va 73, Va 86b). However, at higher spins the anisotropies remain roughly constant, whereas the SPTS model predicts that they should fall

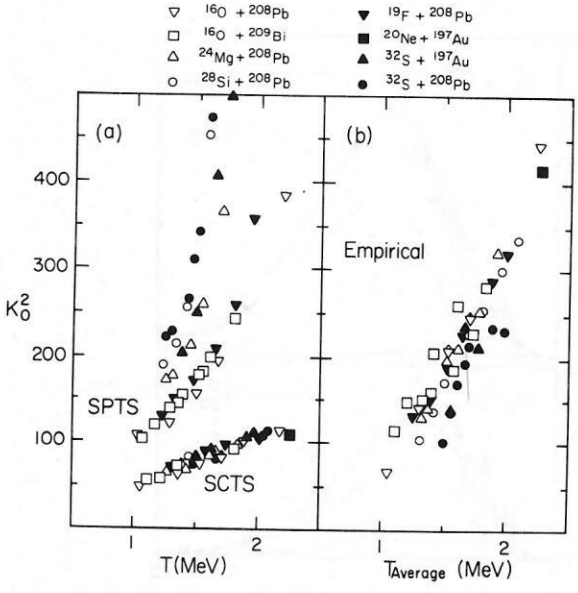


FIG. 3.5. The quantity $K_0^2$ as a function of $T$. (a) Predictions for the standard rigid-rotor saddle-point (SPTS) and scission-point (SCTS) models. (b) Experimental results for compound nuclei with $Z^2/A > 36$ and $J_{\rm rms} > 30$. Values of $T$ are averages calculated for the appropriate models (from Fr 86).

because of the nearly spherical shape of the saddle point when $E_f(J) \approx 0$, giving $\mathscr{I}_{\text{eff}}^{-1} \approx 0$ and $p \approx 0$. Of course this model loses its meaning when $E_f(J) = 0$ and is of doubtful validity even when $T > E_f(J)$ (Kr 40, St 73). The SCTS model gives larger anisotropies than are observed.

The recent observation of greater anisotropies than predicted by the SPTS model for reactions with high-energy heavy ions with $A \geqslant 20$ (Ba 81, Ba 83, Ba 85a, Ga 84a, Le 83, Ro 83, To 84, Ts 83, Ts 83a) has stirred up much interest and controversy. A number of authors have developed scission-point models (Bo 84, Go 87, Ro 84, Ro 86) based on a method suggested by Ericson (Er 60). These models contrast with the standard fission theory in that the separation direction is not limited to the symmetry axis at scission. Three-dimensional decay is allowed as in the statistical decay of light particles. While they give much better agreement than the SPTS for these systems, they do not describe the energy dependence correctly, as illustrated in Fig. 3.6. Alexander (Al 87) points out that there is some difficulty in understanding why "if at high excitation energy and spin, the emerging fission fragments have enough time and flexibility to achieve thermal equilibrium, even as late as scission and so thoroughly as to fill three dimensions, then why do they not have the time and flexibility to do so at low excitation and spin?"

Another approach (Ba 85a, Ba 85b, Ke 87, To 84) to the problem of large anisotropies at high angular momentum is based on the premise that the deviations for projectiles with $A > 20$ indicate that at least part of the "fission" cross section results from reactions which fail to produce completely fused systems inside the fission barrier. Nevertheless

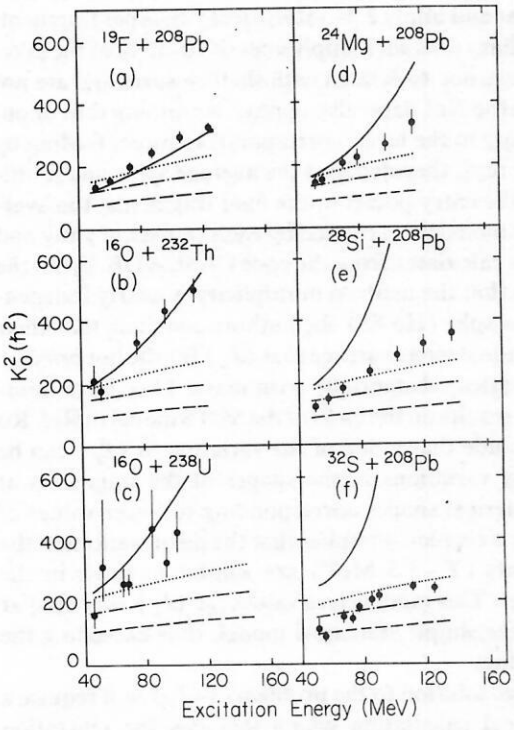


FIG. 3.6. Comparision of $K_0^2$ values, derived from the analysis of experimental fission anisotropies, with the prediction of the SPTS model (solid curves) and SCTS model (dashed curves) as a function of the excitation energy of the fissioning systems. The predictions of the scission-point models of Refs. Bo 84 and Ro 84 are represented by the dot–dash and dotted curves, respectively (from Ba 85a).

these direct reactions, which have been called quasifission (Bj 82, Sw 81) or fast fission (Bo 81, Le 79, Ng 86, Zh 84) are sufficiently slow that approximate equilibration of the mass-asymmetry and energy degrees of freedom is achieved.

This idea can be understood in terms of the extra-push model proposed by Swiatecki (Bj 82, Sw 82, Sw 84). In this it is assumed that the dynamical evolution of two colliding nuclei can be described by a sequence of shapes consisting of two charged spheres connected by conical neck. Classical equations of motion are used, and friction coefficients are taken from the one-body dissipation approach (Bl 78 and see Sec. 4). The two nuclei, represented by liquid drops with sharp edges, remains unchanged until they touch, when they reach the *contact configuration*; this is similar to the one associated with the Coulomb barrier. The neck degree of freedom then comes into play, and a *conditional saddle* configuration is defined as the one corresponding to the maximum of the potential energy with the *initial* mass asymmetry. The *unconditional saddle configuration* is the normal saddle point of the compound nucleus and corresponds in most cases to mass symmetry. If the energy in the initial system is sufficient to overcome the conditional saddle point, the frictional forces trap it, mass exchange occurs, and a mononucleus is formed; otherwise the nuclei rather quickly separate, roughly retaining their initial mass asymmetry (deep-inelastic-scattering). For systems formed with lighter projectiles it turns out that the contact configuration is more compact than the conditional saddle, in which case a mononucleus is formed immediately. For heavier projectiles an extra-push energy $E_{\text{ep}}$ in addition to the Coulomb barrier energy is required to overcome the conditional saddle, because it is now more compact than the contact configuration. Formation of a mononucleus does not necessarily mean that a compound nucleus is also formed; the normal saddle point has also to be overcome. To do this for heavy systems may require an even larger energy than $E_{\text{ep}}$, called the extra-extra-push energy $E_{\text{eep}}$ (Bl 86). If the energy above the Coulomb barrier lies between $E_{\text{ep}}$ and $E_{\text{eep}}$, the mononucleus may remain intact long enough so that approximate equilibration of the mass-asymmetry and energy degrees of freedom can occur, giving rise to the process of quasifission or fast fission. A similar but not identical model was developed in parallel by Gregoire *et al.* (Gr 82) and was reviewed by Ngô (Ng 86). See also Ref. Ge 86.

Experimentally, the predictions of this simple and physically appealing model are qualitatively borne out in practice (Ba 85b, Bo 82, To 85, Sh 87). It has been possible to show the noncompound nature of quasifission for heavy systems through the observation of left–right asymmetries in mass distributions at fixed scattering angle (Bo 82, To 85, Sh 87) and by forward–backward asymmetries in the angular lodistributions for fixed fragment mass or charge (Bu 86, Lu 85, Lu 86, Ke 87). An example of the latter is shown in Fig. 3.7; more symmetric divisions yield symmetry about 90°. From such data it is possible to estimate relaxation times for the tilting mode of $\sim (5\text{–}10) \times 10^{-21}$ s (Bu 86, Lu 86) and for the mass-asymmetry degree of freedom in heavy nuclei of $(5.3 \pm 1) \times 10^{-21}$ s (Sh 86,87). The fact that the asymmetric mass divisions show memory of the initial mass asymmetry suggests that the intermediate system from which they originate retains a dinuclear shape throughout the entire interaction lifetime.

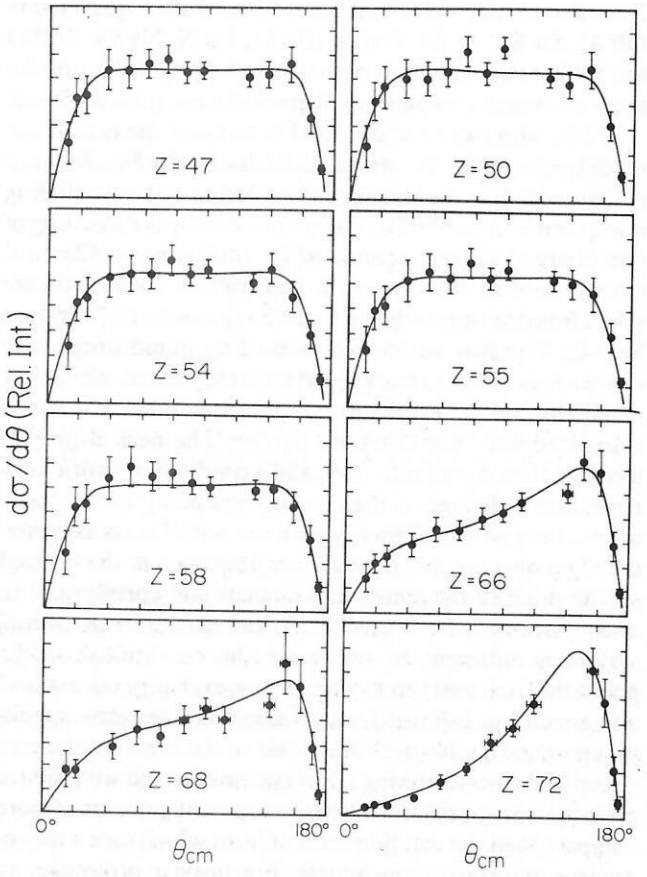


FIG. 3.7. Angular distributions $d^2\sigma/dZd\theta$ of fission fragments in the center-of-mass system for the reaction of 205-MeV $^{40}Ar + ^{208}Pb$. The solid lines are theoretical fits to the data and allow different values of $K_0^2$ near 0° and 180° (from Ke 87).

Recent reviews of this subject are given in Refs. Al 87, Fr 86, Gr 76, Va 73, Va 83a.

### 3.3. Angular momenta of fission fragments

Angular momentum remaining in the fragments following fission can be estimated by measuring $\gamma$-ray multiplicities $\langle M_\gamma \rangle$. Unfortunately there is always some difficulty in translating $\langle M_\gamma \rangle$ into the average total angular momentum of the fragments $\langle J_T \rangle$. The relationship is structure-dependent, and various prescriptions have been used. A simple one is $\langle J_T \rangle = 2(\langle M_\gamma \rangle - 4)$, which could be very roughly interpreted to mean that the $\gamma$ transactions are all of stretched $E2$ multipolarity apart from two statistical $\gamma$ rays per fragment, which on average carry away zero angular momentum, as also do the neutrons.

Measurements of $\langle M_\gamma \rangle$ as a function of mass split have been carried out with $\gamma$ rays, detected in arrays of Na(Tl) counters, taken in coincidence with fission fragments (Bo 82, Di 83, Ho 88, Le 85a, No 82, Sc 83, Sc 84b, Sc 85). The variation of $\langle M_\gamma \rangle$ with mass split changes from case to case, but is usually less than 15% of the average. However, it seems definite that there is structure in the distributions, with dips which are most obvious when shell closures occur in both fragments. The most prominent structure is seen in the case of $^{19}F + ^{197}Au$ (Le 85a). Similar effects have been observed in spontaneous and neutron-induced fission. From such results it is not clear whether these minima arise from reduced angular momenta in the primary fragments, from structure effects in the final $\gamma$-decaying nuclei formed after neutron evaporation, or from both.

The multiplicity averaged over all mass splits $\langle M_\gamma \rangle$, which should be relatively insensitive to shell effects, is always found to be larger than that expected on the basis of rigid rotation about an axis perpendicular to the symmetry axis; for the case of two equal touching spherical fragments $\langle J_T \rangle = (2/7)\langle J_{\text{fis}} \rangle$, $\langle J_{\text{fis}} \rangle$ being the average $J$ for fission. The data have usually been interpreted on the basis of a simple statistical model (Mo 80, Sc 82). The model consists of two touching liquid-drop spheres and assumes that the angular-momentum-carrying collective modes of wriggling, tilting, bending, and twisting have reached thermal equilibrium at this simplified scission point. Excitation of these modes increases the value of $\langle J_T \rangle$ over that for rigid rotation. The increase is larger, the heavier the system, because the larger moment of inertia makes the collective modes easier to excite; this feature appears to be supported by the data (Le 85a). However, the predicted values for $\langle J_T \rangle$ are usually too high. This may be due to the simplicity of the model and/or the possibility that these modes are not fully equilibrated at the scission point.

A different approach, in which discrete $\gamma$ rays were observed in $\gamma$–$\gamma$ coincidence in an array of eight Compton-suppressed Ge detectors and 14 BGO detectors, has been reported for 120-MeV $^{19}F$ on a thick $^{197}Au$ target (Ab 87). Decay schemes for 30 doubly-even fission products and discrete-line mulitplicities $\langle m_i \rangle$ were determined. The shapes of the curves for $\langle m \rangle = \langle m_1 \rangle + \langle m_2 \rangle$ and for $\langle M_\gamma \rangle$ as functions of mass split, from Refs. Le 85a and Ho 88, are qualitatively similar and imply 2.5–3 statistical $\gamma$ rays per fragment. However, sharp dips with amplitudes of 10–15% of the average, which are not associated with shell closures and are not apparent in the NaI data, also appear. Assuming that unobserved feeding to the levels corresponds to direct feeding by statistical $\gamma$ rays, they deduced the average spins and multiplicities at the entry points in the final fragments; the average angular momentum carried by each statistical $\gamma$ ray and neutron was calculated from the code CASCADE. From the observation that the neutron multiplicity is nearly independent of mass split (Ho 88) the authors conclude that their results provide strong evidence that $\langle J_T \rangle$ for the hot *primary* fragments varies substantially with mass. They have interpreted their results on the basis of the SCTS model of Ref. Ro 86 and conclude that much of the variation in $\langle J_T \rangle$ can be explained by variations in the shapes of the fragments at scission, spherical shapes corresponding to lower values of $\langle J_T \rangle$. If this is correct, it implies that the deformations of the hot fragments ($T \sim 1.3$ MeV) are similar to those in the ground states. This model gives values for $\langle J_T \rangle$ very similar to those of the simple statistical model, thus exceeding the observed values.

A proper solution to the problem of $\langle J_T \rangle$ will require a full dynamical calculation which includes the relaxation times of the various collective modes; it is clearly closely related to the problem of the angular distribution of fission fragments. In due course such measurements may provide valuable information on fission dynamics and shell structure at moderate temperatures.

### 3.4. Statistical-model analyses of experimental data

Measurements of fission and fusion excitation functions have been mainly carried out to determine the fission barriers $E_f(J)$, by comparing the results with statistical-model calculations; the codes usually incorporated the RLDM or (later) RFRM barriers. For details, see Refs. An 80, Aw 85, Be 77, Be 78, Bl 80, Bl 81, Bl 82a–c, Bi 78, Ch 86a, De 77, Fo 87, Ga 84, Hi 82, Ka 84, Le 82, Le 85, Le 86, Ne 81a, Pl 78, Pl 80, Pl 82, Pl 83, Pl 84, Sa 87, Si 64, Si 71, Si 82, Vi 80, Vi 82a,b, Wa 83, Ze 74 and references therein. Measurements reported prior to 1982 normally used the sharp cut-off distribution for the fusion angular-momentum distributions input to the code. It was not generally appreciated that the form of this distribution could have major effects on the values of the derived parameters, nor was it always realized that it was necessary to measure the fusion cross sections. Most analyses were carried out by varying only two parameters, the multiplying factor for the RLDM ($k_f$) and $a_f/a_\nu$. However, it was not often realized that equally good fits to the data could frequently be obtained for a large correlated range of the parameters (Hi 82). This led to much confusion between the results of different analyses, and, more importantly, little physical significance could be given to the derived values of the parameters. An excellent review of this subject up to 1984 has been given by Oganessian and Lazarev (Og 85).

Earlier work (see, e.g., Be 78, Pl 80, Hi 82) suggested that the derived values for $E_f(J)$ (usually for $a_f/a_\nu \approx 1.0$) were substantially lower ($k_f \sim 0.5$–$0.8$) than those predicted by the RLDM and that perhaps these results could be understood in terms of finite-range and temperature effects. An exception is Ref. Ka 84, where the RLDM values were found to be satisfactory for $A \approx 200$. Ward *et al.* (Wa 83) showed that it was possible to overcome the problem of the large correlated range of $k_f$ and $a_f/a_\nu$ by measuring the average number of neutrons preceding fission ($\nu_{pre}$). This depends strongly on $a_f/a_\nu$ but not on $k_f$; the dependence on $a_f/a_\nu$ of the multichance fission cross sections for the $^{19}F + ^{181}Ta$ reaction when $k_f$ is adjusted to give acceptable fits for the fission excitation functions is shown in Fig. 3.8. Vigdor *et al.* (Vi 80) have indicated that $\nu_{pre}$ can be indirectly determined from fission-fragment anisotropies, but this method has not been much used.

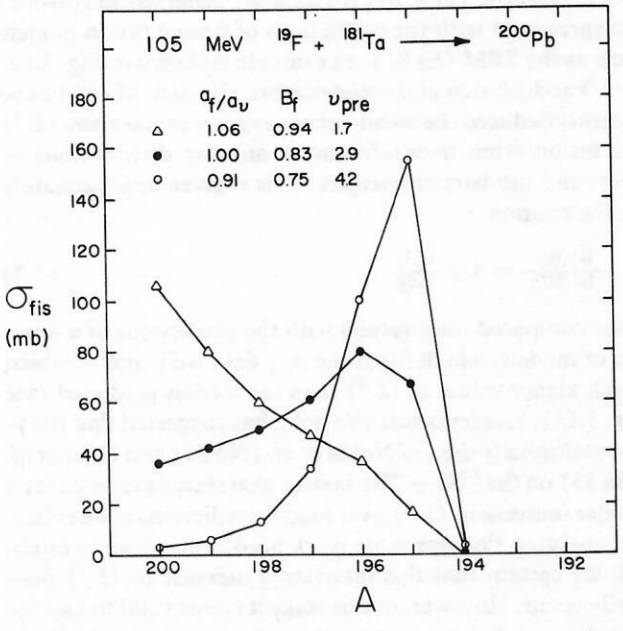


FIG. 3.8. Variation of fission cross section at each evaporation stage for three parameter sets, which give reasonable fits to the total fusion and fission excitation functions, for 105-MeV $^{19}F + ^{181}Ta$. The quantity $\nu_{pre}$ is very sensitive to the parameter set. The calculations were performed with the code MBII (from Wa 83).

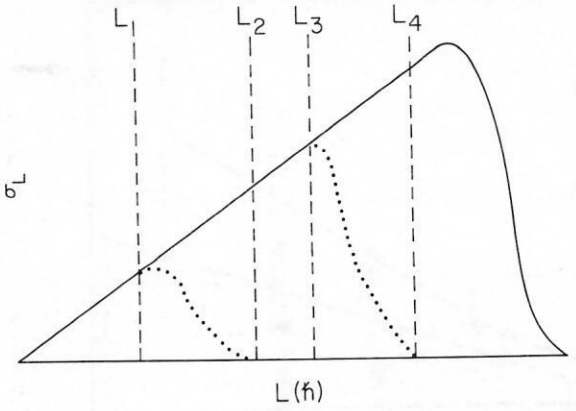


FIG. 3.9. Qualitative representation of the reaction cross-section division which would be required for the saturation hypothesis to be valid (from Bl 82d).

Most recent work has included the possibility of a diffuse angular-momentum distribution for fusion, thus adding a third parameter $\delta L$ [Eq. (2.13)] to the analysis. To avoid to some degree the problem of a third parameter as well as some others, Blann *et al.* (Bl 82c) have suggested the measurement and analysis of $\sigma_{ER}$ in the region where $\sigma_{fis} \gg \sigma_{ER}$ and call this method "saturation analysis." The idea is illustrated in Fig. 3.9, which qualitatively divides the entrance-channel partial cross sections $\sigma_L$ into regions. That from 0 to $L_3$ is assumed to go entirely into compound-nucleus formation, and most of the compound nuclei with $L > L_2$ are assumed to fission. The region with $L > L_3$ may go into any admixture of reaction channels. The dotted curves between $L_1$ and $L_2$ and between $L_3$ and $L_4$ indicate the regions where increasing fractions of the higher $L$ go into fission and non-compound processes, respectively. If this division is correct, i.e., if $\sigma_{EF}$ is limited entirely by compound-nucleus fission, then we can write

$$\sigma_{ER} = \pi\lambda^2 \sum_{L=0}^{\infty} (2L+1)\, T_L\, [1 - P_f(L, E_x)], \quad (3.5)$$

where $P_f$ is the total probability for fission. According to the Bohr hypothesis $\sigma_{ER}/\pi\lambda^2$ should be a function of $E_x$ only and should be independent of entrance channel. Also, provided that $L_3 > L_2$, $\sigma_{ER}$ should not depend on $\sigma L$. Results from a number of reactions are shown in Fig. 3.10 and appear to support the independence idea when saturation is achieved. It is claimed that statistical-model analysis of such data is much less sensitive to choices of transmission coefficient for evaporated particles and level density than analysis of data with low $\sigma_{fis}/\sigma_{ER}$. On the other hand, at least for lighter systems, saturation analysis can only probe the region of high angular momentum where $E_f(J) < B_\nu$. As the authors suggest, it would be worthwhile to explore this method further with more accurate measurements of $\sigma_{ER}$ than they were able to achieve at the time.

In recent analyses (Ch 86a, Le 85, Le 86, Pl 83, Pl 84)

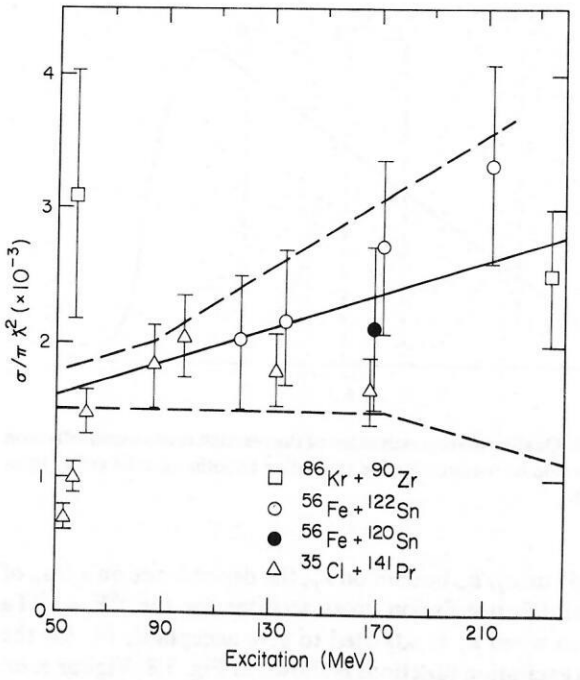


FIG. 3.10. The quantity $\sigma_{ER}/\pi\lambda^2$ as a function of excitation energy for reactions producing osmium nuclei. The solid line represents calculations using the prescription for $a_f/a_\nu$ of Ref. Bi 72, while for the upper (lower) lines $a_f$ is divided (multiplied) by 1.02. The three points at low excitation energy do not satisfy the saturation condition (from B1 82c).

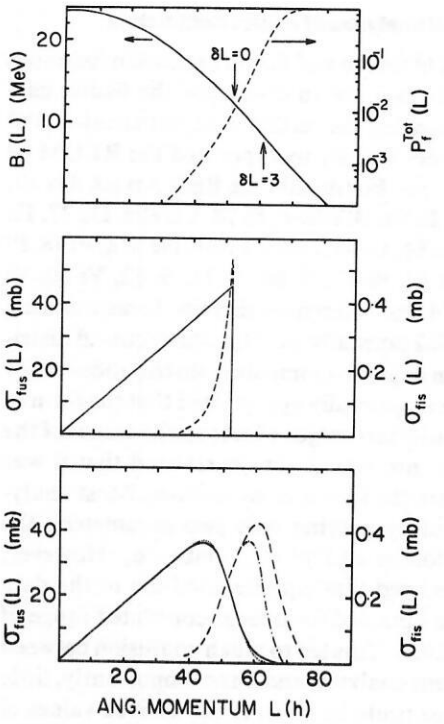


FIG. 3.11. (a) The fission barriers for $^{168}$Yb from the RFRM and the total fission probability for $^{150}$Sm + $^{18}$O at 104 MeV, as a function of angular momentum. The arrows labeled $\delta L = 0$ and $\delta L = 3$ indicate the region of the fission barrier effectively sampled by the fusion angular-momentum distributions in (b) and (c). (b) Sharp cut-off fusion spin-distribution for the same reaction (solid line) and the corresponding fission distribution (dashed line). (c) Same as (b) but for a Fermi distribution with $\delta L = 3.0$ (solid and dashed lines) and for the distribution given by Eq. (3.6) with $\Delta L = 7.0$ (dotted and dot–dash curves) (from Ch 86a).

the RLDM barriers have been replaced by those from the more realistic RFRM and the multiplying parameter $k_f$ has been abandoned. In most cases $a_f/a_\nu$ has been fixed at 1.0 or allowed only a very small variation from unity, and $\delta L$ has been introduced as the only adjustable parameter. Generally good fits to fission excitation functions have been obtained, and there is a tendency to interpret this as evidence that the RFRM barriers rather accurately describe the real barriers. It should, however, be appreciated that changing $\delta L$ is somewhat similar to scaling the barrier height. In Fig. 3.11 results are compared for $\delta L = 0$ and $\delta L = 3.0$. For the former, fission is calculated to come mainly from a narrow region near $L_{max}$, whereas for $\delta L = 3.0$ fission comes mostly from the tail of $L$ distribution and the total fission probability is three times greater than for $\delta L = 0$. Increasing $\delta L$ to 3.0 changes the sampled region of fission barrier from $\sim 13$ MeV to $\sim 9$ MeV. Also shown is the effect of taking the distribution

$$\sigma_{fus}(L) = (1/2)\,\pi\lambda^2\,(2L+1)\{1 - \mathrm{erf}\,[(L - L_0)/\Delta L]\}, \tag{3.6}$$

where erf($x$) is the error function. For $\Delta L = 2.32\delta L$ this distribution closely matches that of the Fermi function if $0.2 < T_L < 0.8$, but approaches its asymptotic value more quickly. Furthermore it reproduces the distribution from the ZPM very accurately (Ch 86a). This very minor change in the $L$ distribution produces a substantial one in the fission cross section.

This case is one of very low fission probability, and the sensitivity to $\delta L$ and to the shape of the distribution is less when the fission probability is higher. However, it is clear that fission barriers cannot be properly tested by arbitrarily adjusting $\delta L$ to fit data. Methods of determining the appropriate $L$ distributions need to be found. Unfortunately, at present there are no direct experimental methods. Gamma-ray multiplicity measurements in conjunction with statistical-model calculations and some other assumptions can provide information on the first and sometimes second moments of the $L$ distributions in cases where fission is not the major decay mode even near $L_{max}$ (Bo 88, Gi 85, Ha 85, No 85, Va 83). These limited data are generally in reasonable agreement with the predictions of simple fusion models such as the ZPM (Es 81); an example is shown in Fig. 3.12.

Vandenbosch and collaborators (Va 86a, Mu 86) have recently deduced the mean-square angular momentum $\langle L^2\rangle$ for fusion from fission-fragment angular distributions at near- and sub-barrier energies. This is given approximately by the relation

$$\frac{W(0°)}{W(90°)} = 1 + \frac{\langle L^2\rangle}{8K_0^2}. \tag{3.7}$$

They compared their results with the predictions of a number of models, which fitted the $\sigma_{fus}$ data well, and obtained much higher values of $\langle L^2\rangle$ than the models predicted (see Fig. 3.13). Vandenbosch (Va 86b) has suggested that the $\gamma$-ray multiplicity data of Nolan *et al.* (No 85) and Haas *et al.* (Ha 85) on the $^{80}$Se + $^{80}$Se system also shows evidence for a similar increase in $\langle L^2\rangle$ over model predictions at near-barrier energies. Perhaps more work needs to be done to establish for certain that this interesting increase of $\langle L^2\rangle$ does really occur. However, at this stage it seems valid to assume that the models do give reasonable values for $\delta L$ (or $\langle L^2\rangle$) at above-barrier energies and possibly underestimate them at sub-barrier energies. If this is correct, we can reject results from statistical-model analyses of fission data which require

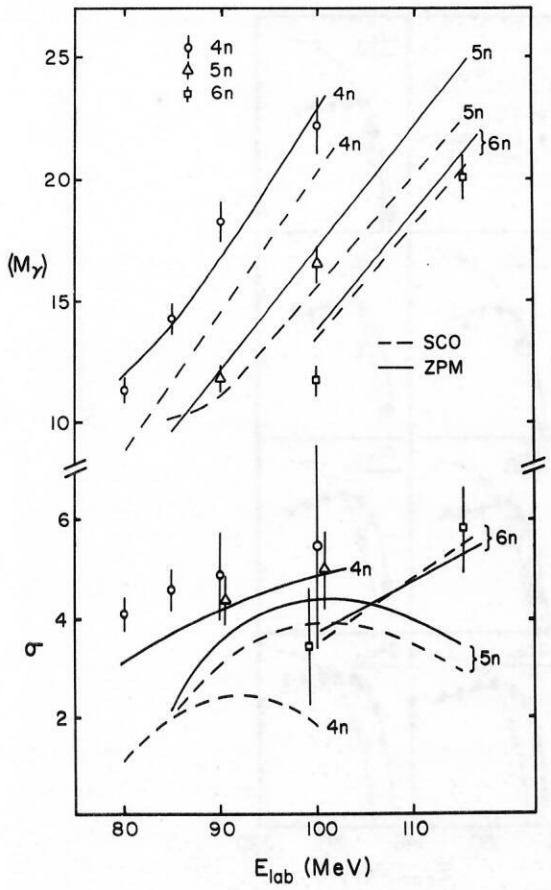


FIG. 3.12. Multiplicities ($M_\gamma$) and widths ($\sigma$) of the $\gamma$-ray multiplicity distributions for the $^{19}F + ^{159}Tb$ reaction. The lines are calculated with the aid of the code ZPACE for $\delta L = 0$ (dashed) and $\delta L = 4.4$ (full), the latter value being the prediction of the zero-point model for energies above the Coulomb barrier. The $4n$ reaction is most sensitive to $M_\gamma$ and $\sigma$ because it derives from the highest available values of $L$ (from Bo 88).

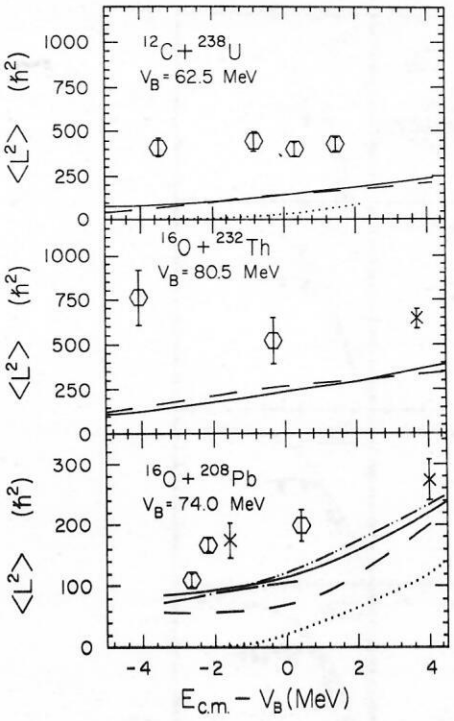


FIG. 3.13. Comparison of mean-square spin values for fusion deduced from fission-fragment anisotropies with the predictions of different models. The dotted curves are based on the sharp cut-off approximation, while the other lines relate to various models: full (Es 81); dashed (Wo 73); dot–dash (Pi 85); dot–dot–dash (Ud 85). The data represented by hexagons are from Ref. Mu 86, and by crosses from Refs. Vu 86 and Ba 85b (from Mu 86).

values for $\delta L$ which are *substantially smaller* than model predictions. The model predictions do not usually differ very much from one another but do differ substantially from the sharp cut-off approximation (Fig. 3.13).

Van der Plicht *et al.* (Pl 83) have made measurements of fission excitation function for the systems $^{158}$Er, $^{186}$Os, and $^{210}$Po formed by a variety of projectiles ranging from $^{9}$Be to $^{64}$Ni. They also studied the nuclei $^{204,206,208}$Po through bombardment with $^{16}$O or $^{18}$O. They determined the velocity distributions for the fissioning systems in order to check for ICF reactions but did not measure fusion cross sections, which were calculated from the Bass model (Ba 77). For the calculations with the code PACE they took the RFRM barriers, $a_f/a_\nu = 1.0$ for the $^{158}$Er and $^{210}$Po systems and 1.015 for $^{186}$Os, $a_\nu = A/7.5$ MeV$^{-1}$, and varied $\delta L$ to get the best fit to the data at the lower energies. Both Fermi-gas and microscopic level densities were used. It is valuable to study one system through a number of different reactions, as hopefully one can use the same parameters for each, apart from $\delta L$. Figure 3.14 illustrates the quality of the fits obtained for $^{158}$Er. There are significant differences between the results for the two types of level-density expression. The values of $\delta L$ ranged between 0.5 and 6.0, with an average of 1.9, and are mostly much smaller than would be expected from the ZPM.

Lesko *et al.* (Le 85, Le 86) have studied systematically the even $^{170-188}$Pt nuclei, whose neutron excesses, $N - Z$, vary by about a factor of 2, by bombarding even $^{112-124}$Sn targets with $^{58,64}$Ni ions. Both $\sigma_{fis}$ and $\sigma_{ER}$ were measured. The heavy nickel projectiles produced compound nuclei

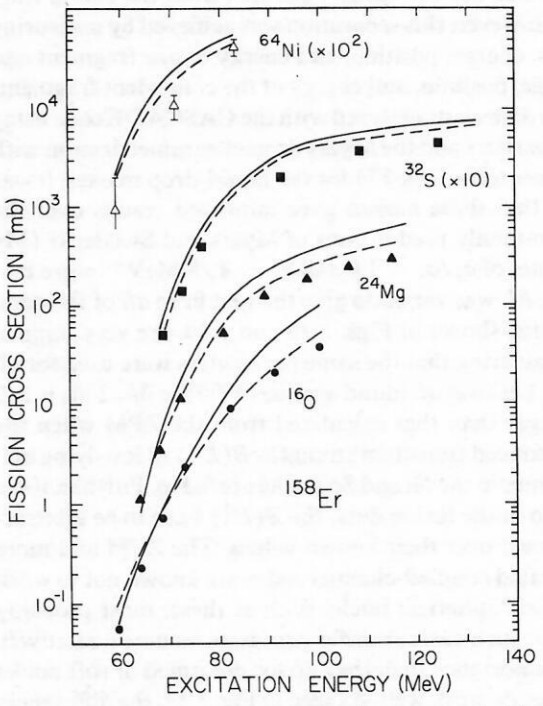


FIG. 3.14. Calculated fission cross sections compared with experimental data for the composite system $^{158}$Er formed by the indicated projectiles. Two level-density expressions were used, Fermi-gas (solid lines) and microscopic (dashed lines) (from Pl 83).

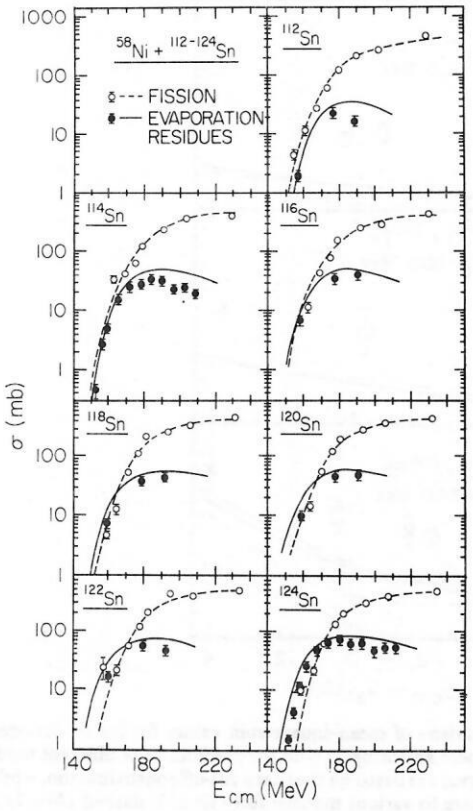


FIG. 3.15. Experimental fission (open circles) and ER (closed circles) cross sections for the systems $^{58}$Ni + $^{112-124}$Sn. The curves are the results of statistical-model calculations (from Le 86).

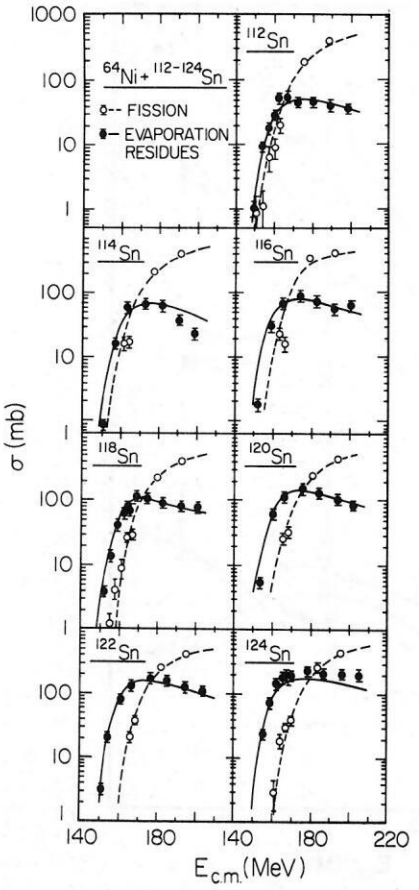


FIG. 3.16. As in Fig. 3.15, for the systems $^{64}$Ni + $^{112-124}$Sn (from Le 86).

with excitation energies 20–50 MeV closer to the yrast line than obtainable with lighter projectiles. The disadvantage of using more symmetric target/projectile combinations is that there is a very significant cross section for deep-inelastic events which are not easily separated from the fission fragments. However, this separation was achieved by measuring the mass, charge, position, and energy of one fragment and the charge, position, and energy of the coincident fragment.

The data were analyzed with the CASCADE code using RFRM barriers and the Myers droplet parametrization with the Wigner term (My 77) for the liquid-drop masses; it was claimed that these masses gave improved results over the more commonly used masses of Myers and Swiatecki (My 67). Values of $a_f/a_\nu = 1.0$ and $a_\nu = A/8$ MeV$^{-1}$ were taken, while $\delta L$ was varied to give the best fit to *all* of the data. The results, shown in Figs. 3.15 and 3.16, are very impressive, considering that the same parameters were used for all 14 cases. Lesko *et al.* found a value of 7.5 for $\delta L$. This is 2–3 times larger than that calculated from the ZPM when the known reduced transition strengths $B(E\lambda)$ to low-lying collective states in the Ni and Sn nuclei are fed in. Further, if the ZPM is to fit the fusion data, the $B(E\lambda)$ have to be arbitrarily increased over their known values. The ZPM and more sophisticated coupled-channel codes are known not to work well for stiff spherical nuclei such as these, most probably because in such cases transfer processes assume a relatively greater importance than they do for deformed or soft nuclei where they do work well. As seen in Fig. 3.17, the diffuseness derived from the fission data agrees rather well with that obtained by requiring the ZPM to fit the fusion data. A less diffuse distribution and correspondingly poor fit to the fusion data is obtained with the coupled-channel code PTOLEMY, which takes collective excitations but not transfer into account.

Kondo *et al.* (Ko 87) have analyzed the data of Ref. Le 85 leading to $^{192}$Pt, i.e., the cases $^{64}$Ni + $^{118}$Sn and $^{58}$Ni + $^{124}$Sn after extending the fission excitation function of the latter to lower energy. They used the code ALERT1,

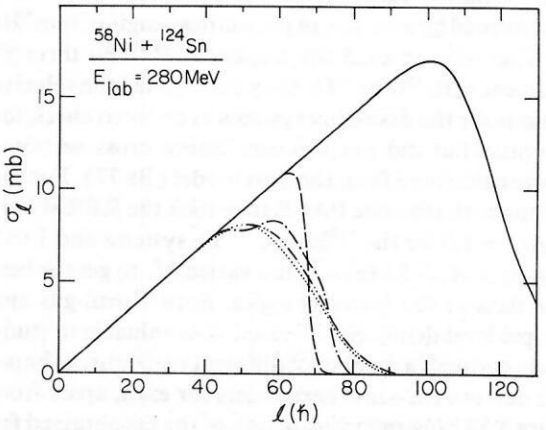


FIG. 3.17. Calculated partial-wave cross-section distributions for fusion of the system $^{58}$Ni + $^{124}$Sn. The solid curve is an optical-model prediction for the total reaction; the dashed and dot–dash curves are, respectively, the predictions for $\sigma_{fus}$ of the coupled-channel code PTOLEMY without and with coupling to the $2^+$ and $3^-$ states in both target and projectile; the dot–dot–dash curve is a result of the ZPM (see text); the dotted curve is deduced from fitting the fission data with statistical-model calculations (from Le 86).

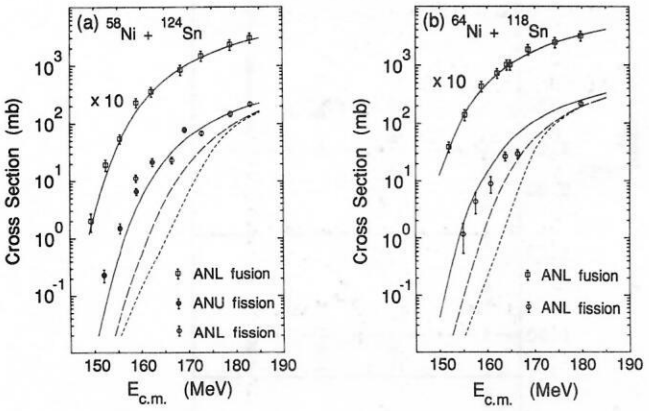


FIG. 3.18. Fusion and fission cross sections for the $^{58}$Ni + $^{124}$Sn and $^{64}$Ni + $^{118}$Sn systems as a function of center-of-mass energy, compared with theoretical calculations with the code ALERT1. The fusion cross sections are multiplied by ten. The data of Ref. Le 86 are denoted by open symbols, and the new data by closed circles. The upper solid curves are model fits to $\sigma_{\rm fus}$, while the dotted, dot–dash, and lower solid curves are calculations of $\sigma_{\rm fis}$ for $\Delta L = 0$, $\Delta L = 16.5$, and for the elastic-fusion model, respectively (from Ko 87).

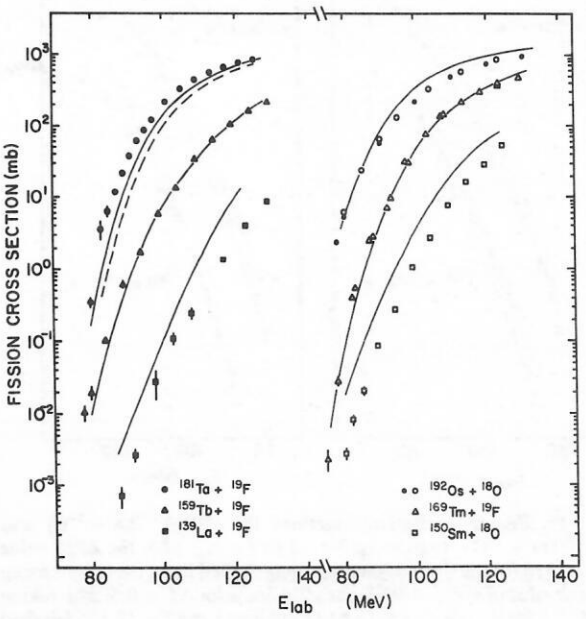


FIG. 3.19. Fission cross sections calculated with the statistical-model parameters given in the text. The dashed curve for $^{200}$Pb was calculated with the RLDM fission barriers (from Ch 86a).

with the RFRM barriers, took $a_f/a_\nu = 1.0$, $a_\nu = A/10$ MeV$^{-1}$, and compared results with fusion $L$ distributions taken from the elastic-fusion model (Ud 85) by requiring it to fit the $\sigma_{\rm fus}$ results and from a smooth cut-off model with the distribution of Eq. (3.6). Their results are shown in Fig. 3.18, where it is seen that only the distribution from the elastic-fusion model fits the data well. They deduced $\Delta L = 16.5$ from the ZPM, which is approximately equivalent to $\delta L = 7.1$, very close to the value of 7.5 taken by Lesko *et al.* which gave excellent fits. Kondo *et al.* state that allowing the fusion cross sections to vary by 20% (the quoted error), and varying $a_\nu$ between $A/11$ and $A/7.5$ and $a_f/a_\nu$ between 1.00 and 1.02 did not produce changes significant enough to alter these conclusions. There appears to be a real discrepancy between the two analyses. The reason for this may reside in differences between the computer codes, in the form of the distribution of $\sigma_{\rm fus}(L)$, in the liquid-drop masses, or elsewhere.

Kondo *et al.* also point out that, if fission probabilities can be calculated reliably, studies of this kind provide a sensitive way of testing the higher angular-momentum components of $\sigma_{\rm fus}(L)$, and hence of fusion models. This cannot be done by methods such as $\gamma$-ray multiplicities or fission-fragment angular distributions which are insensitive to moments higher than the first or second.

The Canberra group (Bo 88, Ch 86a, Hi 82, Hi 83, Hi 84, Ne 84, Ne 88, Wa 83) has made extensive measurements, including fission, evaporation-residue and prefission neutron excitation functions, and in some cases elastic scattering, particle transfer, and $\gamma$-ray multiplicity measurements. Nuclei from $^{158}$Dy to $^{251}$Es with a wide range of fissilities have been studied. Data have been analyzed with the code ALERT1 and MBII, an earlier version. Notable features of the earlier work were the first measurement of the $J$ distribution carried by evaporation residues when limited by fission (Hi 82, Le 82) and the measurements of $\nu_{\rm pre}$ for $^{200}$Pb (Wa 83), which removed the ambiguity in $k_f$ and $a_f/a_\nu$ and showed that $a_f/a_\nu$ had the value $1.02 \pm 0.02$ for this nucleus.

Charity *et al.* (Ch 86a) have taken a slightly different approach in that they have compared their measured data for the systems $^{158}$Dy, $^{168}$Yb, $^{178}$W, $^{188}$Pt, $^{200}$Pb, and $^{210}$Po, formed in reactions induced by $^{19}$F or $^{18}$O beams, with *parameter-free* calculations with ALERT1. For these they took the RFRM barriers $a_f/a_\nu = 1.0$, $a_\nu = A/10$ MeV$^{-1}$, and $\delta L$ values *calculated* from the ZPM model; these had the values 2.3, 3.0, 4.2, 4.4, 4.7, and 2.5, respectively. The results, shown in Fig. 3.19, reveal that the calculations are in remarkably good accordance with experiment except for the light systems $^{158}$Dy and $^{168}$Yb. Apart from these two, very minor adjustment of the parameters would produce very good agreement with the data. For these cases a major part of the fission cross section usually comes from the region where $E_f(J) \leqslant B_\nu$ and only a small part from lower $J$ values, since the fission probability drops rapidly when $E_f(J)$ increases above $B_\nu$. The fission probability soon approaches unity when $E_f(J)$ becomes less than $B_\nu$, so that the rate of decrease of $E_f$ with $J$ is unimportant. Hence the calculations are most sensitive to barriers in the region of $E_f(J) = B_\nu$.

For the two light systems the situation is qualitatively different in that there is no substantial population in the region where $E_f(J) = B_\nu$. The fission arises from the high-$L$ tail of the fusion angular-momentum distribution (Fig. 3.11). Hence the effective $J$ value varies with bombarding energy and $E_f(J)$ is sampled over a wide range of $J$, in contrast to the situation with heavier systems. Clearly the calculated results are critically dependent on the shape assumed for the fusion $L$ distribution and particularly for the high-$L$ tail. In addition the calculations are more sensitive to the values of other parameters than for heavier systems. The effect of varying the form of $\sigma_{\rm fus}(J)$, $a_f/a_\nu$, and $a_\nu$ is shown in Fig. 3.20.

Newton *et al.* (Ne 88) have measured $\nu_{\rm pre}$ for the above systems, excluding $^{158}$Dy, and for some others for which excitation functions for fission and fusion had previously been measured (Hi 82, Hi 83); results are shown in Fig. 3.21. Apart from the two most fissile systems and the $^{28,30}$Si-in-

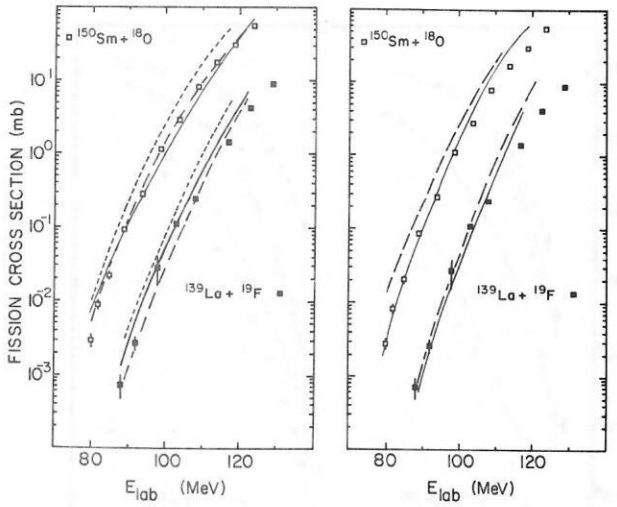


FIG. 3.20. Fission excitation functions for $^{158}$Dy($^{139}$La + $^{19}$F) and $^{168}$Yb($^{150}$Sm + $^{18}$O). Left: using Eq. (3.6) for $\sigma_{fus}$ ($L$); the ZPM value for $\Delta L$ is used for the short dashed and long dashed lines, the latter having a reduced value of $a_f/a_\nu = 0.97$; the solid line is for $\Delta L = 0$. Right: taking $a_\nu = A/7.5$ MeV$^{-1}$, with Eq. (3.6) (solid lines) and Eq. (2.12) (dashed lines) and the ZPM diffuseness (from Ch 86a).

duced reactions, the variation of $\nu_{pre}$ with bombarding energy appears to follow statistical-model predictions for the lower excitation energies, but not for higher $E_x$ where the predictions indicate that $\nu_{pre}$ should fall instead of steadily increasing as observed. Similar deviations have been noted by other authors for still higher $E_x$.

An extensive statistical-model analysis was carried out

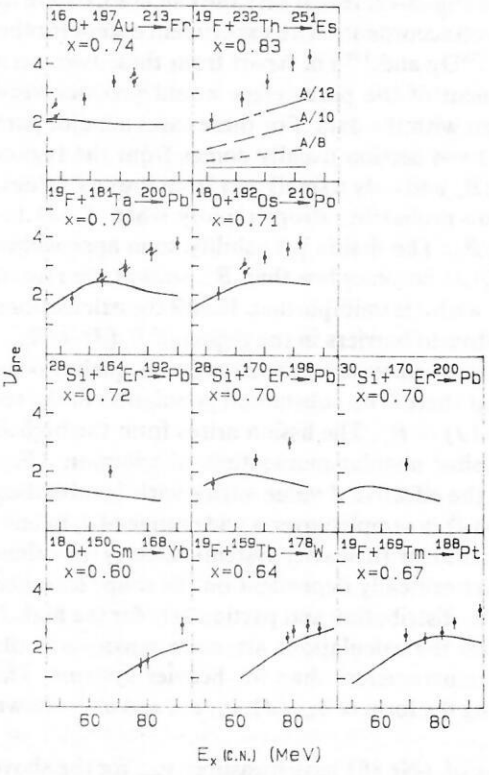


FIG. 3.21. Measured values of $\nu_{pre}$ as functions of compound-nucleus excitation energy. The full lines are statistical-model calculations with $a_f/a_\nu = k_f = 1.00$ and $\delta L$ adjusted to fit the fission and fusion excitation-function data. The dashed lines for $^{251}$Es show the effect of including emission during fragment acceleration (from Ne 88).

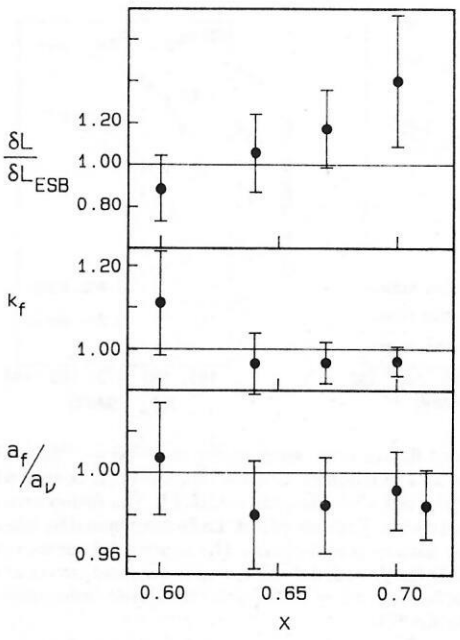


FIG. 3.22. Parameters $a_f/a_\nu$, $k_f$, and $\delta L/\delta L_{ESB}$, derived from statistical-model calculations, plotted against fissility for the systems $^{168}$Yb, $^{178}$W, $^{188}$Pt, $^{200}$Pb, and $^{210}$Po. Results for $k_f$ and $\delta L/\delta L_{ESB}$ are not given for $^{210}$Po because of difficulties in fitting the excitation functions, probably as a consequence of large shell effects. The absolute values of $\delta L$ beginning with $^{168}$Yb are 2.7, 4.4, 4.9, and 6.0, respectively (from Ne 88).

with the code ALERT1 for the five lighter-ion induced systems. The $\sigma_{fis}$, $\sigma_{fus}$, and $\nu_{pre}$ data were included in a $\chi^2$ analysis, except that those values of $\nu_{pre}$ at variance with the model predictions for the three heavier systems were excluded. The importance of including errors in $\sigma_{fus}$ was stressed. Most calculations were done for $a_\nu = A/10$ MeV$^{-1}$, but the effects of variations to $A/12$ and $A/7.5$ were investigated. The RFRM barriers were taken, but a multiplying constant $k_f$ was included. The parameters $k_f$, $a_f/a_\nu$, and $\delta L$ were allowed to vary. The results shown in Fig. 3.22, those for $\delta L$ being divided by the ZPM model value $\delta L_{ESB}$, are consistent with $a_f/a_\nu = 1.0$, $k_f = 1.0$ (the RFRM values) and with the ZPM values of $\delta L$, but only within rather large errors of about 5%, 10–15%, and 40%, respectively. Thus, even within the framework of a statistical-model analysis of more complete data than has been reported in other cases, it is not possible to precisely establish the accuracy of the RFRM barriers. On physical grounds they would be expected to be superior to those of the RLDM; however, it is premature to claim that their accuracy has been experimentally demonstrated, as has frequently been done. This conclusion is made even stronger when dynamical effects are taken into account (see Sec. 3.5).

### 3.5. Fission of light systems

Fission of light systems with fissilities below the Businaro–Gallone (BG) point has been little studied because the clear signature for fission of heavier systems is no longer present. A mass-asymmetric division occurs, and it is not easy to distinguish this from reactions such as deep-inelastic "orbiting" collisions. Recent measurements have indicated that mass-asymmetric fission of light compound systems most probably does occur (Aw 85, Gr 84, Mc 85, Pl 86, Sa 86, Sa 87, So 84). Although there are many uncertainties with this subject, both experimental and theoretical, it is of

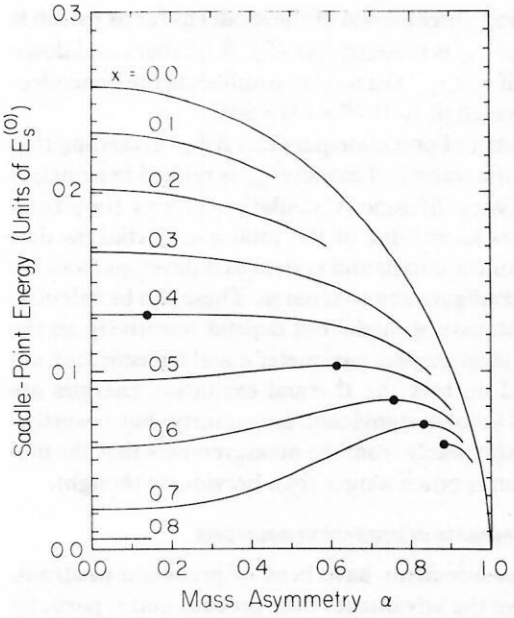


FIG. 3.23. Saddle-point energies as a function of constrained mass asymmetry $\alpha$ for various values of the fissility. Here $\alpha = (M_R - M_L)/(M_R + M_L)$, where $M_R$ and $M_L$ are the masses to the right and left, respectively, of a plane passing through the neck region of the nucleus. The solid points correspond to the Businaro–Gallone family of asymmetric saddle-point shapes with two unstable degrees of freedom (from Da 85).

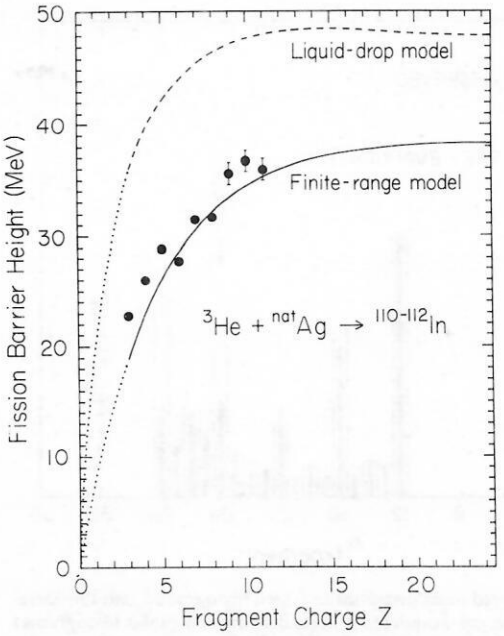


FIG. 3.24. Calculated and experimentally inferred (Mc 85) fission barriers as a function of the charge of the lighter fragment for the fission of indium nuclei. Calculations with the LDM (full line) and FRM (dashed line) are shown; the dotted portions are interpolations (from Si 85).

considerable interest. It would, for example, be very useful to help establish accurate values for fission barriers for light systems to better establish the parameters of the FRM (Si 85). Light might also be thrown on the level densities of the very necked-in saddle points with varying mass asymmetries.

The unity of evaporation and fission decay modes has been emphasized (Mo 75, Sw 83). A major factor determining branching ratios of the various decay modes is the barrier to binary fission into the appropriate masses. This barrier, with constrained mass asymmetry, is known as a conditional saddle point. These have been calculated for the LDM and FRM by Davies and Sierk (Da 85) and are shown in Fig. 3.23 for the LDM ($J = 0$). It can be seen that for $x > x_{BG}$ the mass-symmetric saddle point is lowest, whereas for smaller $x$ this is no longer true. However, even for $x > x_{BG}$, as the asymmetry increases the conditional saddle point reaches a maximum value, corresponding to mass instability, and then rapidly declines to zero. The region beyond these maxima, known as the Businaro–Gallone family, corresponds to evaporation of light particles, and the region inside corresponds to fission. A comparison of experimentally inferred barriers for low $J$ (Mc 85) and those calculated for the LDM and FRM (Si 85) is shown in Fig. 3.24; clearly the FRM is favored.

Neither LDM nor FRM calculations of the conditional saddle points have been reported for rotating systems. However, since the effect of rotation is similar to that of increasing Coulomb energy which increases the effective fissility, one would expect the BG points for the two models to move to lower values of $x$ with increasing $J$. Hence systems with $x < x_{BG}$ ($J = 0$) may still show symmetric fission, particulary as most of the fission comes from the region of highest $J$ as a consequence of the high value of $E_f(0)$. However, no sudden transition from symmetric to asymmetric fission can be expected because the conditional saddle-point barriers are almost independent of asymmetry for a substantial region on either side of $x_{BG}$ (see Fig. 3.23).

Necessary conditions which must be satisfied for fusion/fission are: (1) the kinetic energy of each fission product must be fully relaxed, i.e., consistent with the Coulomb and rotational energies of a nearly touching configuration; (2) mass equilibration must have occurred, i.e., the mass distribution must be the same for all observation angles and show no memory of the entrance channel, and the angular distribution must approximate $1/\sin\theta$ for high-$J$ systems. These conditions are not necessarily sufficient, since it might be possible for the orbiting lifetime to be longer than the mass-equilibration time [$\sim 5\times 10^{-21}$ s for *heavy* systems (Sh 86)]. Some support to the conclusion that fusion/fission was being observed would be given if the cross section were roughly compatible with that expected from a statistical-model calculation using the mass-symmetric fission barrier. However, caution should be exercised here because there are no theoretical calculations for rotating conditional saddle points and, perhaps more important, it may be dangerous to extrapolate the value of $a_f/a_\nu = 1.0$, which seems to work fairly well for heavier systems, to the very necked-in saddle-point shapes for these very light systems.

Sobotka *et al.* (So 84) have studied fragments from the decay of systems formed in the reactions induced by 7.4 and 8.4 MeV/nucleon beams of $^{74}$Ge, $^{93}$Nb, and $^{139}$La on $^{9}$Be and $^{12}$C. The resulting Z distributions are consistent with a change from symmetric to asymmetric fission in the region and $A = 100$, and yields are consistent with the results from a simple fusion/fission calculation. A number of authors have studied the decay of nuclei in the region of $A = 44$–$64$ and attribute the observed decay to fusion/fission (Aw 85, Gr 84, Pl 86, Sa 86, Sa 87). For example, Sanders *et al.* (Sa 86, Sa 87) have studied the fission-like decay of $^{56}$Ni formed

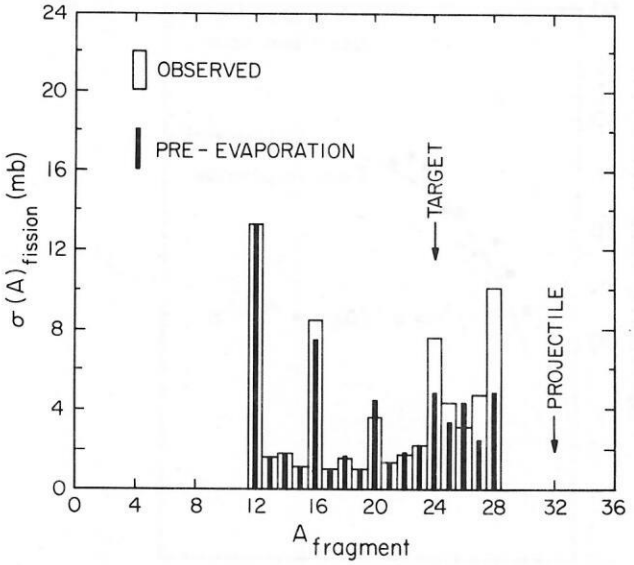


FIG. 3.25. Observed mass distribution (open histograms) and the corresponding deduced pre-evaporation mass distribution (solid histograms) for the fission-like component of the $^{32}S + ^{24}Mg$ reaction at $E_{cm} = 60.8$ MeV (from Sa 87).

in the $^{32}S + ^{24}Mg$ and $^{16}O + ^{40}Ca$ reactions. They have found rather flat mass distributions (see, e.g., Fig. 3.25), full energy damping, a $1/\sin\theta$ angular dependence in the range studied, and qualitative agreement with statistical-model calculations with the CASCADE code. The possibility that the observed mass distribution resulted from an "orbiting" mechanism was explored within two models, neither of which indicated the presence of such a component. However, the models were developed for heavy systems (see also Bl 85a) and assume a sharp nuclear surface which is not a good approximation for light systems. On the other hand Shivakumar *et al.* (Sh 86b), who studied the $^{28}Si + ^{14}N$ system and also found evidence for equilibration of charge and mass, claim that compound-nucleus evaporation underpredicts the yield by a factor of six; hence they favor an orbiting mechanism. Clearly much more experimental and theoretical work needs to be done before we attain a good understanding of the fission-like decay of light systems.

### 3.6. Prefission particle emission

In the statistical model it is assumed that the collective fission degree of freedom reaches equilibrium in a time $\tau_{fe}$ short compared with that for particle emission $\tau_p$. This need not necessarily be the case, and it is interesting that as long ago as 1940 Kramers (Kr 40) considered the possible effects of nuclear viscosity (or friction) on fission decay. However, this work was overlooked until recently. If $\tau_p \leqslant \tau_{fe}$, then on the average more particles will be emitted before fission than the statistical model predicts. Further, the statistical model in its usual form does not take into account the possibility of particle emission during the time $\tau_{ss}$ taken in the transition between the saddle and scission configurations. It used to be assumed that $\tau_{ss}$ was sufficiently short that an insignificant number of particles would be evaporated in this time. However, it should be appreciated that extra particle emission due to a long $\tau_{ss}$ would not in itself invalidate the statistical model or change the calculated fission cross section; this possibility was simply ignored. On the other hand, if $\tau_p \leqslant \tau_{fe}$, there is a definite breakdown of the model as far as fission is concerned and $\sigma_{fis}$ is reduced (Kr 40). A further breakdown would occur if $\tau_p \leqslant \tau_{eq}$, the time to equilibrate the noncollective modes, which is $\lesssim 10^{-22}$ s (We 80).

The number of prefission particles $\Delta P_{pre}$ exceeding that predicted by the statistical model $P^s_{pre}$ is related in principle to the prescission lifetime. Calculation of this time from $\Delta P_{pre}$ requires knowledge of the total and partial particle decay times for the compound system as it develops from the equilibrium configuration to scission. These can be calculated from the statistical model but depend sensitively on the values of the level-density parameter $a$ and transmission coefficients, and on how the thermal excitation energies are deduced. All involve significant uncertainty, but nevertheless it seems very likely from the measurements that the lifetime for fission is much longer than previously thought.

#### *3.6.1. Measurements of prefission neutrons*

Most measurements have been of prefission neutrons. Neutrons have the advantages over protons and $\alpha$ particles that their transmission coefficients are less sensitive to deformation effects and that, apart from very neutron-deficient systems, they are the most abundantly emitted light particles. Partial reviews of this subject have been given by Hilscher (Hi 87, Hi 87a). The measurements can be roughly divided into two classes, those at low energies ($E_x \leqslant 100$ MeV) and those at higher energies. The former have the advantage that complete fusion, without significant preequilibrium effects, is the dominant reaction mechanism but the disadvantage that $\nu^s_{pre}$ forms a major part of the measured $\nu_{pre}$. The latter have the advantage that $\nu^s_{pre}$ is relatively unimportant, but there may be difficulties with pre-equilibrium emission and incomplete fusion. A significant part of the fission-like cross section may arise from angular momenta where $E_f(J) = 0$, so that no compound nucleus can be formed. This process is similar to quasifission and would be expected to involve a shorter lifetime than compound-nucleus fission.

Most of the low-energy work has been carried out by the Canberra group (Hi 84, Hi 86, Hi 87, Hi 89b, Ne 88). Hinde *et al.* have stressed the desirability for all $\nu_{pre}$ measurements of plotting $\nu_{tot}$ against the available excitation energy for fission, $E_x(f)$ (for definition, see Hi 86); $\nu_{tot}$ should exclude pre-equilibrium neutrons, and $E_x(f)$ is reduced by 20 MeV per pre-equilibrium neutron (Hi 88). Such a plot is a very useful guide to the reliability of the results, and should lie on a nearly straight line which is almost independent of mass.

Some of the results for $\nu_{pre}$ have been shown in Fig. 3.21. These data have been analyzed by modifying the code ALERT1 to include a fission delay time and to take account of saddle-to-scission emission as well as neutron emission during fragment acceleration (Hi 86); no account was taken of the reduction of $\sigma_{fis}$ arising from the finite value of $\tau_{fe}$. The results, based on good fits to fission and ER excitation functions with $a_f/a_\nu = 1.0$, $a_\nu = A/10$, the RLDM fission barriers, and allowing $k_f$ and $\delta L$ to vary, are that *all* of the data can be fitted well with $\tau_{ss} = 30\times10^{-21}$ s, or with $\tau_{fe} = 70\times10^{-21}$ s, or with $\tau_{ss} = \tau_{fe} = 20\times10^{-21}$ s. Changing $a_\nu$ to $A/8$ ($A/12$) increases (decreases) these times by a factor of $\sim 2$. The results for $\tau_{ss}$ were based on $E_x$ being the average of that at the saddle point and that for spherical fragments at scission. This is probably an overestimate. An-

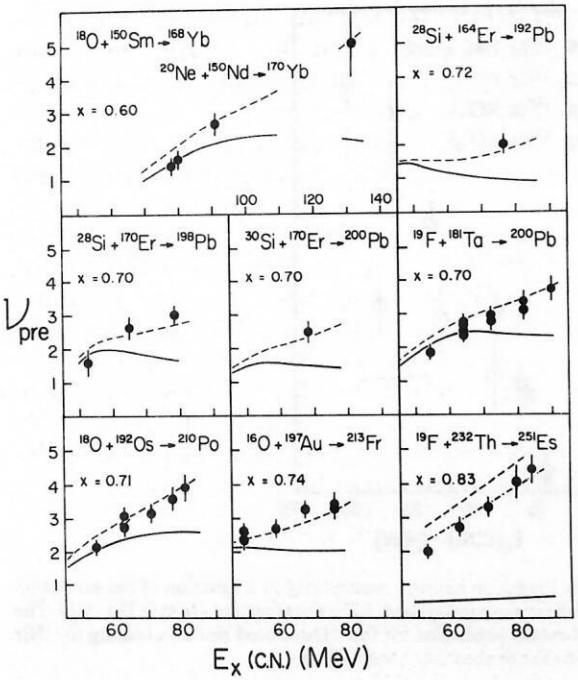


FIG. 3.26. Prefission neutron multiplicities as a function of excitation energy in the compound nucleus. The full curves are the results of statistical-model calculations (see text). The dashed lines show the effect of allowing neutron evaporation during a saddle-to-scission time of $30\times10^{-21}$ s. The result of neglecting the effect of neutron emission during fragment acceleration is shown by the dot–dash line in the $^{251}$Es panel; for other cases the reduction is much smaller (from Hi 86).

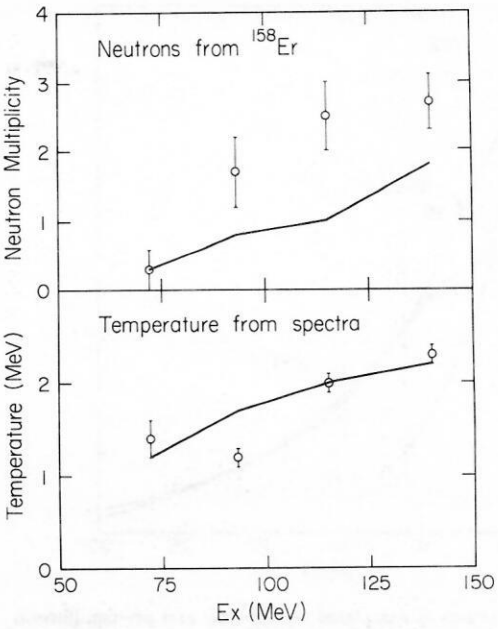


FIG. 3.27. Comparison between experimental results of the number of neutrons preceding fission and statistical-model calculations (full lines). The lower half of the figure shows a similar comparison for the temperature. The points, starting at the lowest excitation energy, refer to the reactions induced by $^{50}$Ti, $^{32}$S, $^{24}$Mg, and $^{16}$O, respectively (from Ga 87).

other extreme value would be to take $E_x$ at the saddle point, on the basis that most time is probably spent there. If this is done, $\tau_{ss}$ is increased by factors of $\sim2$ for $A\sim160$ to $\sim4$ for $A\sim250$. These long times correspond to overdamped motion of the nuclear fluid. The fits for $\tau_{ss}$ alone are shown in Fig. 3.26.

Newton *et al.* (Ne 88; see also Ga 86) have also considered how these viscous effects might affect the values of the parameters deduced from a standard statistical-model analysis. They point out that even in the region of low energy, when the shape of the $\nu_{pre}$ excitation function appears to be well described by the model calculation, a significant fraction of the observed $\nu_{pre}$ still comes from viscous effects. Hence the measured value should be reduced for use in a standard statistical-model analysis. This requires $a_f/a_\nu$ to be increased by $\sim0.02$ to reduce $\nu^s_{pre}$ and $k_f$ to be increased by $\sim0.04$ to bring $\sigma_{fis}$ back to its correct value. Likewise they indicate that the reduction in $\sigma_{fis}$ due to viscosity [see Eq. (4.10)] may require an increase in $a_f/a_\nu$ of up to $\sim10\%$, while temperature variations in $E_f(J)$ might require a reduction of about 5%. Thus, the experimentally derived values of $a_f/a_\nu$ and $k_f$ shown in Fig. 3.22 (and those from similar analyses) are much more uncertain than appear there. Until the theory for these effects is much more developed, accurate and physically meaningful values of the statistical-model parameters are not attainable.

Measurements of $\nu_{pre}$ at higher energies have been carried out at Oak Ridge (Ga 81, Ga 86, Ga 87), at the H.M.I., Berlin (Ho 83, Hi 89a, Ro 89, Za 86), and at Osaka (Hi 88, Hi 89c). Gavron *et al.* (Ga 86, Ga 87) have carried out a detailed study of the $^{158}$Er system formed in the reactions induced by 207-MeV $^{16}$O, 180-MeV $^{24}$Mg, 180-MeV $^{32}$S, and 216-MeV $^{50}$Ti on appropriate targets. They measured neutrons in coincidence with ER and fission fragments. For the $^{16}$O reaction a significant pre-equilibrium (PE) multiplicity ($\sim1$) was apparent. The neutron spectra in coincidence with ER were analyzed by assuming that the PE component came from a source moving with an average velocity $v_{PE}$, while the equilibrium (EQ) component's velocity was that of the compound system. The shapes of the neutron-energy ($\varepsilon$) spectra were given the arbitrary form $\varepsilon^\alpha\exp(-\varepsilon/T)$ in the appropriate center-of-mass frames, with $\alpha_{PE}=1.0$ and $\alpha_{EQ}=0.6$. Results were $T_{PE}=5.5\pm0.2$ MeV, $T_{EQ}=1.9\pm0.2$ MeV, $v_{PE}=1.4\pm0.2$ cm/ns. The values $v_{PE}$ and $T_{PE}$ were then used in a four-moving-source fit to the neutron spectra in coincidence with fission fragments, the extra sources being those of the moving fission fragments. Results are shown in Fig. 3.27 and compared with those from the code PACE2.

Blann and Remington (Bl 88) have drawn attention to the danger in using the commonly used moving-source method for separating EQ and PE spectra. They point out that it has little physical basis and might give sizable errors at low neutron energies. This is illustrated in Fig. 3.28 for the case of the $^{16}O+^{142}Nd$ reaction of Ga 87.

Hinde *et al.* (Hi 88, 89c) concluded that the results of Ref. Ga 87 were in error because their values of $\nu_{tot}$ lay well below those for other similar cases and from calculated expectations when plotted agains $E_x(f)$. They confirmed this expectation by making a measurement for the $^{16}O+^{142}Nd$ reaction at 178 MeV, shown in Fig. 3.29. Their result for $\nu_{pre}$ of $3.95\pm0.3$ (Hi 89c) is much higher than the value of $2.7\pm0.4$ (Ga 87) taken at considerably higher energy. As can be seen in Fig. 3.30, which shows values for $\nu_{pre}$ for a number of nearby systems, the apparent error in the Ga 87 results makes a much larger error in the values for $\Delta\nu_{pre}$, which are relevant to the determination of viscous effects.

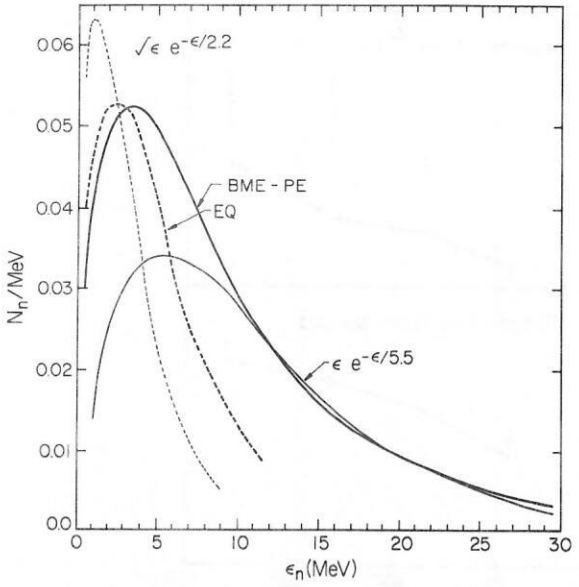


FIG. 3.28. Comparison of calculated equilibrium and pre-equilibrium neutron spectra for the $^{16}O + ^{142}Nd$ reaction. The heavy solid and dashed lines are the PE and EQ results of the Boltzmann master equation (BME); the thin solid curve is that used in Ref. Ga 87 to represent the PE result; the thin dashed line is the result of the indicated expression, similar to that used for EQ emission in Ref. Ga 87. It is seen that the $\varepsilon_n$ greater than $\sim 12$ MeV there is good agreement between the two approaches, but very bad agreement below this (from B1 88).

The data of Ga 87 have had the most detailed theoretical analysis of any (see Sec. 4), and this must have considerable implication on its conclusions.

Holub *et al.* (Ho 83) and Zank *et al.* (Za 86) have measured $\nu_{pre}$ for the systems $^{165}Ho + ^{20}Ne$ (220, 292, and 402 MeV), $^{141}Pr + ^{40}Ar$ (316 MeV), and $^{175}Lu + ^{12}C$ (192 MeV) leading to iridium nuclei. They have measured neutron spectra, in coincidence with ER and fission fragments,

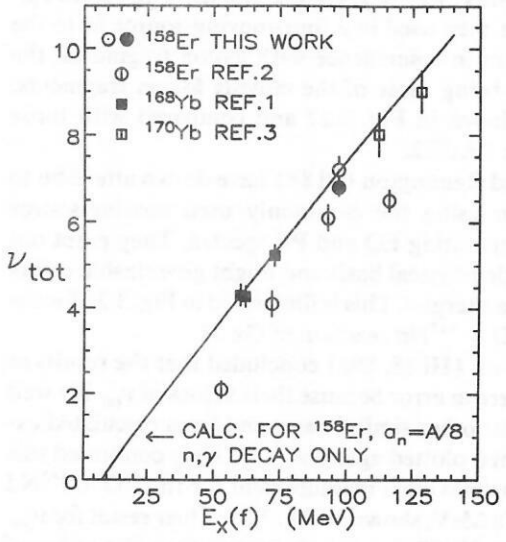


FIG. 3.29. Total neutron multiplicity shown as a function of available decay energy. The new result for $^{158}$Er (Hi 88) is shown by the filled circle, while the open circle just above it includes a correction of $0.42 \pm 0.15$ to account for charged-particle emission. The other results for $^{158}$Er are those of Ref. Ga 87 not corrected for charged-particle emission (see caption to Fig. 3.27 for identification). The data for $^{168}$Yb and $^{170}$Yb are from Refs. Hi 86 and Ga 81, respectively (from Hi 88).

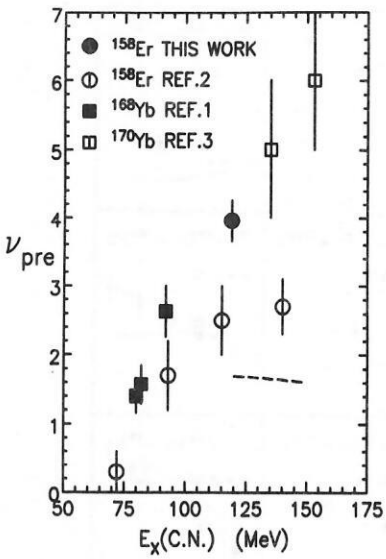


FIG. 3.30. Prefission neutron multiplicity as a function of the excitation energy of the compound system. References to data are as in Fig. 3.29. The statistical-model prediction for the $^{16}$O-induced reaction leading to $^{158}$Er is shown by the dashed line (from Hi 88).

and fission-fragment angular distributions. Significant PE-neutron emission was seen in all cases apart from the $^{40}$Ar-induced reaction. They analyzed the data with a four-moving-source method, somewhat more complex than that of Ga 86. An example of a fit to the neutron/fission data is shown in Fig. 3.31. They checked their results for $\nu_{tot}$ by making measurements with a $4\pi$ neutron detector. Again their values for $\nu_{pre}$ are well in excess of those predicted by a statistical-model code, though the $^{20}$Ne and $^{40}$Ar induced reactions predominantly fission from configuration for which $E_f(J) = 0$ and to which the statistical code cannot be correctly applied. The data were analyzed assuming saddle-to-scission emission, giving $\tau_{ss} = 14^{+35}_{-8}$, $60^{+45}_{-25}$ and $49^{+}_{-15}$

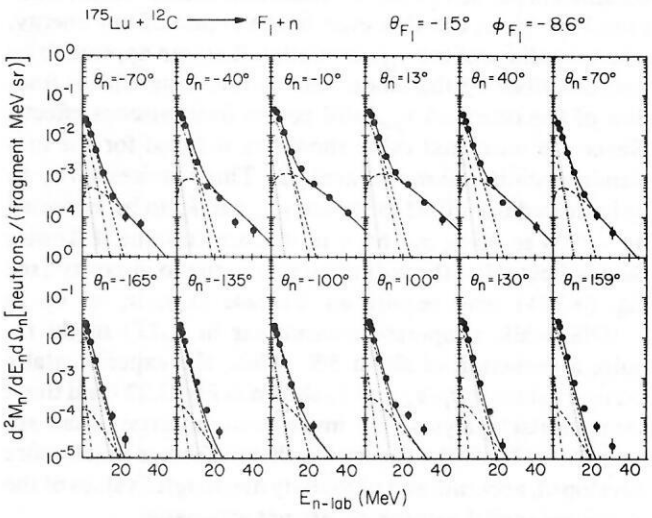


FIG. 3.31. An example of measured neutron energy spectra in coincidence with fusion–fission events for the reaction Lu + C. The lines represent the evaporative components from the system: the solid lines are the sums of all components; the short dashed lines are the components from the compound system before scission; the dot–dash lines and the dotted lines are the components from the detected and complementary fragments, respectively. A highly energetic pre-equilibrium component shown by the long dashed lines is also present (from Za 86).

$\times 10^{-21}$ s for the Ar, Ne, and C induced reactions, respectively (Za 86, Hi 87a).

The processes of fission without barrier and quasifission involve shorter lifetimes and wider mass distributions than compound-nucleus fission. When these lifetimes are less than the orbiting time of the system ( $\lesssim 10\times 10^{-21}$ s), it is possible to measure them from the mass–angle correlations (see, e.g., To 85, Sh 87). A comparison of lifetimes measured by the latter method and by $\nu_{\text{pre}}$ might be useful because of the difficulties in deriving absolute time values from $\nu_{\text{pre}}$.

During the time that the orbiting complex stays together there is a mass drift towards a symmetrical system. Therefore the more asymmetric mass splits correspond to shorter lifetimes. Measurements of $\nu_{\text{pre}}$ as a function of mass split may offer a way of studying this to somewhat longer times than orbiting periods. So far few attempts have been made. Hinde *et al.* (Hi 89c) studied the dependence of $\nu_{\text{pre}}$ on total kinetic energy and mass split for 215-MeV $^{20}$Ne + $^{232}$Th, which should result in little quasifission but considerable fission with $E_f(J) = 0$. Within errors they found $\nu_{\text{pre}}$ to be consistent with no dependence on mass split. They also claim to be able to observe shorter lifetimes for fission without barrier. Hilscher *et al.* (Hi 87b, Hi 89a) have studied the 838-MeV $^{32}$S + $^{144,154}$Sm reactions and found $\nu_{\text{pre}}$ smaller for asymmetric mass splits.

### 3.6.2. Systematics of $\nu_{\text{pre}}$ and $\nu_{\text{post}}$

The systematics of $\nu_{\text{pre}}$ as a function of compound-system excitation energy (Hi 89c) are shown in Fig. 3.32. There

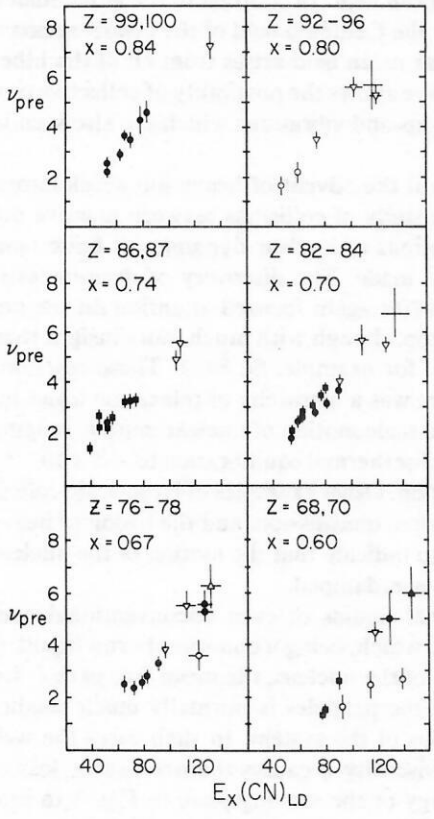


FIG. 3.32. Systematics of $\nu_{\text{pre}}$ as a function of the excitation energy above the liquid-drop ground state of the compound nucleus for systems with differing fissilities. Results for neighboring compound nuclei have been included in the plots as indicated. Data are from Refs. Ch 70, Ga 81, Ga 87, Hi 88, Hi 89a, Hi 89c, Ho 83, Ne 88, and Za 86 (from Hi 89c).

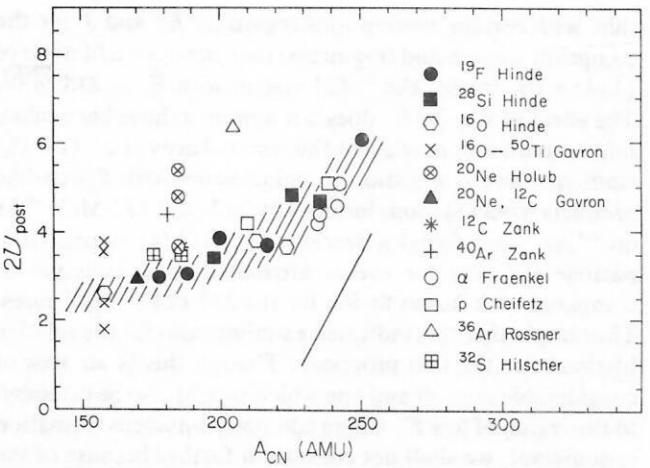


FIG. 3.33. Experimental postfission neutron multiplicities as a function of mass number. The data are from the references given for Fig. 3.31 plus Fr 75, Hi 89a, and Ro 88. The solid line represents the average number of neutrons emitted in spontaneous fission or thermal induced fission corrected for zero excitation energy (Va 73) (from Hi 87b).

is remarkable good consistency between the data of all the groups, apart from that of Ref. Ga 87. The data for systems of differing fissilities increase approximately linearly with $E_x$ and with roughly the same slope. The principal difference is that the intercept with $\nu_{\text{pre}} = 0$ increases with fissility; this may result in part from the corresponding increase of the $Q$ value for fission ($Q_{\text{fis}}$).

Hilscher *et al.* (Hi 87b) have pointed out that $\nu_{\text{post}}$ would be expected to be roughly constant if the prescission lifetimes were constant for all nuclei and independent of temperature. This is because the evaporation time decreases roughly exponentially with increasing excitation energy, so that the time taken to evaporate additional neutrons is small compared with that for emission of the last neutron prior to scission. Hence emission of this last neutron always takes place at approximately the same temperature. Of course, $\nu_{\text{post}}$ depends also on $B_\nu$ and $Q_{\text{fis}}$ for the particular system, so that $\nu_{\text{post}}$ would be expected to rise with increasing fissility. Values for $2\nu_{\text{post}}$ for a wide variety of systems are shown plotted against compound-nucleus mass in Fig. 3.33 and show reasonable agreement with this conclusion. They point out that investigation of any change in the prescission lifetime with temperature will be difficult because, even if the system is initially at very high temperature, it will spend little time there because of the very short evaporation times. They also emphasize the rather constant and low temperatures at the scission point which, for example, are relevant to the calculations with the scission-point model.

### 3.6.3. Measurements of prefission protons and α particles

A number of measurements of $\pi_{\text{pre}}$ and $\alpha_{\text{pre}}$, mostly at high ($\sim$10 MeV/nucleon) bombarding energies with medium-heavy projectiles, have been carried out (Br 88, Du 83, Du 84, La 88, Mo 87a, Sh 84). In contrast to $\nu_{\text{pre}}$, the proton and $\alpha$ multiplicities are small ($\sim$0.1). Further, interpretation of the data to obtain fission lifetimes is difficult because of the considerable uncertainties involved with the transmission coefficients for hot deformed shapes, a topic of great interest in itself. Scad *et al.* (Sh 84) have observed the shadowing effect produced by one fission fragment on $\alpha$ emission from the other, and so deduced the fragment lifetime. From

this, with certain assumptions regarding $E_x$ and $J$ for the composite system and fragments, they deduced a lifetime of $(1–3)\times10^{-20}$ s for the $^{143}$Gd system with $E_x = 218$ MeV. The effect of $\nu_{pre}$ on $E_x$ does not appear to have been taken into account and may affect the result. Lacey *et al.* (La 88) studied $\pi$ and $\alpha$ emission in coincidence with fission-like products from reactions induced by 247- and 337-MeV $^{40}$Ar on $^{nat}$Ag. They found a decrease of 1/2(1/4) in prefission particle emission for events attributed to quasifission as compared with fusion fission for the 337 (247) MeV cases. They imply that this indicates a similar ratio for the relative lifetimes for the two processes. Though this is an area of considerable interest and one which should also be extended to the region of low $E_x$ where compound-nucleus formation is dominant, we shall not consider it further because of the many uncertainities in lifetime determination.

#### *3.6.4. Measurement of giant-dipole $\gamma$ rays*

An interesting measurement has recently been carried out by Thoennessen *et al.* (Th 87), who observed $\gamma$ rays in coincidence with fission fragments from the $^{16}O + ^{208}Pb$ reaction. The $\gamma$ rays were detected in a 25.4 cm$\times$38.1 cm NaI(Tl) detector placed collinearly with two of four fission detectors, each separated by 90° in the plane perpendicular to the beam direction. The results, shown in Fig. 3.34, indicate that there is a large discrepancy between the observed results and those calculated with the modified statistical-model code CASCADE for the region $8 < E_\gamma < 12$ MeV. Note that the GDR energy is lower for the compound system than for the fragments. The discrepancy can be removed if the intensity of the prefission $\gamma$ rays is increased 3–4 times over that predicted with use of the GDR sum rule, which fits other cases well (Sn 86). The authors attribute this to a hindrance of the fission degree of freedom in the early decay steps, i.e., $\tau_p \leqslant \tau_{fe}$, and include this effect in their CASCADE code giving excellent fits. However, they do not appear to consider the possibility that some or all of the excess $\gamma$ rays may originate during the saddle-to-scission transition. From these and from the yields at 0° and 90° they deduce that the prefission $\gamma$ rays arise from a prolate system with a deformation $\beta \simeq 0.33 \pm 0.06$. Unfortunately there is some doubt (Hi 89b) regarding the ER cross sections and consequent statistical-model parameters (Vu 86) on which the above analysis has been based. It would be of considerable interest to repeat this after remeasuring $\sigma_{ER}$ and also taking into account the $\nu_{pre}$ measurements for this system which are now available (Hi 89b). Measurement of giant-dipole $\gamma$ rays should prove a valuable addition to our methods of studying dissipative effects in fission. Study of systems lighter than $^{224}$Th may be in some respects easier because of smaller $Q_{fis}$ and the consequent larger ratio of pre- to post-fission $\gamma$ rays.

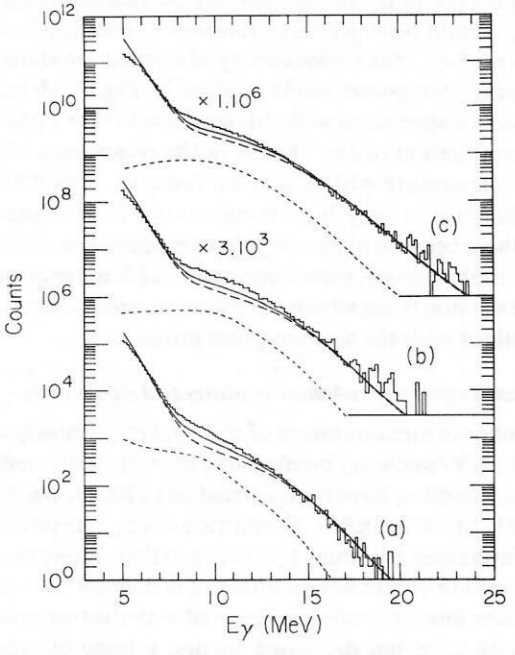


FIG. 3.34. Experimental $\gamma$ spectra measured in the reaction $^{16}O + ^{208}Pb$ at (a) 100, (b) 120, and (c) 140 MeV. Calculated prefission (short dashed lines), postfission (long dashed lines), and total (solid lines) $\gamma$ spectra, calculated with the code CASCADE, are shown (from Th 87).

## 4. NUCLEAR DYNAMICS AND DISSIPATION

The dynamics of fission is one of the more challenging topics in nuclear-structure physics at the present time. It involves the study of a unique superdense quantum Fermi liquid with a finite number of constituents, of its conservative potentials and dissipative processes. For excellent discussion of the basic physics, see Refs. Bj 85, 86. Although there was early interest in the liquid-drop model of the nucleus, this interest waned for many years, partly because of the great success of the shell and related models applied to nuclear spectroscopy. These models were applied mainly to nuclei with zero or very low temperatures. They take the nucleons to move almost independently, apart from pairing correlations, in a mean field. In contrast to the atom, which is held together by the Coulomb field of the massive central nucleus, the nuclear mean field arises from all of the other nucleons. It therefore allows the possibility of collective motion such as rotations and vibrations which are also seen in liquid drops.

It was not until the advent of heavy-ion accelerators, which allowed the study of collisions between massive nuclei, that investigations of nuclear dynamics at finite temperatures could be made. The discovery of deep-inelastic collisions in the 1970's again focused attention on the nucleus as a liquid drop, though with much more insight than in the 1930's (see, for example, Sc 84a). These reactions indicated that there was a hierarchy of relaxation times involved in this large-scale motion of nuclear matter, ranging from $\sim 4\times40^{-22}$ s for thermal equilibration to $\sim 5\times10^{-21}$ s for mass equilibration. Other examples of large-scale collective motion are fission, quasifission, and the fusion of heavy nuclei; all appear to indicate that the motion of the nuclear fluid is creepy and overdamped.

In conventional liquids or even unconventional ones such as liquid $^3$He, which, being a quantum Fermi liquid, is the nearest analog of the nucleus, the mean free path $\lambda$ for collisions between the particles is normally much smaller than the dimensions of the system. In such cases the well known two-body viscosity $\eta$ causes the irreversible loss of the collective energy of the moving plate in Fig. 4.1a into thermal energy. Taking $\eta$ from the kinetic theory of gases, the rate of energy loss per unit area is given by

$$\frac{dE}{dt} = \eta \frac{U^2}{d} \simeq \frac{1}{3} \rho \bar{c} \frac{\lambda}{d} U^2, \tag{4.1}$$

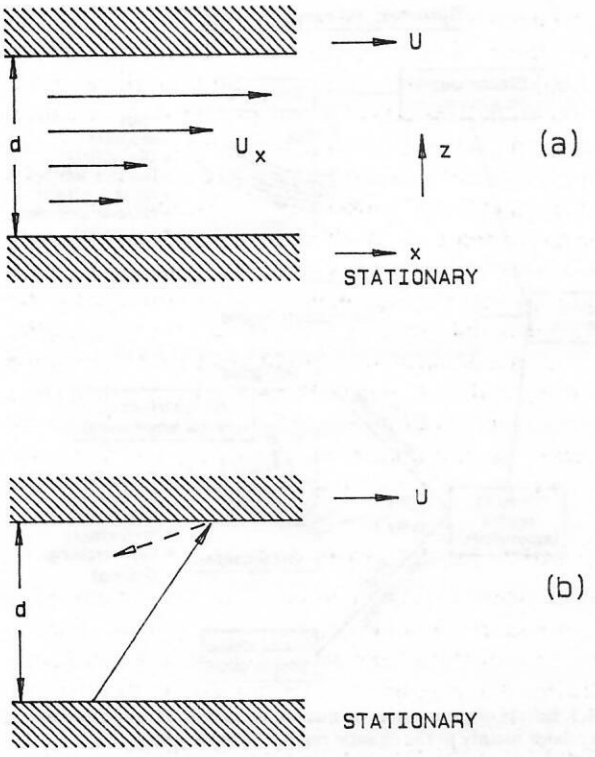


FIG. 4.1. Simple illustration of two extreme forms of dissipation leading to loss of collective energy of the top plate moving with velocity $U$. (a) Conventional two-body viscosity. The horizontal lines indicate the velocities at various points in the gas. A linear velocity gradient $dU_x/dz$ is assumed. (b) One-body dissipation. The full line shows the trajectory of a particle, emitted from the bottom plate, which hits the moving top plate, sticks to it, and is later emitted in a random direction (dashed line).

where $\bar{c}$ is the average velocity of the particles and $\rho$ is the density. For a system of Fermi particles, collisions are inhibited by the Pauli principle, so that $\lambda$ decreases with temperatures as $\sim T^{-2}$, whereas $\bar{c}$ is roughly independent of $T$; hence $\eta$ and $dE/dt$ vary as $T^{-2}$ as observed in bulk liquid $^3$He (Wi 67). The total dissipative loss in a system is given by a volume integral over the square of the velocity gradients.

In contrast to liquid $^3$He, the nucleus contains only a small number of constituents and $\lambda$ is significantly greater than nuclear dimensions, so that dissipation through two-body collisions inside the nucleus become small. Dissipative energy loss can also be caused by collisions with the surface as in a Knudsen gas. A simple illustration of this "one-body dissipation" is given in Fig. 4.1b. The important assumption for this process is that when a particle hits either plate, it first sticks to the plate and is then emitted in a random direction with a velocity distribution appropriate to the temperature of that plate; it is essential that the particle loses all memory of hitting the moving plate before it hits it again. Under these conditions, *on the average* each particle of mass $m$ transfers momentum $-mU$ to the moving plate. Hence

$$dE/dt \simeq (1/4)\,\rho\bar{c}U^2, \tag{4.2}$$

which is approximately independent of $T$. In a nucleus the collisions are with the moving "walls" of the nuclear surface. The dissipative loss is given by a surface integral over the squares of velocity components perpendicular to the surface, quite different from that for two-body dissipation. Because of this, the type of "viscosity" which is operative has a profound effect on the dynamics of nuclear collective motion. This is illustrated in Fig. 4.2., which shows scission-point shapes calculated by Blocki *et al.* (Bl 78). Note that two-body (one-body) dissipation gives more (less) stretched-out shapes than zero viscosity. This is because the system tries to minimize velocity gradients for two-body viscosity, while for the one-body case it tries to minimize the number of nucleons which can cross between the two moving "walls."

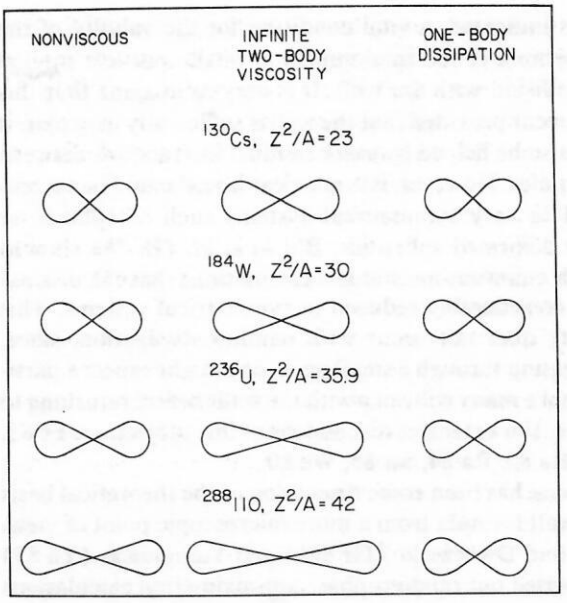


FIG. 4.2. Effect of dissipation on the scission shapes for the fission of four nuclei with $J = 0$. The reference shapes for nonviscous flow are shown in the first column, while the other columns show the shapes for infinite two-body viscosity and for one-body dissipation (from Bl 78).

The theory of one-body dissipation was developed by Swiatecki and collaborators, originally on the basis of classical kinetic theory (Bl 78, Ra 84). They derived the wall formula [similar to Eq. (4.2)], applying to nuclear shapes with little or no neck, and the window formula for necked-in shapes. If we denote the two elements of the necked-in shape by $A$ and $B$, the area of the neck or window between them by $\Delta\sigma$, and the velocity of $B$ relative to $A$ by $\mathbf{u}$, then the window formula for the dissipative force on $A$ due to $B$ is

$$\mathbf{F}_{BA} = (1/4)\,\rho\bar{c}\Delta\sigma\,(2\mathbf{u}_{\parallel} + \mathbf{u}_{\perp}), \tag{4.3}$$

Here $\mathbf{u}_{\parallel}$ and $\mathbf{u}_{\perp}$ are the velocity components along and at right angles to the normal to $\Delta\sigma$. Note that this force is not in general parallel to $\mathbf{u}$, the coefficient for normal friction being twice that for tangential friction. Also, the dissipative mechanism is not reflection from the surface but transfer of particles between the two drops $A$ and $B$ in relative motion. The window formula really applies to systems with very small necks. In the intermediate situation with larger necks both the wall and window mechanisms should be operative, but a satisfactory way of treating this case has not been developed. So far only simple *ad hoc* interpolations between the two extreme regimes have been used (see, e.g., Bl 86), but attempts are being made to solve this problem on the basis of linear response theory (Ko 77, Do 87). The one-body mechanism does predict that the nuclei do exhibit very high viscosity and overdamped motion, as is required by the data on deep-inelastic collisions.

As indicated, a vital condition for the validity of the wall formula is the randomization of the particle motion after collision with the wall. It is easy to imagine that this might occur provided that the wall is sufficiently irregular; it might also be helped by *weak* residual interactions between the particles. However, it is not clear how it could be accomplished in very symmetrical systems such as spheres or weakly deformed spheroids. Blocki *et al.* (Bl 78) showed through quantum-mechanical calculations that the dissipation is considerably reduced in symmetrical systems. This difficulty does not occur with window dissipation, since, after passing through a small neck, one might expect a particle to make many collisons with the walls before returning to the neck. For extensive discussions of this subject, see Fe 85, Fe 87, Ra 80, Ra 84, Sw 85, We 80.

There has been come discussion of the theoretical basis of the wall formula from a more microscopic point of view. Griffin and Dworzecke (Gr 86a) and Yannouleas (Ya 85) have carried out random-phase approximation calculations for the damping of giant resonances, which indicate that for these cases the simple wall formula overpredicts the one-body dissipation by about ten times. They also imply that this result should be general and suggest that surface-dominated two-body dissipation may play a significant role; the Pauli principle, which suppresses collisions in the interior, is not effective in the surface region. Fiolhais (Fi 86) concludes that one-body damping is not appropriate for low-multipolarity giant resonances, but is appropriate to describe dissipation involving distortions of high multipolarity such as occur in fission and heavy-ion reactions. Reinhard *et al.* (Re 86b), who used dissipative adiabatic mean-field theory, report that one-body dissipation vanishes under certain conditions. Much more work needs to be done to gain a real understanding of dissipative mechanisms in nuclei. It does seem clear that the wall formula overestimates the damping for cases with high symmetry. Further, even if a substantial part of the dissipation does arise from two-body interactions in the surface, the wall formula multiplied by a strength parameter does provide a useful phenomenological tool (Gr 86a, Ni 86, Ni 87). An indication, due to Swiatecki (Sw 85), of some of the possible effects of symmetries on the dynamics is shown in Fig. 4.3. The wall formula applies to the higher-temperature (chaotic) regime, while the zero-temperature (ordered) regime is dominated by symmetries. Neither this nor the intermediate regime have yet been properly addressed and remain challenging problems for future study.

So far we have assumed that the meaning of dissipation, viscosity, or friction in nuclei is obvious. However, this is very far from the case. In the case of a sphere injected into a viscous liquid with zero gravity and velocity $u_0$ the velocity at time $t$ will be given by applying Stokes's law

$$u(t) = u_0 \exp[-t/(M/6\pi\eta R)] = u_0 \exp(-t/\tau), \quad (4.4)$$

where $M$ and $R$ are the mass and radius of the sphere and $\tau$ is a relaxation time. The velocity and kinetic energy tend to zero with increasing $t$, and the probability of the sphere ever regaining the velocity $u_0$ is essentially zero. In this case the essentially infinite heat sink, with which the sphere is in contact, takes up its initial collective energy.

The nucleus is a completely isolated system with a small number of constituents, and the situation is entirely different. It is more analogous to that for Brownian motion in

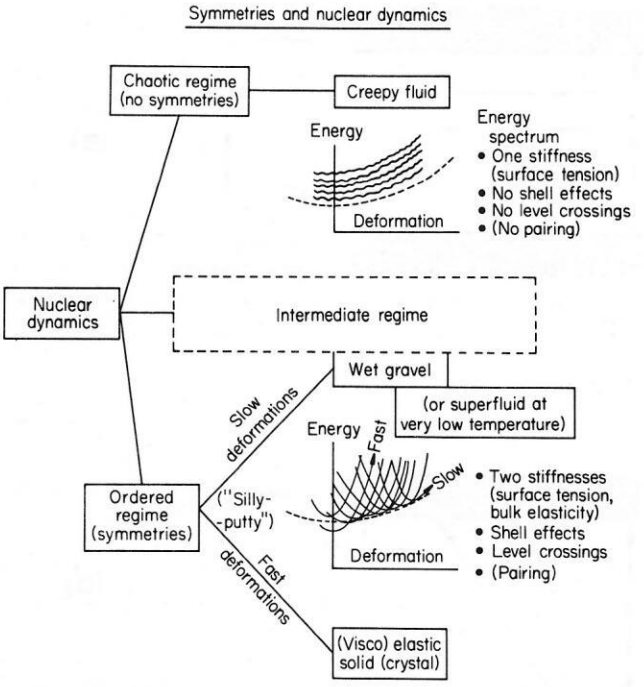


FIG. 4.3. Effects of symmetries on nuclear dynamics. Heavy-ion induced fission relates mainly to the chaotic regime (from Sw 85).

which a small particle of mass $M$ is kicked around by irregular collisions with the fluid molecules of mass $m \ll M$. The particle makes a random walk in normal space and is subject to a fluctuating force (Fig. 4.4)

$$\mathbf{F}(t) = \langle \mathbf{F}(t) \rangle + \delta\mathbf{F}(t). \quad (4.5)$$

Experience tells that often $\langle \mathbf{F}(t) \rangle = -\xi \mathbf{u}(t)$, where $\xi$ is a friction coefficient. The fluctuating force has the properties that its average value is zero and that its correlation function is given by

$$\langle \delta F_i(t)\, \delta F_j(t) \rangle = 2D\delta_{ij}\delta(t-s), \quad i, j = 1, 2, 3. \quad (4.6)$$

The quantity $D$ is related to the strength of the fluctuating force, and $\delta(t-s)$ is sharply peaked around $t=s$ with a characteristic width $\tau_m$ related to the time between collisions with the Brownian particle. The equation of motion

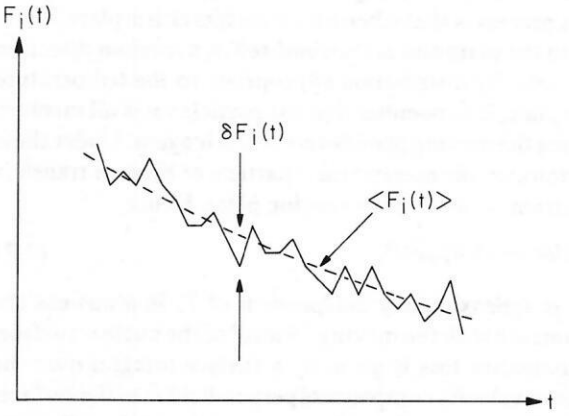


FIG. 4.4. Sketch of a component of the fluctuating force, which is decomposed into a mean (dashed line) and fluctuating part (from Fe 87).

(Langevin equation) is

$$M \frac{d}{dt} \mathbf{u}(t) = -\xi \mathbf{u}(t) + \delta \mathbf{F}(t). \tag{4.7}$$

One solution to this is

$$\langle \mathbf{u}(t) \rangle = \mathbf{u}_0 \exp\left[-t/(M/\xi)\right], \tag{4.8}$$

which shows that the average collective velocity $\langle \mathbf{u}(t) \rangle$ tends to zero with a relaxation time $M/\xi$. However, the mean kinetic energy *does not* tend to zero, as the particle is still being kicked around. It can be shown that

$$\left\langle \frac{M}{2} [\mathbf{u}(t)]^2 \right\rangle = \frac{M}{2} \mathbf{u}_0^2 \exp\left(-\frac{2\xi}{M} t\right) + \frac{3}{2} \frac{D}{\xi} \left[1 - \exp\left(-\frac{2\xi}{M} t\right)\right]. \tag{4.9}$$

For $t \to \infty$ this gives the value $\frac{3}{2}(D/\xi)$ for the thermal energy of the particle, which has now lost its initial collective energy $\frac{1}{2}Mu_0^2$. From classical equipartition we expect the thermal energy to be $\frac{3}{2}T$ (Boltzmann's constant = 1). Hence

$$D = T\xi. \tag{4.10}$$

This is a simple form of the Einstein relation, which relates the friction coefficient, temperature of heat bath, and the strength of the fluctuating force. Note that in some sense $D$ represents the strength of the interaction between the collective and thermal modes; if $D = 0$, there is no interaction and no friction. The Brownian motion of a particle which at time $t_1$ has velocity $u_1$ results in a diffusion-like process in velocity space as illustrated in Fig. 4.5. The mean value tends to zero, and the probability distribution widens with time.

Because it involves the fluctuating force $\delta F(t)$ the Langevin equation is not easily soluble with analytical methods, though it can be solved by numerical trajectory computations (Ab 86). For this reason it has been more usual in nuclear applications to use the classical Fokker–Planck equation (FPE), which can be derived from the Langevin equation under certain assumptions. An important one is that the process is Markovian, i.e., that $\tau_m \ll \tau_{\text{col}}$, where $\tau_{\text{col}}$ is the typical time for the collective motion.

Though dissipative phenomena in nuclei do resemble those of Brownian motion, there are significant differences which make the solution of the nuclear problem a much more delicate matter. The ratio $M/m$ is only $\sim 10^2$ for the nucleus, compared with $\sim 10^{20}$ for Brownian motion; therefore large fluctuations and strong friction forces are expected [Eq. (4.10)]. The probability of building up collective motion from a nucleus which initially has only thermal excitation is certainly not zero as it was for the sphere in the viscous liquid. The nucleus is isolated with a small number of constituents, and the various relaxation times are not greatly different. For further details of this complex subject, see the excellent reviews of Weidenmüller (We 80) and Feldmeier (Fe 85, 87), which we have mainly followed in this brief introduction, and for a discussion of the possible effects of quantum mechanics on classical transport equations (Sa 87a).

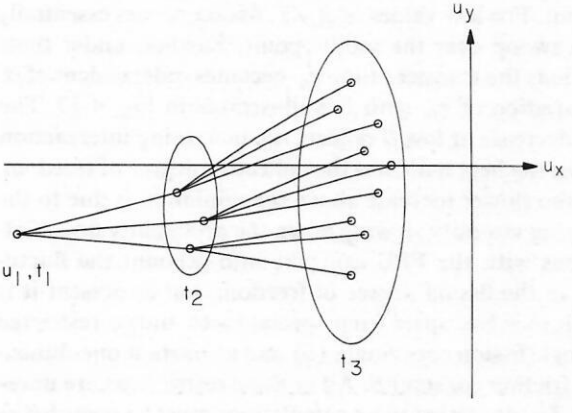


FIG. 4.5. Markovian diffusion in velocity space of a Brownian particle with initial velocity $u_1$ at time $t_1$ (from Fe 87).

#### 4.1. Application of dissipation theory to fission

The study of deep-inelastic collisions has given much information on nuclear dissipation. However, it relates to nearly grazing collisions where the dinucleus is connected by a small neck. There is little mass transfer on average, and the interpretation of the data, although indicating high dissipation, is ambiguous. The study of dissipation in fission and quasifission is of great interest because it should throw light on dissipation in mononuclear systems and perhaps give information on the effects of symmetries, particularly in the period before the saddle point is reached.

The systematics of fission-fragment kinetic energies together with the $\nu_{\text{pre}}$ data, which appear to require overdamped motion, support the hypothesis of one-body rather than two-body dynamics. The kinetic energies result from the Coulomb energies and fragment velocities at scission together with a small contribution from rotation. As seen in Fig. 4.2, scission shapes for two-body viscosity are more stretched out and hence have lower Coulomb energy than those for one-body friction. However, by arbitrarily choosing a low value for the two-body viscosity, corresponding to $\sim 30\%$ of critical damping, it is possible to get sufficient kinetic energy at scission to give an excellent fit to the experimental data; a good fit can also be obtained with one-body dissipation (Si 80). Kinetic energies are sensitive to viscosity only for systems with $Z \gtrsim 80$ because the difference between the saddle and scission shapes for lighter nuclei is relatively small. Perhaps one should not take too seriously the *exact* correspondence between calculations and the data because of the various approximations which have to be made. Nevertheless the fact that a good fit can be obtained with one-body theory without major parameter adjustment is encouraging. Recently, however, Nix and Sierk (Ni 87) have applied their surface-plus-window dissipation model to this problem and find that the strength of the simple wall formula has to be reduced by factors of $k_s \sim 0.5$ for lighter systems to $\sim 0.2$ for the heaviest, in order to get a good fit. Possibly this is an indication that symmetries really do cause a reduction in the wall-formula result, since the heavier the nucleus, the more nearly does the saddle point approach the spherical shape. On the other hand, if this were so, one might expect $k_s$ to be a function of the shape of the evolving system. The calculated evolution in time of the nuclear shape after passing the saddle point is illustrated in Fig. 4.6. Notice that $\tau_{ss}$ is roughly proportional to $k_s$ in this case, probably because the system appears to spend most of its time near the

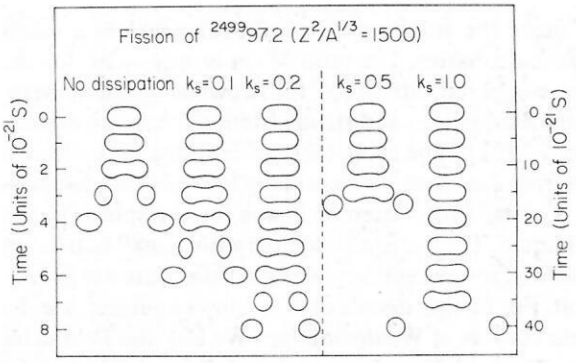


FIG. 4.6. Effect of surface-plus-window dissipation of the dynamical evolution beyond its saddle point of a nucleus, with $Z^2/A^{1/3} = 1500$ in Green's valley of stability and with $J = 0$; the nuclear temperature is taken to be 2 MeV (from Ni 87).

saddle point, as might be expected, since the driving force is least there.

Kramers (Kr 40) was the first to apply a one-dimensional FPE to nuclear fission. He deduced that the stationary value of $\Gamma_{fk}$ (the flow over the barrier) after the Boltzmann distribution at the saddle point has built up ($t \gg \tau_{fe}$) is given by (for $\beta \gtrsim \omega_0/10$)

$$\Gamma_{fk} = \Gamma_f^{BW} \{[1 + (\beta/2\omega_0)^2]^{1/2} - \beta/2\omega_0\}, \qquad (4.11)$$

where $\beta$ is the "reduced frictional constant" (Ha 84), $\omega_0$ is the frequency of the inverted oscillator which osculates the nuclear potential at the saddle point, and $\Gamma_f^{BW}$ is very close to the statistical-model width for fission decay. Note that $\beta$ is related to the $\xi$ of Eq. (4.7) by $\beta = \xi/M$ and has the dimensions $s^{-1}$. The result has been extended to $n$-dimensions (We 84, Zh 83). For critical damping $\gamma = \beta/2\omega_0 = 1$. Substantial reductions on $\Gamma_f^{BW}$ occur because the viscosity reduces the flow over the barrier; e.g., for $\gamma = 1$, we have $\Gamma_{fk} = 0.41\Gamma_f^{BW}$. This is illustrated in Fig. 4.7, which shows that an increasing proportion of the flux at the saddle point returns to the equilibrium deformation as $\gamma$ increases. It also emphasizes the large fluctuations which occur in the Brownian-type diffusion and the fact that quantities such as $\tau_{ss}$ are only average values.

Grangé, Weidenmüller, and collaborators have treated

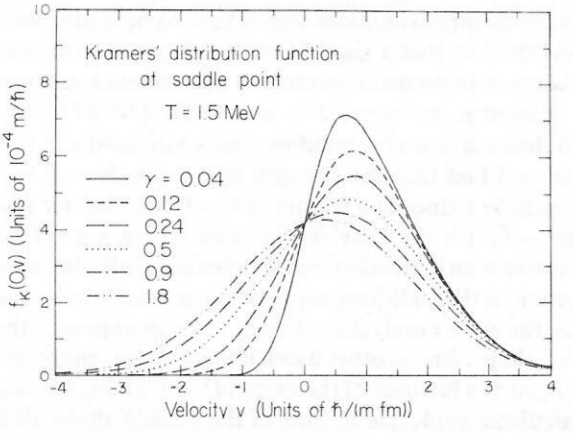


FIG. 4.7. Distribution $f_k(0,v)$ in velocity at the saddle point corresponding to Kramers' stationary solution, for various values of the dissipation strength $\gamma$ (from Ni 84).

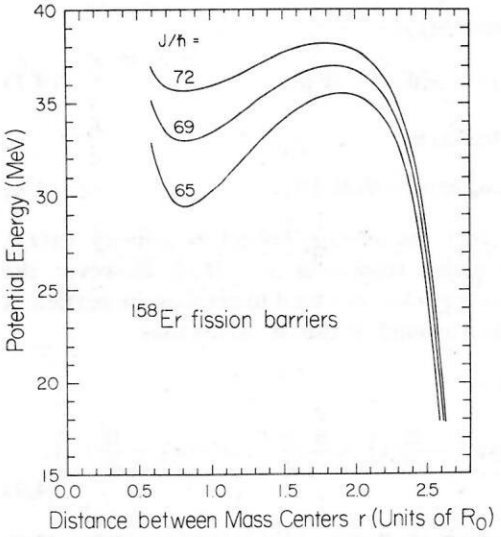


FIG. 4.8. Potential energy as a function of the distance $r$ between the centers of mass of the two halves of the dividing nucleus $^{158}$Er for three angular momenta. The zero of potential energy is taken as that for the nonrotating spherical nucleus, while $R_0 = 1.6 \times (158)^{1/3}$ fm = 6.27 fm (from Gr 86).

the time evolution of the classical probability density at the saddle point by means of the FPE in the two-dimensional phase space of the deformation degree of freedom $q$ and its associated velocity $p$ (Bh 86, Da 87, Gr 80, Gr 83, Gr 86, Ha 84, Ha 86a, La 86, We 84, We 84a, Zh 83). They have related this to the number of neutrons emitted before the saddle point is reached. For a review, see Ref. We 87.

To solve this problem correctly would require a dynamical calculation from the time that the projectile and target made contact until the saddle point is reached. This task has not yet been attempted, and it has been assumed that at $t = 0$ the nucleus starts off with the fission degree-of-freedom cold and a Gaussian distribution of $p$ and $q$ centered at the first minimum (equilibrium deformation) of the static nuclear potential $V(q)$; the widths in $p$ and $q$ are approximately related to the zero-point motion in $V(q)$. Examples of $V(q)$ are shown in Fig. 4.8, and of the development of the fission decay rate as a function of time in Fig. 4.9. Notice in the latter, undertaken for $E_f = 4$ MeV, that the decay rate overshoots the asymptotic value of Kramers for $T = 5$ MeV, i.e., when $E_f < 1$. This is an indication that transient effects are beginning to dominate and that there is no meaning in talking of the build-up of the Boltzmann distribution at the saddle point. For low values of $E_f/T$, fission occurs essentially in one swoop over the saddle point. Further, under these conditions the transient time $\tau_{fe}$ becames independent of $\beta$. The variation of $\tau_{fe}$ with $\beta$ is illustrated in Fig. 4.10. The sharp decrease at low $\beta$ reflects the increasing intereaction between the heat bath and the collective degree of freedom, while the slower increase above the minimum is due to the increasing viscosity slowing down the probability flow. Calculations with the FPE can take into account the fluctuations in the fission degree of freedom, but at present it is difficult to solve, apart from special cases, unless restricted to a single fission coordinate ($q$) and a constant one-dimensional friction constant $\beta$. All of these restrictions are unrealistic. To this extent these calculations must be regarded as schematic.

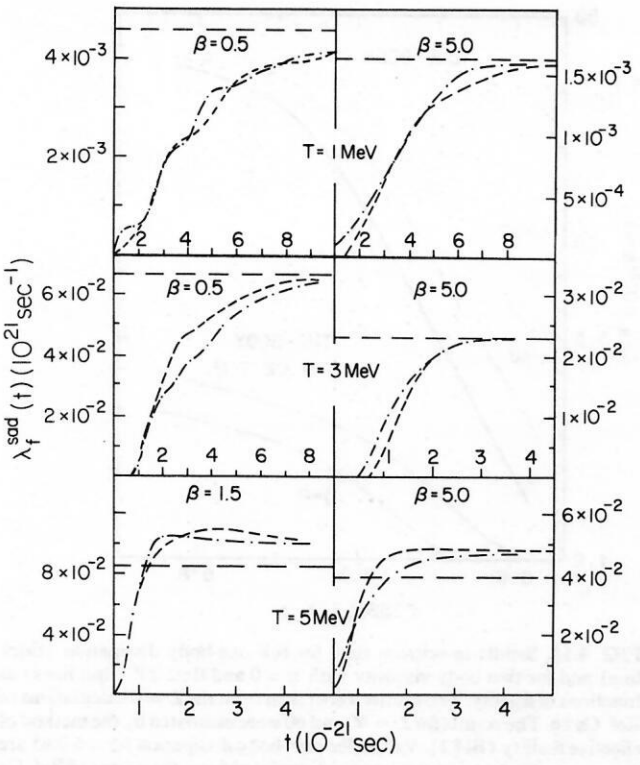


FIG. 4.9. The fission rate $\gamma_f(t)$ (in units of $10^{21}$ s$^{-1}$), evaluated at the saddle point for a nucleus with $A = 248$ and $E_f = 4$ MeV, as a function of time for various friction constants. The left-hand (right-hand) side of the figure corresponds to underdamped (overdamped) motion of the collective variable in the potential pocket. The dashed curves are the results of numerical calculations, and the dash–dot curves of analytical approximations. The horizontal dashed lines give the quasistationary values of Kramers (from Bh 86).

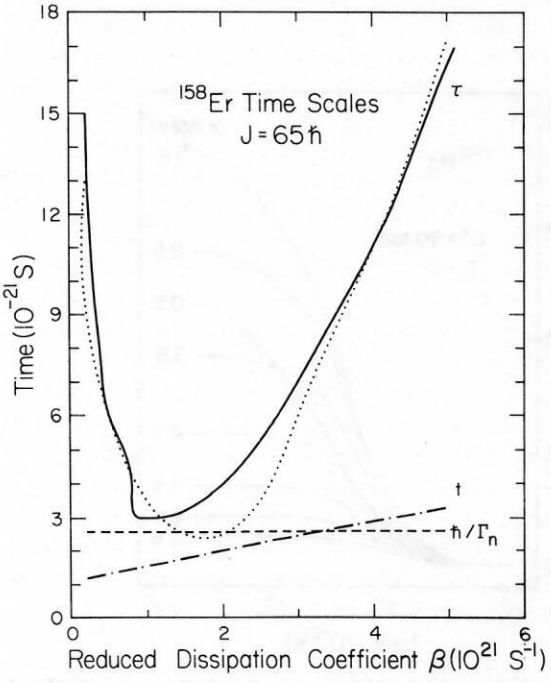


FIG. 4.10. Time scale of various processes as a function of friction coefficient. Curves marked $\tau$ are the transient time. The solid and dotted lines are the results of a solution of the Fokker–Planck equation and an analytical approximation to it, respectively. The dot–dash line ($t$) represents the saddle–to–scission time, and $\hbar/\Gamma_n$ is the average emission time of the first neutron (from Ga 87).

The most detailed theoretical analysis of $\nu_{pre}$ data has been carried out by Grangé *et al.* (Gr 86) and Gavron *et al.* (Ga 87) on the four reactions leading to $^{158}$Er (Ga 86,87). They have calculated $\nu_{pre}$ utilizing the ideas above, either by the numerical solution of coupled equations (Gr 86) or with the Monte-Carlo statistical code PACE2, which was modified to take them into account and included the RFRM fission barrier (Ga 87). Neutron emission during the saddle-to-scission transition was also included with the aid of an analytical expression deduced by Nix *et al.* (Ho 83b, Ni 84) using the Fokker–Planck equation. The potential $V(q)$ (Fig. 4.8) at the equilibrium and saddle points for a given $J$ was calculated as in Si 86, while those between the equilibrium and saddle point were deduced on the assumption that the shapes were the equilibrium configurations for larger values of $J$. Beyond the saddle point the shapes were generated by following the nondissipative dynamical evolution of the rotating nucleus constrained to be axially symmetric (Si 80). Various analytical approximations to results from Fokker–Planck calculations were used (Bh 86, Gr 83) to give values for the "transient time" $\tau$, defined as the time taken to reach 90% of the Kramers stationary flow.

The calculations used the statistical-model parameters deduced in Ref. Pl 83, with the exception of $a_f/a_\nu$, which had to be increased to bring the calculated values of $\sigma_{fis}$ into agreement with experiment; both the Kramers correction and $\tau_{fe}$ reduce $\sigma_{fis}$ (see Fig. 4.11). A comparison of calculated and experimental results for the $^{16}O + ^{142}Nd$ case is shown in Fig. 4.12. The $^{24}$Mg and $^{32}$S induced reactions exclude the region of low $\beta$, and the authors claim that the results indicate that $\beta \sim 6\times10^{21}$ s$^{-1}$ (Ga 87), a value 2–3 times that required for critical damping. A higher value would be required if the experimental results of Ga 87 are too low as indicated by Refs. Hi 88, Hi 89c. For the $^{16}$O-induced reaction, $\beta \sim 6\times10^{21}$ s$^{-1}$ implies that $\tau \sim (20\text{–}30)\times10^{-21}$ s

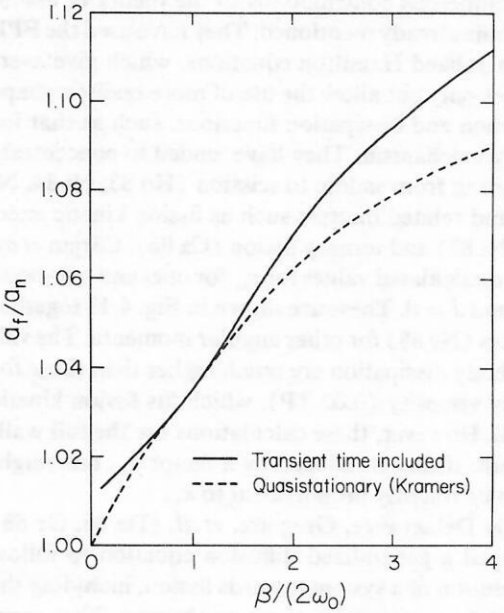


FIG. 4.11. Dependence of $a_f/a_\nu$ on $\gamma = \beta/2\omega_0$ determined from fitting the low-energy fission probability. The dashed curve gives the result when Eq. (4.10) alone is taken into account. Note that the greatest effects of the transient time occur when it is greatest, i.e., when $\beta$ is large or small (see Fig. 4.10) (from Gr 86).

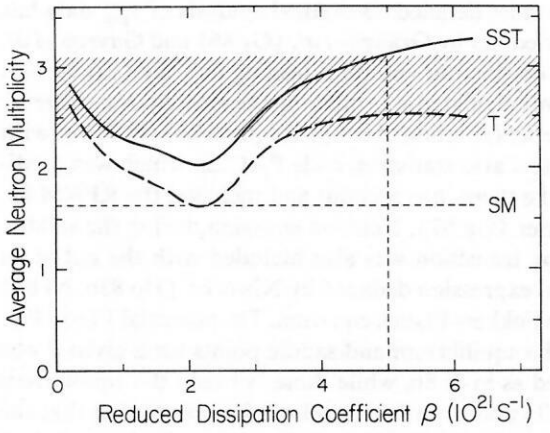


FIG. 4.12. Average neutron multiplicity $\nu_{pre}$ for the 207-MeV $^{16}O + ^{142}Nd$ reaction as a function of dissipation strength $\beta$. The curves labeled SM, T, and SST refer to calculations with the statistical model, calculations including transients, and including both transients and saddle-to-scission time, respectively. The experimental result of Ref. Ga 87 is shown by the shaded band, whose intersection with the solid curve determines the upper limit to $\beta$ indicated by the vertical dashed line (from Gr 86).

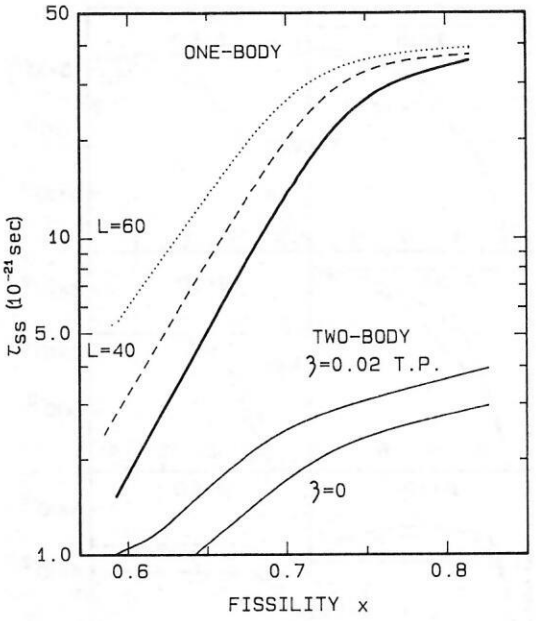


FIG. 4.13. Saddle-to-scission time for full one-body dissipation (thick line) and for two-body viscosity with $\eta = 0$ and 0.02 TP (thin lines) as functions of fissility. The results were taken from the $L = 0$ calculations of Ref. Ca 86. The results for $L = 40$ and 60 were estimated by the method of effective fissility (Bl 82). Values for one–body dissipation for $x \lesssim 0.65$ are not very accurate, since they were extrapolated from the curves of Ref. Ca 86 (from Ne 88).

and $\tau_{ss} \sim 5 \times 10^{-21}$ s. When $\Gamma_{fk} \ll \Gamma_\nu$, the average time when fission occurs is $\sim \hbar/\Gamma_\nu > \tau$. However, when $\Gamma_{fk} \gg \Gamma_\nu$ (for higher $J$), fission strongly competes with neutron emission for times $< \tau$, so that on the average fission occurs before equilibration of the fission degree of freedom at the saddle point; this might have implications for fission-fragment angular distributions (Ga 87). The effect of friction on lifetimes for spontaneous fission has been investigated (Da 87) and an upper limit to $\beta$ of $3 \times 10^{20}$ s$^{-1}$ established. This is consistent with zero and the expectations for the ordered regime of low-temperature collective nuclear dynamics (Fig. 4.3).

Nix, Sierk, and collaborators (Ca 86, Da 85, Gr 86, Ho 83b, Kr 79, Ni 84, Ni 86, Ni 87, Si 80, Si 85, Si 86, Si 86a) have made numerous contributions to the theory of fission dynamics, some already mentioned. They have used the FPE and also generalized Hamilton equations, which give average properties only but allow the use of more realistic shape parametrization and dissipation functions, such as that for the one-body mechanism. They have tended to concentrate on the transition from saddle to scission (Ho 83, Ni 84, Ni 86, Ni 87) and related matters such as fission kinetic energies (Si 80, Ni 87) and ternary fission (Ca 86). Cârjan *et al.* (Ca 86) have calculated values for $\tau_{ss}$ for one- and two-body dissipation and $J = 0$. These are shown in Fig. 4.13 together with estimates (Ne 88) for other angular momenta. The values for one-body dissipation are much higher than those for the two-body viscosity (0.02 TP), which fits fission kinetic energies well. However, these calculations use the full wall-formula result; if this is reduced by a factor $k_s$, one might expect $\tau_{ss}$ to be roughly proportional to $k_s$.

Recently Delagrange, Grégoire, *et al.* (De 86, Gr 88) have developed a generalized diffusion equation to follow the time evolution of a system towards fission, including the emission of light particles ($\nu$, $\pi$, $\alpha$) on the way. They comment that their method is very flexible and would allow the inclusion of coordinate-dependent inertia and dissipation coefficients. In the calculations they have included the temperature dependence of $E_f$, have taken the friction constant as that obtained from the wall-plus-window expression of Ref. Si 80 at the saddle point, and have parametrized the potential $V(q)$ with a cubic function. They have paid particular attention to the shapes of the neutron spectra as a functions of time (Gr 88); an example is shown in Fig. 4.14. They have also calculated $\nu_{pre}$ for the $^{16}O$ reaction leading to $^{158}Er$

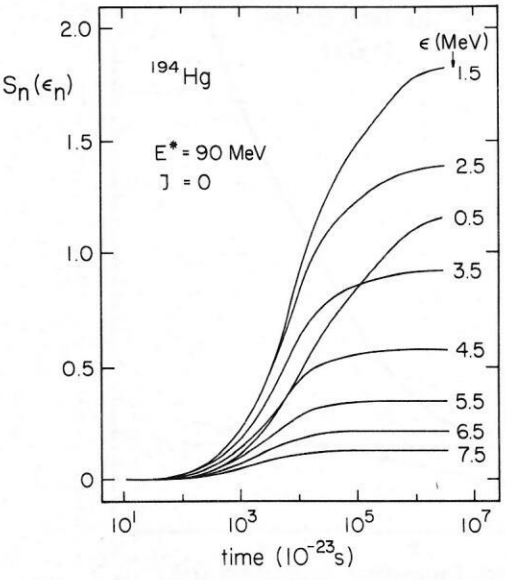


FIG. 4.14. Time variation of the number of emitted neutrons $S_n(E_n)$ for the dynamical decay of a $^{194}Hg$ nucleus with an initial excitation energy of 90 MeV and zero angular momentum. The curves correspond to the indicated neutron energy bins. Note that higher-energy neutrons are predominately emitted at earlier times where the excitation energy of the decaying system is still high, and at longer times only low-energy neutrons are emitted (from Gr 88).

and obtain a value of 3.2 in good agreement with the experimental value $2.7 \pm 0.4$ (Ga 86,87), but low if the results of Refs. Hi 88,89c are correct. However, the theoretical value appears not to include saddle-to-scission emission.

A number of authors have used the Gaussian-bundle propagation method to solve the FPE for two- or three-dimensional collective coordinates, to determine mass and kinetic-energy distributions (Ad 86, Ad 86a, Sh 84a). For this purpose it appears adequate to start with the stationary distribution at the saddle point because, for reasonable values of the friction, memory of the initial distribution at the equilibrium deformation is lost by the time that the saddle point is reached (Ad 86a).

An analytical approach to calculating the competition between first-chance fission and the emission of the first neutron has been achieved by solving the Smoluchowski equation, which is derived from the FPE for overdamped motion (Lu 86a). An alternative phenomenological approach to the FPE method, for use with statistical-model codes, has been proposed (We 84b); the parametrization of the delay function is related to the frequencies of the lowest modes of collective vibration. An interesting possibility is that the time delay in fission arises from the transition from ordered to chaotic motion, which occurs when the curvature of the nuclear potential surface becomes negative near the saddle point (Bo 85). Another matter which might have relevance to the scission process, particularly mass distributions, is the possibility of random neck rupture due to hydrodynamical instability (Br 83, Br 85, Ca 86); surface vibrations along the neck of a classical fluid grow catastrophically when their wavelength exceeds about nine times the neck radius. Extensive calculations have been carried out (Ge 86) showing the quasi- or fast-fission appears as the natural link between deep-inelastic reactions and compound-nucleus formation, and deriving many properties such as mass–angle correlations and fragment angular distributions.

A self-consistent microscopic approach to fission dynamics has not yet been successfully achieved. It appears necessary to use extended time-dependent Hartree–Fock theory (ETDHF) which includes two-body correlations; see, for example, Ref. Ni 87a.

### 4.2. Conclusions

The recent experimental data, indicating an excess of prefission neutrons over that predicted by the statistical model, can be reproduced with fair quantitative accuracy by calculations based on classical diffusion theory, which may be appropriate at high temperature. A large dissipation coefficient, indicating overdamped motion, is required and is also suggested by the concept of one-body dissipation. Further development of the theory is desirable to include multidimensional collective coordinates together with shape- and temperature-dependent dissipation tensors. The calculations should be followed from contact in the entrance channel, rather than from an arbitrary starting point of thermal equilibrium for all except the collective degrees of freedom in the compound nucleus. The question as to whether the adiabatic approximation to $V(q)$ is adequate for large dissipation should be explored (We 87). The nature of the dissipative mechanism needs further study, and in the longer term one would hope that microscopic approaches such as ETDHF might become possible.

More experimental studies for systems with a wide range of fissilities, bombarding energies, and entrance channels, including $\pi$, $\alpha$, and $\gamma$ emission as well as neutron emission, are required. It would be of great interest to be able to separate the contributions to $\nu_{\text{pre}}$ from the pre- and post-saddle periods.

Great advances in our understanding of fission dynamics have occurred in the last few years. However, much more remains to be done in both theory and experiment, and we might expect a rapid development of this field in the near future.

The survey of material for this review was completed in August 1988.


### ACKNOWLEDGMENTS

I would like to express my warm appreciation to Mary Winch and Gavin Gilmour for their patience and excellent work in preparing the manuscript and figures. Thanks are due to J. R. Leigh, for reading the manuscript and for useful comments, and to all those who sent data in advance of publication.


**Note from the American Institute of Physics*: The English version of this article was provided by the author. The style of the references and illustrations were followed from the original manuscript.


Ab 86 Y. Abe, C. Grégoire, and H. Delagrange, J. Phys. (Paris) Colloq. **47**, 329 (1986).

Ab 87 Y. Abdelrahman, J. L. Durell, W. Gelletly, W. R. Phillips, I. Ahmad, R. Holzmann, R. V. F. Janssens, T. L. Khoo, W. C. Ma, and M. W. Drigert, Phys. Lett. **199B**, 504 (1987).

Ad 86 G. D. Adeev, I. I. Gonchar, L. A. Marchenko, and N. I. Pischasov, Yad. Fiz. **43**, 1137 (1986) [Sov. J. Nucl. Phys. **43**, 727 (1986)].

Ad 86a G. D. Adeev and N. I. Pischasov, Yad. Fiz. **44**, 897 (1986) [Sov. J. Nucl. Phys. **44**, 579 (1986)].

Aj 86 N. N. Ajitanand, G. La Rana, R. Lacey, D. J. Moses, L. C. Vaz, G. F. Peaslee, D. M. de Castro Rizzo, M. Kaplan, and J. M. Alexander, Phys. Rev. C **34**, 877 (1986).

Al 82 J. M. Alexander, D. Guerreau, and L. C. Vaz, Z. Phys. A **305**, 313 (1982).

Al 87 J. M. Alexander, Ann. Phys. (Paris) **12**, 603 (1987).

An 79 G. Andersson, M. Areskoug, H. Å. Gustafsson, G. Hyltén, B. Schroder, and E. Hagebo, Z. Phys. A **293**, 241 (1979).

An 80 J. U. Andersen, A. S. Jensen, K. Jørgensen, E. Lægsgaard, K. O. Nielsen, J. S. Forster, I. V. Mitchell, D. Ward, W. M. Gibson, and J. J. Cuomo, K. Dan. Vidensk. Selsk. Mat.–Fys. Medd. **40:7**, 1 (1980).

Aw 85 T. C. Awes, R. L. Ferguson, R. Novotny, F. E. Obenshain, F. Plasil, V. Rauch, G. R. Young, and H. Sann, Phys. Rev. Lett. **55**, 1062 (1985).

Ba 70 H. Baba, Nucl. Phys. **A159**, 625 (1970).

Ba 77 R. Bass, Phys. Rev. Lett. **38**, 265 (1977).

Ba 81 B. B. Back, H. G. Clerc, R. R. Betts, B. G. Glagola, and B. D. Wilkins, Phys. Rev. Lett. **46**, 1068 (1981).

Ba 83 B. B. Back, R. R. Betts, K. Cassidy, B. G. Glagola, J. E. Gindler, L. E. Glendenin, and B. D. Wilkins, Phys. Rev. Lett. **50**, 818 (1983).

Ba 85 J. Bartel, and P. Quentin, Phys. Lett. **152B**, 29 (1985).

Ba 85a B. B. Back, Phys. Rev. C **31**, 2104 (1985).

Ba 85b B. B. Back, R. R. Betts, J. E. Gindler, B. D. Wilkins, S. Saini, M. B. Tsang, C. K. Gelbke, W. Lynch, M. A. McMahan, and P. A. Baisden, Phys. Rev. C **32**, 195 (1985).

Ba 87 G. Batko, O. Civitarese, and A. L. De Paoli, Z. Phys. A **327**, 323 (1987).

Be 77 M. Beckerman and M. Blann, Phys. Lett. **68B**, 31 (1977); Phys. Rev. Lett. **38**, 272 (1977).

Be 78 M. Beckerman and M. Blann, Phys. Rev. C **17**, 1615 (1978).

Be 80 G. Bertsch, Phys. Lett. **95B**, 157 (1980).

Be 83 F. D. Becchetti, H. H. Hicks, C. A. Fields, R. J. Peterson, R. S. Raymond, R. A. Ristinen, J. L. Ullmann, and C. S. Zaidins, Phys. Rev. C **28**, 1217 (1983).

Be 85 M. Beckerman, Phys. Rep. **129**, 145 (1985).

Be 86 M. Beckerman, *Proc. Symp. on "The Many Facets of Heavy-Ion Fusion Reactions"* (1986), Argonne National Laboratory Report ANL-PHYS-86-1, p. 1.

Bh 86 K. H. Bhatt, P. Grangé, and B. Hiller, Phys. Rev. C **33**, 954 (1986).

Bi 72 C. J. Bishop, I. Halpern, R. W. Shaw, Jr., and R. Vandenbosch, Nucl. Phys. **A198**, 161 (1972).

Bi 78 J. Bisplinghoff, P. David, M. Blann, W. Scobel, T. Mayer-Kuckuk, J. Ernst, and A. Mignerey, Phys. Rev. C **17**, 177 (1978).

Bj 73 S. Bjørnholm, A. Bohr, and B. Mottelson, *Proc. Third IAEA Symp. on Physics and Chemistry of Fission*, Rochester (1973), p. 367.

Bj 82 S. Bjørnholm and W. J. Swiatecki, Nucl. Phys. **A391**, 471 (1982).

Bj 85 S. Bjørnholm, Nucl. Phys. **A447**, 117c (1985).

Bj 86 S. Bjørnholm, *Proc. Symp. on Nuclear Fission and Heavy-Ion Induced Reactions*, Rochester (H. Freiesleben and W. U. Schröder, eds.) (1986), p. 1.

Bl 76 M. Blann, OVERLAID ALICE, A Statistical Model Computer Code Including Fission and Pre-equilibrium Models, U. S. Energy Research and Development Administration Report No. COO-3494-29 (1976), unpublished.

Bl 78 J. Blocki, Y. Boneh, J. R. Nix, J. Randrup, M. Robel, A. J. Sierk, and W. J. Swiatecki, Ann. Phys. (N. Y.) **113**, 330 (1978) and references therein.

Bl 80 M. Blann, Phys. Rev. C **21**, 1770 (1980).

Bl 81 M. Blann and T. T. Komoto, Phys. Rev. C **24**, 426 (1981).

Bl 82 M. Blann and T. T. Komoto, Phys. Rev. C **26**, 472 (1982).

Bl 82a M. Blann, Phys. Rev. Lett. **49**, 505 (1982).

Bl 82b M. Blann and T. T. Komoto, University of California Radiation Laboratory Report UCID 19390 (1982), unpublished.

Bl 82c M. Blann, D. Akers, T. A. Komoto, F. S. Dietrich, L. F. Hansen, J. G. Woodworth, W. Scobel, J. Bisplinghoff, B. Sikora, F. Plasil, and R. L. Ferguson, Phys. Rev. C **26**, 1471 (1982).

Bl 85 M. Blann, Phys. Rev. C **31**, 1245 (1985).

Bl 85a J. Blocki, K. Grotowski, R. Planeta, and W. J. Swiatecki, Nucl. Phys. **A445**, 367 (1985).

Bl 86 J. P. Blocki, H. Feldmeier, and W. J. Swiatecki, Nucl. Phys. **A459**, 145 (1986).

Bl 88 M. Blann and B. Remington, Phys. Rev. C **37**, 2231 (1988).

Bo 39 N. Bohr and J. A. Wheeler, Phys. Rev. **56**, 426 (1939).

Bo 69 A. Bohr and B. R. Mottelson, *Nuclear Structure, Vol. 1* (Benjamin, New York, 1969).

Bo 81 B. Borderie, M. Berlanger, D. Gardès, F. Hanappe, L. Nowiki, J. Peter, B. Tamain, S. Agarwal, J. Girard, C. Gregoire, J. Matuszek, and C. Ngô, Z. Phys. A **299**, 263 (1981).

Bo 82 R. Bock, Y. T. Chu, M. Dakowski, A. Gobbi, E. Grosse, A. Olmi, H. Sann, D. Schwalm, U. Lynen, W. F. J. Müller, S. Bjørnholm, H. Esbensen, W. Wölfli, and E. Morenzoni, Nucl. Phys. **A388**, 334 (1982).

Bo 84 P. D. Bond, Phys. Rev. Lett. **52**, 414 (1984); Phys. Rev. C **32**, 471, 483 (1985).

Bo 85 Yu.L. Bolotin and I. V. Krivosheĭ, Yad. Fiz. **42**, 53 (1985) [Sov. J. Nucl. Phys. **42**, 32 (1985)].

Bo 87 P. F. Bortignon and C. H. Dasso, Phys. Lett. **189B**, 381 (1987).

Bo 88 J. J. M. Bokhorst, J. R. Leigh, J. O. Newton, and D. J. Hinde, to be published.

Br 83 U. Brosa and S. Grossmann, Z. Phys. A **310**, 177 (1983).

Br 85 U. Brosa, Phys. Rev. C **32**, 1438 (1985).

Br 88 A. Brucker, B. Lindl, M. Bantel, H. Ho, R. Muffler, L. Schad, M. G. Trauth, and J. P. Wurm, Phys. Lett. **206B**, 13 (1988).

Bu 86 M. A. Butler, S. S. Datta, R. T. de Souza, J. R. Huizenga, W. A. Schröder, J. Töke, and J. L. Wile, Phys. Rev. C **34**, 2016 (1986).

Ca 79 N. Carjan, H. Delagrange, and A. Fleury, Phys. Rev. C **19**, 2267 (1979).

Ca 86 N. Cârjan, A. J. Sierk, and J. R. Nix, Nucl. Phys **A452**, 381 (1986).

Ch 70 E. Cheifetz, Z. Fraenkel, J. Galin, M. Lefort, J. Peter, and X. Tarrago, Phys. Rev. C **2**, 256 (1970).

Ch 86 Y. Chan, C. Albiston, M. Bentel, A. Budzunowski, D. DiGregorio, R. G. Stokstad, S. Wald, S. Zhou, and Z. Zhou, Proc. Symp. on "The Many Facets of Heavy-Ion Fusion Reactions" (1986), Argonne National Laboratory Report ANL-PHY-86-1, p. 219.

Ch 86a R. J. Charity, J. R. Leigh, J. J. M. Bokhorst, A. Chatterjee, G. S. Foote, D. J. Hinde, J. O. Newton, S. Ogaza, and D. Ward, Nucl. Phys. **A457**, 441 (1986).

Ch 87 D. R. Chakrabarty, M. Thoennessen, N. Alamanos, P. Paul, and S. Sen, Phys. Rev. Lett. **58**, 1092 (1987).

Ci 85 O. Civitarese and A. L. De Paoli, Nucl. Phys. **A440**, 480 (1985).

Co 74 S. Cohen, F. Plasil, and W. J. Swiatecki, Ann. Phys. (N. Y.) **82**, 557 (1974).

Da 80 B. Dalton, S. Grimes, J. Vary, and S. Williams, eds., *Theory and Applications of Moment Methods in Many Fermion Systems* (Plenum Press, New York, 1980).

Da 85 K. T. R. Davies and A. J. Sierk, Phys. Rev. C **31**, 915 (1985).

Da 87 N. R. Dagdeviren and H. A. Weidenmüller, Phys. Lett. **186 B**, 267 (1987).

De 77 H. Delagrange, A. Fleury, and J. M. Alexander, Phys. Rev. C **16**, 706 (1977).

De 82 H. Delagrange, Ann. Phys. (Paris) **7**, 193 (1982).

De 86 H. Delagrange, C. Grègoire, F. Scheuter, and Y. Abe, Z. Phys. A **323**, 437 (1986).

Di 73 W. Dilg, W. Schantle, H. Vonach, and M. Uhl, Nucl. Phys. **A217**, 269 (1973).

Di 83 F. A. Dilmanian, L. Grodzins, J. W. Ball, M. Beckerman, R. Boisseau, S. Gazes, R. Ledoux, and A. Sperduto, Phys. Lett. **127B**, 172 (1983).

Do 86 R. Donangelo and L. F. Canto, Nucl. Phys. **A451**, 349 (1986).

Do 86b T. Døssing and J. Randrup, *Proc. Workshop on Nuclear Dynamics* (Copper Mountain, Colorado, 1986), p. 13.

Do 87 T. Døssing and J. Randrup, Nucl. Phys. **A475**, 557 (1987).

Du 83 E. Duek, N. N. Ajitanand, J. M. Alexander, D. Logan, M. Kildir, L. Kowalski, L. C. Vaz, D. Guerreau, M. S. Zisman, and M. Kaplan, Phys. Lett. **131B**, 297 (1983).

Du 84 E. Duek, N. N. Ajitanand, J. M. Alexander, D. Logan, M. Kildir, L. Kowalski, L. C. Vaz, D. Guerreau, M. S. Zisman, M. Kaplan, and D. J. Moses, Z. Phys. A **317**, 83 (1984).

Er 60 T. Ericson, Adv. Phys. **9**, 425 (1960).

Es 81 H. Esbenson, Nucl. Phys. **A352**, 147 (1981).

Fe 60 H. Feshbach, In *Nuclear Spectroscopy, Part B* (Academic Press, New York, 1960), p. 625.

Fe 85 H. T. Feldmeier, Argonne National Laboratory Report ANL-Phy-85-2 (1985), unpublished.

Fe 87 H. Feldmeier, Rep. Prog. Phys. **50**, 915 (1987).

Fi 86 C. Fiolhais, Ann. Phys. (N. Y.) **171**, 186 (1986).

Fo 87 J. S. Forster, I. V. Mitchell, J. U. Andersen, A. S. Jensen, E. Læsgaard, W. M. Gibson, and K. Reichelt, Nucl. Phys. **A464**, 497 (1987).

Fr 75 Z. Fraenkel, I. Mayk, J. P. Unik, A. J. Gorski, and W. D. Loveland, Phys. Rev. C **12**, 1809 (1975).

Fr 86 R. Freifelder, M. Prakash, and J. M. Alexander, Phys. Rep. **133**, 315 (1986).

Ga 72 J. B. Garg, ed., *Statistical Properties of Nuclei* (Plenum, New York, 1972).

Ga 80 A. Gavron, Phys. Rev. C **21**, 230 (1980).

Ga 81 A. Gavron, J. R. Beene, B. Cheynis, R. L. Ferguson, F. E. Obenshain, F. Plasil, G. R. Young, G. A. Petitt, M. Jääskeläinen, D. G. Sarantites, and C. F. Maguire, Phys. Rev. Lett. **47**, 1255 (1981); **48**, 835(E) (1982).

Ga 84 A. Gavron, J. Boissevain, H. C. Britt, K. Eskola, P. Eskola, M. M. Fowler, H. Ohm, J. B. Wilhelmy, T. C. Awes, R. L. Ferguson, F. E. Obenshain, F. Plasil, G. R. Young, and S. Wald, Phys. Rev. C **30**, 1550 (1984).

Ga 84a A. Gavron, P. Eskola, A. J. Sierk, J. Boissevain, H. C. Britt, K. Eskola, M. M. Fowler, H. Ohm, J. B. Wilhelmy, S. Wald, and R. L. Ferguson, Phys. Rev. Lett. **52**, 589 (1984).

Ga 86 A. Gavron, A. Gayer, J. Boissevain, H. C. Britt, J. R. Nix, A. J. Sierk, P. Grangé, S. Hassani, H. A. Weidenmüller, J. R. Beene, B. Cheynis, D. Drain, R. L. Ferguson, F. E. Obenshain, G. A. Petitt, and C. Butler, Phys. Lett. **176B**,

312 (1986).
Ga 87 A. Gavron, A. Gayer, J. Boissevain, H. C. Britt, T. C. Awes, J. R. Beene, B. Cheynis, D. Drain, R. L. Ferguson, F. E. Obenshain, F. Plasil, G. R. Young, G. A. Pettitt, and C. Butler, Phys. Rev. C **35**, 579 (1987).
Ge 82 C. Gerschel, Nucl. Phys. **A387**, 297c (1982).
Ge 86 A. van Geertruyden and Ch. Leclercq-Willain, Nucl. Phys. **A459**, 173 (1986); **A459**, 196 (1986).
Gi 65 A. Gilbert and A. G. W. Cameron, Can. J. Phys. **43**, 1446 (1965).
Gi 85 S. Gil, R. Vandenbosch, A. J. Lazzarini, D.-K. Lock, and A. Ray, Phys. Rev. C **31**, 1752 (1985).
Go 77 P. A. Gottschalk and T. Ledergerber, Nucl. Phys. **A278**, 16 (1977).
Go 87 L J. B. Goldfarb, Nucl. Phys. **A465**, 529 (1987).
Gr 76 I. S. Grant, Rep. Prog. Phys. **39**, 955 (1976).
Gr 80 P. Grangé and H. A. Weidenmüller, Phys. Lett. **96B**, 26 (1980).
Gr 82 C. Gregoire, C. Ngô, and B. Remaud, Nucl. Phys. **A383**, 392 (1982).
Gr 83 P. Grangé, Li Jun-Qing, and H. A. Weidenmüller, Phys. Rev. C **27**, 2063 (1983).
Gr 84 K. Grotowski, Z. Majka, R. Planeta, M. Szczodrak, Y. Chan, G. Guarino, L. G. Moretto, D. J. Morrissey, L. G. Sobotka, R. G. Stokstad, I. Tserruya, S. Wald, and G. J. Wozniak, Phys. Rev. C **30**, 1214 (1984).
Gr 86 P. Grangé, S. Hassani, H. A. Weidenmüller, A. Gavron, J. R. Nix, and A. J. Sierk, Phys. Rev. C **34**, 209 (1986).
Gr 86a J. J. Griffin and M. Dworzecka, Nucl. Phys. **A455**, 61 (1986).
Gr 88 C. Grègoire, H. Delagrange, K. Pomorski, and K. Dietrich, Z. Phys. A **329**, 497 (1988).
Ha 39 O. Hahn and F. Strassmann, Naturwissenschaften **27**, 11 (1939); **27**, 89 (1939).
Ha 52 W. Hausser and H. Feshbach, Phys. Rev. **87**, 366 (1952).
Ha 73 R. W. Hasser and W. Stocker, Phys. Lett. **44B**, 26 (1973).
Ha 83 G. Hansen and A. S. Jensen, Nucl. Phys. **A406**, 236 (1983).
Ha 84 S. Hassani and P. Grangé, Phys. Lett. **137B**, 281 (1984).
Ha 85 B. Haas, G. Duchêne, F. A. Beck, T. Byrski, C. Gehringer, J. C. Merdinger, A. Nouvredine, V. Rauch, J. P. Vivien, J. Berrette, S. Tobbeche, E. Bozek, J. Styczen, J. Keinonen, J. Dudek, and W. Nazarewicz, Phys. Rev. Lett. **54**, 398 (1985).
Ha 86 R. W. Hasser and P. Schuck, Phys. Lett. **179B**, 313 (1986).
Ha 86a S. Hassani and P. Grangé, Z. Phys. A **325**, 95 (1986).
He 88 S. Henss, A. Ruckelschausen, R. D. Fischer, W. Kühn, V. Metag, R. Novotny, R. V. F. Janssens, T. L. Khoo, D. Habs, D. Schwalm, D. Freeman, G. Duchène, B. Haas, F. Haas, S. Hlavac, and R. S. Simon, Phys. Rev. Lett. **60**, 11 (1988).
Hi 82 D. J. Hinde, J. R. Leigh, J. O. Newton, W. Galster, and S. Sie, Nucl. Phys. **A385**, 109 (1982).
Hi 83 D. J. Hinde, J. O. Newton, J. R. Leigh, and R. J. Charity, Nucl. Phys. **A398**, 308 (1983).
Hi 84 D. J. Hinde, R. J. Charity, G. S. Foote, J. R. Leigh, J. O. Newton, S. Ogaza, and A. Chatterjee, Phys. Rev. Lett. **52**, 986 (1984); **53**, 2275 (E) (1984).
Hi 86 D. J. Hinde, R. J. Charity, G. Foote, J. R. Leigh J. O. Newton, S. Ogaza, and A. Chatterjee, Nucl. Phys. **A452**, 550 (1986).
Hi 86a D. Hilscher, H. Rossner, A. Gamp, U. Jahnke, A. Giorni, C. Morano, A. Dauchy, P. Stassi, B. Cheynis, B. Chambon, D. Drain, C. Pastor, and G. Petitt, J. Phys. (Paris) Colloq. **C4**, 381 (1986).
Hi 87 D. J. Hinde, J. R. Leigh, J. J. M. Bokhorst, J. O. Newton, R. L. Walsh, and J. W. Boldeman, Nucl. Phys. **A472**, 318 (1987).
Hi 87a D. Hilscher, Nucl. Phys. **A471**, 77c (1987).
Hi 87b D. Hilscher, D. J. Hinde, and H. Rossner, Hahn-Meitner Institute, Berlin, Report No. HMI-P87/15R, unpublished.
Hi 88 D. J. Hinde, H. Ogata, M. Tanaka, T. Shimoda, N. Takahashi, A. Shinohara, S. Wakamatsu, K. Katori, and H. Okamura, Phys. Rev. C **37**, 2923 (1988).
Hi 89a D. Hilscher, H. Rossner, B. Cramer, B. Gebauer, U. Jahnke, M. Lehmann, E. Schwinn, M. Wilpert, Th. Wilpert, H. Frobeen, E. Mordhorst, and W. Scobel, Phys. Rev. Lett. **62**, 1099 (1989).
Hi 89b D. J. Hinde, J. J. M. Bokhorst, J. R. Leigh, and J. O. Newton, to be published.
Hi 89c D. J. Hinde, H. Ogata, M. Tanaka, T. Shimoda, N. Takahashi, A. Shinohara, S. Wakamatsu, K. Katori, and H. Okamaura, Phys Rev. C **39** 2268 (1989).
Ho 83 E. Holub, D. Hilscher, G. Ingold, U. Jahnke, H. Orf, and H. Rossner, Phys. Rev. C **23**, 252 (1983).
Ho 83b H. Hofmann and J. R. Nix, Phys. Lett. **122B**, 117 (1983).
Ho 88 D. Hook, G. C. Colvin, J. L. Durell, W. Gelletly, J. Lukasiak, J. O. Newton, and W. R. Phillips, to be published.
Hu 72 J. R. Huizenga and L. G. Moretto, Ann. Rev. Nucl. Sci. **22**, 427 (1972).
Ig 75 A. V. Ignatyuk, G. N. Smirenkin, and A. S. Tishin, Yad. Fiz. **21**, 485 (1975) [Sov. J. Nucl. Phys. **21**, 255 (1975)].
Ig 85 A. V. Ignatyuk, International Atomic Energy Agency Report INDC (CCP)-223/L (1985).
Ka 66 P. B. Kahn and N. Rosenzweig, Phys. Lett. **22**, 307 (1986).
Ka 69 P. B. Kahn and N. Rosenzweig, Phys. Rev. **187**, 1193 (1969).
Ka 78 S. A. Karmayan, Yad. Fiz. **27**, 1472 (1978) [Sov. J. Nucl. Phys. **27**, 775 (1978)].
Ka 84 H. J. Karwowski and S. E. Vigdor, Phys. Rev. C **29**, 872 (1984).
Ke 87 H. Keller, K. Lützenkirchen, J. V. Kratz, G. Wirth, W. Brüchle, and K. Sümmerer, Z. Phys. A **326**, 313 (1987).
Ki 87 M. Kicinska-Habior, K. A. Snover, C. A. Gossett, J. A. Behr, G. Feldman, H. K. Glatzel, J. H. Gundlach, and E. F. Garman, Phys. Rev. C **36**, 612 (1987).
Ko 77 S. E. Koonin and J. Randrup, Nucl. Phys. **A289**, 475 (1977).
Ko 87 Y. Kondō, B. A. Robson, J. J. M. Bokhorst, D. J. Hinde, and J. R. Leigh, Phys. Rev. C **35**, 828 (1987).
Kr 40 H. A. Kramers, Physika **7**, 284 (1940).
Kr 79 H. J. Krappe, J. R. Nix, and A. J. Sierk, Phys. Rev. C **20**, 992 (1979).
La 86 E. G. Lanza and H. A. Weidenmüller, Z. Phys. A **323**, 157 (1986).
La 87 R. Lacey, N. N. Ajitanand, J. M. Alexander, D. M. de Castro Rizzo, P. DeYoung, M. Kaplan, L. Kowalski, G. LaRara, D. Logan, D. J. Moses, W. E. Parker, G. F. Peaslee, and L. C. Vaz, Phys. Lett. **191B** 253 (1987).
La 88 R. Lacey, N. N. Ajitanand, J. M. Alexander, D. M. de Castro Rizzo, G. F. Peaslee, L. C. Vaz, M. Kaplan, M. Kildir, G. La Rana, D. J. Moses, W. E. Parker, D. Logan, M. S. Zisman, P. De Young, and L. Kowalski, Phys. Rev. C **37**, 2540, 2561 (1988).
Le 79 C. Lebrun, F. Hanappe, J. F. Lecolley, F. Levebvres, C. Ngô, J. Peter, and B. Tamain, Nucl. Phys. **A321**, 207 (1979).
Le 82 J. R. Leigh, D. J. Hinde, J. O. Newton, W. Galster, and S. H. Sie, Phys. Rev. Lett. **48**, 527 (1982).
Le 83 K. T. Lesko, S. Gil, A. Lazzarini, V. Metag, A. G. Seamster, and R. Vandenbosch, Phys. Rev. C **27**, 2999 (1983).
Le 85 K. T. Lesko, W. Henning, K. E. Rehm, G. Rosner, J. P. Schiffer, G. S. F. Stephans, B. Zeidman, and W. S. Freeman, Phys. Rev. Lett. **55**, 803 (1985).
Le 85a J. R. Leigh, W. R. Phillips, J. O. Newton, G. S. Foote, D. J. Hinde, and G. D. Dracoulis, Phys. Lett. **159B**, 9 (1985).
Le 86 K. T. Lesko, W. Henning, K. E. Rehm, G. Rosner, J. P. Schiffer, G. S. F. Stephans, B. Zeidman, and W. S. Freeman, Phys. Rev. C **34**, 2155 (1986).
Lu 85 K. Lützenkirchen, J. V. Kratz, G. Wirth, W. Brüchle, L. Dörr, K. Sümmerer, R. Lucas, J. Poitou, C. Gregoire, and S. Bjørnholm, Z. Phys. A **320**, 529 (1985).
Lu 86 K. Lützenkirchen, J. V. Kratz, G. Wirth, W. Brüchle, K. Sümmerer, R. Lucas, J. Poitou, and C. Gregoire, Nucl. Phys. **A452**, 351 (1986).
Lu 86a Z. Lu, J. Zhang, R. Feng, and T. Zhuo, Z. Phys. A **323**, 477 (1986).
Ma 79 C. Mahaux and H. Weidenmüller, Ann. Rev. Nucl. Part. Sci. **29**, 1 (1979).
Mc 80 M. A. McMahan and J. M. Alexander, Phys. Rev. C **21**, 1261 (1980).
Mc 85 M. A. McMahan, L. G. Moretto, M. L. Padgett, G. J. Wozniak, L. G. Sobotka, and M. G. Mustafa, Phys. Rev. Lett. **54**, 1995 (1985).
Me 39 L. Meitner and O. R. Frisch, Nature **143**, 239 (1939); **143**, 471 (1939).
Mo 72 L. G. Moretto, Nucl. Phys. **A182**, 641 (1972).
Mo 75 L. G. Moretto, Nucl. Phys. **A247**, 211 (1975).

Mo 80 L. G. Moretto and R. P. Schmitt, Phys. Rev. C **21**, 204 (1980).

Mo 85 U. Mosel, in *Treatise on Heavy-Ion Science, Vol. 2* (D. A. Bromley, ed.) (Plenum, New York, 1985), p. 1.

Mo 87 D. J. Moses, M. Kaplan, G. La Rana, W. E. Parker, R. Lacey, and J. M. Alexander, Phys. Rev. C **36**, 422 (1987).

Mo 87a D. J. Moses, M. Kaplan, M. Kildir, D. R. G. Logan, G. La Rana, W. E. Parker, R. Lacey, G. F. Peaslee, J. M. Alexander, N. N. Ajitanand, L. C. Vaz, and M. S. Zisman, Nucl. Phys. **A465**, 339 (1987).

Mu 82 M. G. Mustafa, P. A. Baisden, and H. Chandra, Phys. Rev. C **25**, 2524. (1982).

Mu 86 T. Murakami, C.-C. Sahm, R. Vandenbosch, D. D. Leach, A. Ray, and M. J. Murphy, Phys. Rev. C **34**, 1353 (1986).

Mu 88 T. Murakami, J. Kasagi, K. Yoshida, H. Harada, H. Tachibanaki, S. Kubono, M. Yasue, M. H. Tanaka, S. M. Lee, M. Ogiwara, H. Fugiwara, and S. C. Jeong (1988), to be published.

My 66 W. D. Myers and W. J. Swiatecki, Nucl. Phys. **81**, 1 (1966).

My 67 W. D. Myers and W. J. Swiatecki, Ark. Fys. **36**, 343 (1967).

My 77 W. D. Myers *Droplet Model of the Atomic Nucleus* (IFI/Plenum, New York, 1977).

Ne 81 J. O. Newton, B. Herskind, R. M. Diamond, E. L. Dines, J. E. Draper, K. H. Lindenberger, C. Schück, S. Shih, and F. S. Stephens, Phys. Rev. Lett. **46**, 1383 (1981).

Ne 81a J. O. Newton, Phys. Scr. **24**, 83 (1981).

Ne 84 J. O. Newton, *Proc. Int. Symp. on Nuclear Spectroscopy and Nuclear Interactions, Osaka, Japan* (H. Ejiri and T. Fukuda, ed.) (World Scientific, Singapore, 1984), p. 58.

Ne 86 G. Nebbia, K. Hagel, D. Fabris, Z. Majka, J. B. Natowitz, R. P. Schmitt, B. Sterling, G. Mouchaty, G. Barkowitz, M. Strozewski, G. Viesti, P. L. Gonthier, B. Wilkins, M. N. Namboodiri, and H. Ho, Phys. Lett. **176B**, (1986).

Ne 88 J. O. Newton, D. J. Hinde, R. J. Charity, J. R. Leigh, J. J. M. Bokhorst, A. Chatterjee, G. S. Foote, and S. Ogaza, Nucl. Phys. **A483**, 126 (1988).

Ng 86 C. Ngô, Prog. Part. Nucl. Phys. **16**, 139 (1986).

Ni 69 J. R. Nix, Nucl. Phys. **A130**, 241 (1969).

Ni 84 J. R. Nix, A. J. Sierk, H. Hofmann, F. Scheuter, and D. Vautherin, Nucl. Phys. **A424**, 239 (1984).

Ni 86 J. R. Nix and A. J. Sierk, Los Alamos National Laboratory Report LA-UR-86-698 (1986), unpublished.

Ni 87 J. R. Nix and A. J. Sierk, Los Alamos National Laboratory Reports. LA-UR-87-133, LA-UR-87-1705 (1987), unpublished.

Ni 87a K. Niita, W. Nörenberg, and S. J. Wang, Z. Phys. A **326**, 69 (1987).

No 82 L. Nowicki, M. Berlanger, B. Borderie, C. Cabot, P. del Marmol, Y. El Masri, C. Grégoire, F. Hanappe, C. Ngô, and B. Tamain, Phys. Rev. C **26**, 1114 (1982).

No 85 P. J. Nolan, D. J. G. Love, A. Kirwan, D. J. Unwin, A. H. Nelson, P. J. Twin, and J. D. Garrett, Phys. Rev. Lett. **54**, 2211 (1985).

Oe 80 W. von Oertzen, H. Fuchs, A. Gamp, H. Homeyer, U. Jahnke, and J. C. Jacmart, Z. Phys. A **298**, 207 (1980).

Og 85 Yu. Ts. Oganessian and Yu. A. Lazarev, *Treatise on Heavy-ion Science* (D. A. Bromley, ed.) (Plenum, New York, 1985), Vol. IV, p. 1.

Pi 82 M. Pi, X. Vinas, and M. Barranco, Phys. Rev. C **26**, 733 (1982).

Pi 85 S. C. Pieper, M. J. Rhoades-Brown, and S. Landowne, Phys. Lett. **162B**, 43 (1985).

Pl 78 F. Plasil, Phys. Rev. C **17**, 823 (1978).

Pl 80 F. Plasil, R. L. Ferguson, R. L. Hahn, F. E. Obenshain, F. Pleasonton, and G. R. Young, Phys. Rev. Lett. **45**, 333 (1980).

Pl 82 F. Plasil, R. L. Ferguson, R. L. Hahn, F. E. Obenshain, F. Pleasonton, and G. R. Young, Phys. Rev. Lett. **49**, 506 (1982).

Pl 83 J. van der Plicht, H. C. Britt, M. M. Fowler, Z. Fraenkel, A. Gavron, J. B. Wilhelmy, F. Plasil, T. C. Awes, and G. R. Young, Phys. Rev. C **28**, 2022 (1983).

Pl 84 F. Plasil, T. C. Awes, B. Cheynis, D. Drain, R. L. Ferguson, F. E. Obenshain, A. J. Sierk, S. G. Steadman, and G. R. Young, Phys. Rev. C **29**, 1145 (1984).

Pl 86 R. Planeta, P. Belery, J. Brzychczyk, P. Cohilis, Y. El Masri, Gh. Grégoire, K. Grotowski, Z. Majka, S. Micek, M. Szczodrak, A. Wieloch, and J. Albinski, Phys. Rev. C **34**, 512 (1986).

Po 62 S. M. Polikanov, V. A. Druin, V. A. Karnaukov, V. L. Mikhaev, A. A. Pleve, N. K. Sobeliev, V. G. Subbortin, G. M. Ter-Akopyan, and V. A. Fomichev, Zh. Eksp. Teor. Fiz. **42**, 1464 (1962) [Sov. Phys. JETP **15**, 1016 (1962)].

Pr 84 M. Prakash, V. S. Ramamurthy, S. S. Kapoor, and J. M. Alexander, Phys. Rev. Lett. **52**, 990 (1984).

Pu 77 F. Pühlhoffer, Nucl. Phys. **A280**, 267 (1977).

Ra 80 J. Randrup and W. J. Swiatecki, Ann Phys. (N.Y.) **125**, 193 (1980).

Ra 84 J. Randrup and W. J. Swiatecki, Nucl. Phys. **A429**, 105 (1984).

Ra 87 G. La Rana, D. J. Moses, W. E. Parker, M. Kaplan, D. Logan, R. Lacey, J. M. Alexander, and R. J. Welberry, Phys. Rev. C **35**, 373 (1987).

Ra 87a J. Randrup and R. Vandenbosch, Nucl. Phys. **A474**, 219 (1987).

Re 81 W. Reisdorf, Z. Phys. A **300**, 227 (1981).

Re 86 K. E. Rehm, Proc. Symp. on "The Many Facets of Heavy-Ion Fusion Reactions" (1986), Argonne National Laboratory Report ANL-PHY-86-1, p. 27.

Re 86a W. Reisdorf, *Proc. Int. Conf. on Nuclear Physics, Harrogate*, Vol. 2 (1986), p. 205.

Re 86b P. G. Reinhard, H. Reinhardt, and K. Goeke, Ann Phys. (N.Y.) **166**, 257 (1986).

Ri 82 M. F. Rivet, D. Logan, J. M. Alexander, D. Guerreau, E. Duek, M. S. Zisman, and M. Kaplan, Phys. Rev. C **25**, 2430 (1982).

Ro 83 H. Rossner, D. Hilscher, E. Holub, G. Gingold, U. Jahnke, H. Orf, J. R. Huizenga, J. R. Birkland, W. U. Schröder, and W. W. Wilki, Phys. Rev. C **27**, 2666 (1983).

Ro 84 H. Rossner, J. R. Huizenga, and W. U. Schröder, Phys. Rev. Lett. **53**, 38 (1984).

Ro 86 H. Rossner, J. R. Huizenga, and W. U. Schröder, Phys. Rev. C **33**, 560 (1986).

Ro 89 H. Rossner, D. Hilscher, D. J. Hinde, B. Gebauer, M. Lehmann, M. Wilpert, and E. Mordhorst, Phys. Rev. C, in press.

Sa 76 G. Sauer, H. Chandra, and U. Mosel, Nucl. Phys. **A264**, 221 (1976).

Sa 86 S. J. Sanders, R. R. Betts, I. Ahmad, K. T. Lesko, S. Saini, B. D. Wilkins, F. Videbaek, and B. K. Dichter, Phys. Rev. C **34**, 1746 (1986).

Sa 87 S. J. Sanders, D. G. Kovar, B. B. Back, C. Beck, B. K. Dichter, D. Henderson, R. V. F. Janssens, J. G. Keller, S. Kaufman, T.-F. Wang, B. Wilkins, and F. Videbaek, Phys. Rev. Lett. **59**, 2856 (1987).

Sa 87a T. Sami and J. Richert, Nucl. Phys. **A472**, 168 (1987).

Sc 82 R. P. Schmitt and A. J. Pacheco, Nucl. Phys. **A379**, 313 (1982).

Sc 83 R. P. Schmitt, G. Mouchaty, D. R. Haenni, and P. Bogucki, Phys. Lett. **127B**, 327 (1983).

Sc 84 K. H. Schmídt, J. G. Keller, and D. Vermeulen, Z. Phys. A. **315**, 159 (1984).

Sc 84a W. U. Schröder and J. R. Huizenga *Treatise in Heavy-Ion Science* (D. A. Bromley, ed.), Vol. 2 (Plenum, New York, 1984), p. 115.

Sc 84b R. P. Schmitt, G. Mouchaty, and D. R. Haenni, Nucl. Phys. **A427**, 614 (1984).

Sc 85 R. P. Schmitt, G. Mouchaty, D. R. Haenni, and M. Tirion, Z. Phy. A **321**, 411 (1985).

Sh 84 L. Schad, H. Ho, G.-Y. Fan, B. Lindl, A. Pfoh, R. Wolski, and J. P. Wurm, Z. Phys. A **318**, 179 (1984).

Sh 84a F. Scheuter, C. Grégoire, H. Hofmann, and J. R. Nix, Phys. Lett. **149B**, 303 (1984).

Sh 86 W. Q. Shen, J. Albinski, R. Bock, A. Gobbi, S. Gralla, K. D. Hildenbrand, N. Herrmann, J. Kuzminski, W. F. J. Müller, H. Stelzer, J. Töke, B. B. Back, S. Bjørnholm, S. P. Sørensen, A. Olmi, and G. Guarino, Europhys. Lett. **1**, 113 (1986).

Sh 86b B. Shivakumar, D. Shapira, P. H. Stelson, M. Beckerman, B. A. Harmon, K. Teh, and D. A. Bromley, Phys. Rev. Lett. **57**, 1211 (1986).

Sh 87 W. Q. Shen, J. Albinski, A. Gobbi, S. Gralla, K. D. Hildenbrand, N. Herrmann, J. Kuzminski, W. F. J. Müller, H. Stelzer, J. Toke, B. B. Back, S. Bjørnholm, and S. P. Sørensen, Phys. Rev. C **36**, 115 (1987).

Si 64 T. Sikkeland, Phys. Rev. **135**, B669 (1964).

Si 71 T. Sikkeland, J. E. Clarkson, N. H. Steiger-Shafrir, and V. E. Viola, Phys. Rev. C **3**, 329 (1971).

Si 80 A. J. Sierk and J. R. Nix, Phys. Rev. C **21**, 982 (1980).

Si 82 B. Sikora, W. Scobel, M. Beckerman, J. Bisplinghoff, and M. Blann, Phys. Rev. C **25**, 1446 (1982).

Si 83 R. H. Siemssen, Nucl. Phys. **A400**, 245 (1983).

Si 85 A. J. Sierk, Phys. Rev. Lett. **55**, 582 (1985).

Si 86 A. J. Sierk, Phys. Rev. C **33**, 2039 (1986).

Si 86a A. J. Sierk, Proc. Symp. on "The Many Facets of Heavy-Ion Fusion Reactions" (1986), Argonne National Laboratory Report ANL-PHY-86-1, p.135.

Sn 86 K. A. Snover, Ann. Rev. Nucl. Part. Sci. **36**, 545 (1986) and references therein.

Sn 88 K. A. Snover, Nucl. Phys. **A482**, 13 (1988).

So 84 L. G. Sobotka, M. A. McMahan, R. J. McDonald, C. Signarbieux, G. J. Wozniak, M. L. Padgett, J. H. Gu, Z. H. Liu, Z. Q. Yao, and L. G. Moretto, Phys. Rev. Lett. **53**, 2004 (1984).

St 66 V. M. Strutinskiĭ, Yad. Fiz. **3**, 614 (1966) [Sov. J. Nucl. Phys. **3**, 449 (1966)].

St 73 V. M. Strutinsky, Phys. Lett. **47B**, 121 (1973).

St 85 R. G. Stokstad, *Treatise on Heavy-Ion Science, Vol. 3* (D. A. Bromley, ed.) (Plenum, New York, 1985), p. 83.

St 85a S. G. Steadman, ed., *Fusion Reactions Below the Coulomb Barrier* (Lecture Notes in Physics, Vol. 219, Springer-Verlag, Berlin, 1985).

St 86 S. G. Steadman and M. J. Rhoades-Brown, Ann. Rev. Nucl. Part. Sci. **36**, 649 (1986).

St 88 A. Stolk, W. H. A. Hesselink, H. Rijneveld, A. Balanda, J. Penninga, and H. Verheul, Phys. Lett. **200B**, 13 (1988).

Sw 81 W. J. Swiatecki, Phys. Sci. **24**, 113 (1981).

Sw 82 W. J. Swiatecki, Nucl. Phys. **A376**, 275 (1982).

Sw 83 W. J. Swiatecki, Aust. J. Phys. **36**, 641 (1983).

Sw 84 W. J. Swiatecki, Nucl. Phys. **A428**, 199 (1984).

Sw 85 W. J. Swiatecki, in *Proc. of Niels Bohr Centennial Symp. on Semiclassical Descriptions of Atomic & Nuclear Collisions*, eds J. de Boer and J. Bang, Copenhagen (North-Holland, Amsterdam, 1985), p.281.

Th 68 T. D. Thomas, Ann. Rev. Nucl. Sci. **18**, 343 (1968).

Th 87 M. Thoennessen, D. R. Chakrabarty, M. G. Herman, R. Butsch, and P. Paul, Phys. Rev. Lett. **59**, 2860 (1987).

Th 88 M. Thoennessen, D. R. Chakrabarty, R. Butsch, M. G. Herman, P. Paul, and S. Sen, Phys. Rev. C **37**, 1762 (1988).

To 81 J. Toke and and W. J. Swiatecki, Nucl. Phys. **A372** 141 (1981).

To 84 J. Toke, R. Bock, Dai Guang-xi, A. Gobbi, S. Gralla, K. D. Hildenbrand, J. Kuzminski, W. F. J. Müller, A. Olmi, W. Reisdorf, S. Bjørnholm, and B. B. Back, Phys. Lett. **142B**, 258 (1984).

To 85 J. Toke, R. Bock, Dai Guang-xi, A. Gobbi, S. Gralla, K. D. Hildenbrand, J. Kuzminski, W. F. J. Müller, A. Olmi, H. Stelzer, B. B. Back, and S. Bjørnholm, Nucl. Phys. **A440**, 327 (1985).

To 86 S. Tobbeche, J. Barrette, B. Haas, F. A. Beck, T. Byrski, G. Duchene, C. Gehringer, J. C. Merdinger, A. Nourreddine, and J. P. Vivien, Z. Phys. A **325**, 85 (1986).

Ts 83 M. B. Tsang, H. Utsunomiya, C. K. Gelbke, W. G. Lynch, B. B. Back, S. Saini, P. A. Baisden, and M. A. McMahan, Phys. Lett. **129B**, 18 (1983).

Ts 83a M. B. Tsang, D. Ardouin, C. K. Gelbke, W. G. Lynch, Z. R. Xu, B. B. Back, R. R. Betts, S. Saini, P. A. Baisden, and M. A. McMahan, Phys. Rev. C **28**, 747 (1983).

Ts 88 T. Tserruya, V. Steiner, Z. Fraenkel, P. Jacobs, D. G. Kovar, W. Henning, M. F. Vineyard, and B. B. Glagola, Phys. Rev. Lett. **60**, 14 (1988).

Ud 85 T. Udagawa, B. T. Kim, and T. Tamura, Phys. Rev. C **32**, 125 (1985); B. T. Kim, T. Udagawa, and T. Tamura, Phys. Rev. C **33**, 370 (1986).

Va 73 R. Vandenbosch and J. R. Huizenga, *Nuclear Fission* (Academic, New York, 1973).

Va 74 L. C. Vaz and J. M. Alexander, Phys. Rev. C **10**, 464 (1974).

Va 83 R. Vandenbosch, B. B. Back, S. Gil, A. Lazzarini, and A. Ray, Phys. Rev. C **28**, 1161 (1983).

Va 83a L. C. Vaz and J. M. Alexander, Phys. Rep. **97**, 1 (1983).

Va 84 L. C. Vaz and J. M. Alexander, Z. Phys. A. **318**, 231 (1984).

Va 86 R. Vandenbosch, Proc. Symp. on "The Many Facets of Heavy-Ion Fusion Reactions" (1986), Argonne National Laboratory Report ANL-PHY-86-1, p. 155.

Va 86a R. Vandenbosch, T. Murakami, C. C. Sahm, D. D. Leach, A. Ray, and M. J. Murphy, Phys. Rev. Lett. **56**, 1234, 1498 (1986).

Va 86b R. Vandenbosch, in *Proc. Int. Symp on Physics at Tandem* (1986), (C. Jiang, S. Li, Z. Sun, and H. Zhang, eds.) (World Scientific, Singapore, 1987), p.315.

Vi 80 S. E. Vigdor, H. J. Karwowski, W. W. Jacobs, S. Kailas, P. P. Singh, F. Soga, and P. Yip, Phys. Lett. **90B**, 384 (1980).

Vi 82 S. E. Vigdor and H. J. Karwowski, Phys. Rev. C **26**, 1068 (1982).

Vi 82a V. E. Viola, B. B. Back, K. L. Wolf, T. C. Awes, C. K. Gelbke, and H. Breuer, Phys. Rev. C **26**, 178 (1982).

Vi 82b S. E. Vigdor, H. J. Karwowski, W. W. Jacobs, S. Kailas, P. P. Singh, F. Soga, and T. G. Throwe, Phys. Rev. C **26**, 1035 (1982).

Vo 68 E. Vogt, *Advances in Nuclear Physics, Vol. 1* (M. Baranger and E. Vogt, ed.) (Plenum, New York, 1968), p. 261.

Vu 86 E. Vulgaris, L. Grodzins, S. G. Steadman, and R. Ledoux, Phys. Rev. C **33**, 2017 (1986).

Wa 83 D. Ward, R. J. Charity, D. J. Ninde, J. R. Leigh, and J. O. Newton, Nucl. Phys. **A403**, 189 (1983).

We 80 H. A. Weidenmüller, Prog. Part. Nucl. Phys. **2**, 49 (198).

We 84 H. A. Weidenmüller and J. S. Zhang, Phys. Rev. C **29**, 879 (1984).

We 84a H. A. Weidenmüller and J. S. Zhang, J. Stat. Phys. **34**, 191 (1984).

We 84b W. Westmeier and R. A. Esterlund, Z. Phys. A **316**, 27 (1984).

We 87 H. A. Weidenmüller, Nucl. Phys. **A471**, 1c (1987).

Wi 67 J. Wilks, *The Properties of Liquid and Solid Helium* (Clarendon, Oxford, 1967).

Wo 73 C. Y. Wong, Phys. Rev. Lett. **31**, 766 (1973).

Ya 85 C. Yannouleas, Nucl. Phys. **A439**, 336 (1985).

Za 86 W. P. Zank, D. Hilscher, G. Ingold, U. Jahnke, M. Lehmann, and H. Rossner, Phys. Rev. C **33**, 519 (1986).

Ze 74 A. M. Zebelman, L. Kowalski, J. Miller, K. Beg, Y. Eyal, G. Jaffe, A. Kandil, and D. Logan, Phys. Rev. C **10**, 200 (1974).

Zh 83 J. S. Zhang and H. A. Weidenmüller, Phys. Rev. C **28**, 2190 (1983).

Zh 84 Z. Zheng, B. Borderie, D. Gardès, H. Gauvin, F. Hanappe, J. Peter, M. F. Rivet, B. Tamain, and A. Zaric, Nucl. Phys. **A422**, 447 (1984).